Reconstruction of the sedimentary history offshore NW Africa: Application of core-logging tools

Dissertation zur Erlangung

des Doktorgrades am

Fachbereich Geowissenschaften

der Universität Bremen

vorgelegt von

Holger Kuhlmann

Bremen, November 2003

Tag des Kolloquiums:

10. Februar 2004

Gutachter:

Prof. Dr. Gerold Wefer

Prof. Dr. Gerhard Bohrmann

Prüfer:

Prof. Dr. Katrin Huhn

Prof. Dr. Jörn Peckmann

Table of contents

Abstract

Wide regions of the open oceans are characterized by a general uniformity of their physical and biological properties. In contrast, coastal upwelling regions, which are comparatively small in size, present a highly variable pattern. As a consequence investigations of regional factors in coastal upwelling regions based on a single or just a few cores seem to lack sufficient information, as is confirmed by their differing results. The goal of this thesis is to reconstruct, with high spatial resolution, the influence of coastal upwelling and Saharan dust on the magnitude and composition of sediment accumulation in the Canary region, and to investigate how this influence has varied through the last glacial and interglacial periods. The investigation was carried out within a small region containing a zonal productivity gradient from the eutrophic Northwest African upwelling system to the oligotrophic North Atlantic subtropical gyre. Additionally, the meridional transition from the North Atlantic / Mediterranean climate system, influencing the northern part of the investigation area (down to 30° N), to the dominating influence of the NW African monsoonal climate system further to the south characterizes the diversity of the Canary Islands region. To achieve dense coverage for paleoceanographic reconstruction in the investigation area, a large number of sediment cores has been analyzed with rapid and non-destructive core-logging systems.

The results of this thesis show that even the small region of the Canary Islands can be separated into several areas, with each reflecting its own sediment characteristics. Recent remote sensing images of chlorophyll concentration reflecting the present upwelling conditions are mirrored by the accumulation rates of the underlying sediment. At the last deglaciation the highest sediment accumulation rates of the last 40,000 years before present (B.P.) are observed, which is interpreted to reflect the strongest upwelling intensity. During glacial periods, areas of high accumulation achieved their widest extent, as a result of sea-level changes. These findings provide possible explanations for the conflicting results of single-core reconstructions from the NW African continental margin.

The contribution of terrigeneous material to the marine sediments can be separated into eolian and a fluvial portions. Three characteristic areas could be delineated within the Canary Islands region. The ratio of eolian to fluvial transport of the terrigeneous material increases with wider distance to the coast. The fluvial

contribution reflects river activity throughout the last 130,000 years B.P. north of 30° N at near-coastal sites. South of 30° N fluvial input occurs only during wet phases of interglacial time intervals, reflecting the influence of the NW African monsoon.

Holocene climate, studied in great detail on the highest-resolution core from the northern part of the Canary Islands region is characterized by significant environmental changes at 8,500 years B.P., as indicated by the sedimentation rates and the periodicity of the terrigeneous signal. These findings document the separation of the climatic regime dominating the area north of 30° N from influences of the NW African monsoonal system further to the south, where the main Holocene climate shift occurs at 5,000 years B.P..

Zusammenfassung

Die großen Ozeangebiete der Erde sind über weite Strecken von relativ einheitlichen physikalischen und biologischen Parametern geprägt. Im Gegensatz dazu zeigen die vergleichsweise kleinen Auftriebsgebiete entlang der Ozeanränder ein sehr uneinheitliches und sich veränderndes Bild. Die Untersuchung der kleinräumigen, regionalen Einflussfaktoren in Küstenauftriebsgebieten, basierend auf Arbeiten an einem oder wenigen Sedimentkernen, ist deshalb häufig unzureichend, was durch die teilweise gegensätzlichen Ergebnisse dieser Studien belegt wird. Das Ziel dieser Dissertation ist es, mit hoher regionaler Auflösung den Einfluss des Küstenauftriebes vor NW Afrika und des Saharastaubes auf die Akkumulation und die Zusammensetzung der Sedimente in der Region der Kanarischen Inseln zu bestimmen. Besondere Beachtung finden hierbei die Veränderungen der genannten Einflussfaktoren im Wechsel der letzten Glazial- und Interglazialzeiten. Als Arbeitsgebiet wurde die Region der Kanarischen Inseln ausgewählt, die einen deutlichen, zonalen Produktivitätsgradienten von der eutrophen Afrikanischen Küstenregion zu oligotrophen Oberflächenwassermassen der subtropischen Gyre des Nordatlantiks aufweist. Zusätzlich zu dieser zonalen Komponente ist die Region durch den meridionalen Übergang der Einflussbereiche des Nordatlantischen Klimasystems (> 30°N) zu dem weiter südlich vorherrschenden NW Afrikanischen Monsoonsystems charakterisiert. Für die hochauflösende, paläozeanographische Rekonstruktion dieser variablen Region wurde eine große Anzahl von Sedimentkernen mit Hilfe von relativ schnell und zerstörungsfrei arbeitenden Kernlogging-Systemen analysiert.

Die Ergebnisse dieser Arbeit verdeutlichen, dass selbst ein relativ kleines Gebiet wie die Region der Kanarischen Inseln aufgrund ihrer hohen Diversität in kleinere Bereiche aufteilt werden muss, um ihre Charakteristika zu erfassen. Satelliten gestützte Beobachtungen der Chlorophyllverteilung im Oberflächenwasser, die als Indikator für Pirmärproduktion und damit Auftrieb gelten, zeigen die gleichen Verteilungsmuster wie die Akkumulationsraten der jüngsten Sedimente am Ozeanboden. Während der Abschmelzphase der Gletscher der letzten Vereisung erreichten die Sedimentakkumulationsraten die höchsten Werte der letzten 40.000 Jahre. Daraus wird auf eine maximale Auftriebsintensität zu dieser Zeit geschlossen. In der Zeit des vorangegangenen Glazials erreichte das Gebiet hoher Sedimentakkumulation seine größte Ausdehnung, was mit dem zu dieser Zeit niedrigeren Meeresspiegel und der

damit veränderten Küstenmorphologie erklärt wird. Diese Ergebnisse und die Charakterisierung der verschiedenen Bereiche bieten eine Erklärung und Zusammenführung der unterschiedlichen Ergebnisse von Einzelkernstudien in der NW Afrikanischen Auftriebsregion.

Der Anteil der terrigenen Komponenten in den marinen Sedimenten kann sowohl über fluviatilen als auch über äolischen Transport eingetragen werden. Auch für diesen Themenschwerpunkt wurde eine Unterteilung des Untersuchungsgebietes in drei charakteristische Teilbereiche vorgenommen. Der Anteil äolisch eingetragenen Staubes am terrigenen Material erhöht sich mit zunehmender Entfernung von der Küste. Im küstennahen Bereich nördlich von 30° N wird aufgrund der Flussfracht auf eine kontinuierliche Aktivität der das Atlasgebirge entwässernden Flusssysteme während der letzten 130.000 Jahre geschlossen. In den weiter südlich gelegenen Bereichen des Arbeitsgebietes gibt es nur während der Feuchtphasen der Interglaziale Anzeichen für Flusseintrag. Diese werden als Hinweise auf einen im Vergleich zu heutigen Bedingungen weiter nach Norden (maximal bis 30° N) ausgedehnten Einfluss des NW Afrikanischen Monsoonsystems gedeutet.

Das Klima des bis heute andauernden Interglazials (Holozän) wurde in höchstmöglicher zeitlicher Auflösung an einem Kern aus dem nördlichen Bereich des Arbeitgebietes untersucht. Änderungen, die sowohl in der Sedimentakkumulation als auch in der Zyklizität des terrigenen Eintrags vor 8.500 Jahren auftreten, weisen auf eine tiefgreifende Veränderung des damaligen Klimas in der Region hin. Weiterhin dokumentieren die Ergebnisse die Unterscheidung vom weiter südlich dominierenden Einfluss des NW Afrikanischen Monsoonsystems, das eine vergleichbare Klimaänderung vor 5.000 Jahren erfahren hat.

1. INTRODUCTION

Evidence for climate variations can be found throughout the Earth´s geologic record. Slight changes in the Earth´s orbit (Milankovic, 1930) as well as differences in solar activity are responsible for a continuous variation of the energy balance of different regions. Additionally, changes on our planet itself, such as the distribution of landmasses following the theory of Wegener (1915), contribute to the climatic changes. On more recent time scales, the opportunity to study past atmospheric conditions, such as the greenhouse gas CO_2 trapped in ice cores (Barnola et al., 1987; Bender et al., 1994), lead to a recognition of the important role of the world´s oceans with respect to the climate system (Siegenthaler and Sarmiento, 1993; Schlesinger, 1997). As a consequence, marine productivity (Broecker and Henderson, 1998) and marine sediment have been identified as both, as important sources and sinks in the carbon cycle (Broecker and Peng, 1993). Coastal upwelling regions are of special interest due to the high fluxes within the biogeochemical cycles. Paleoceanographic reconstructions of the NW African coastal upwelling system using sediment records have frequently been applied to infer the behaviour of the system in the alternation of glacial and interglacial conditions (Sarnthein et al., 1982; Bertrand et al., 1996; Martinez et al., 1999; Freudenthal et al., 2002; Moreno et al., 2002). These studies are often based on single or a limited number of cores, and produce different results regarding determination of maximum marine productivity. This thesis is aimed at investigating the factors and processes that account for the differences within a small region using a large number of sediment cores in order to achieve a high spatial resolution. A common trend in paleoceanography and climate understanding is to achieve high-resolution reconstructions. The application of core-logging systems provides the unique opportunity to work on a large number of sediment cores at a high temporal resolution.

1.1. Investigation area

1.1.1 Geographic setting

The investigation area is located at the passive continental margin region off the NW African continent from 27 to 34° N and 9 to 18° W. It is bounded by the Moroccan coast to the east and includes the Canary Islands in the south and Madeira at the northwestern tip. The Moroccan landscape is characterized in the northwestern part by two mountain chains consisting of highly diverse material of up to Precambrian ages. The High Atlas reach an altitude of more than 4,000 m. The Anti Atlas are located

further to the south separated from the High Atlas by the valley of the Souss River (Fig. 1.1). The southwestern part of Morocco is comparatively flat and characterized by sand dunes and dried lakes. The coastal morphology exhibits two cape locations: Cape Ghir at 31° N, and Cape Yubi between 27 and 28° N (Fig. 1.1). In the adjacent North

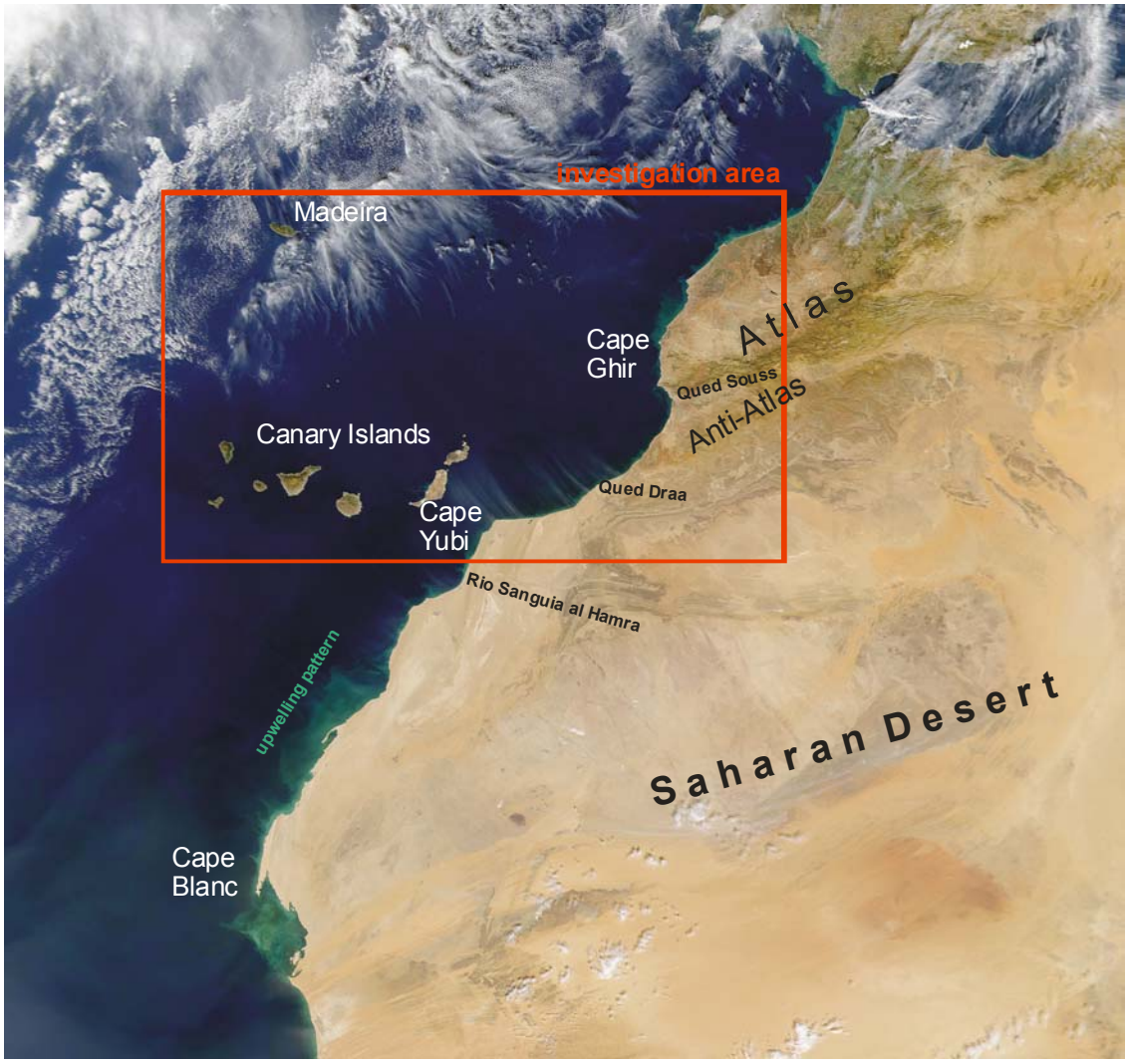

Figure 1.1 The NW African continental margin as observed by the SeaWiFS sensor of the OrbView 2 satellite on Dec. 11th, 2000; provided by the SeaWiFS Project, NASA/Goddard Space Flight Center, and ORBIMAGE.

Atlantic Ocean the Canary Islands, consisting of 7 major islands, extend from 27 to about 29° N and 13 to 18 °W. The island of Madeira is located farther to the north at the northwestern tip of the investigation area (33° N, 17° W).

The Canary Islands as well as the island of Madeira are of volcanic origin (Schmincke, 2000). They are suspected to represent the youngest parts of the Canary (Geldmacher and Hoernle, 2000) and the Madeira (Geldmacher et al., 2001) hotspot tracks, respectively. The volcanic edifice of the Canary Islands grew upon basaltic series that range in age from 12 to 3 Ma (Martí et al., 1994; Ancochea, 1999; Abratis et al., 2002; Edgar et al., 2002; Huertas et al., 2002). The further development generated various types of volcanic activity, which lasted until the 20th century (Klügel et al., 2000), and probably will continue in the future (Rihm et al., 1998). The geologic history of the Canary Islands and their related influence on the region was investigated, among others, by a cruise of the Ocean Drilling Program (Leg 157, Site 953 – 955) in 1994 ,drilling down into the volcanic apron of the Islands (Shipboard, 1995; Rodehorst et al., 1998; van den Bogaard, 1998). The imprint of volcanic activity seen on the landscape (Cantagrel et al., 1999) extends onto the surrounding seafloor, as investigated in great detail by the use of sonar techniques (Fig. 1.2) (Krastel et al., 2001; Watts and Masson, 2001).

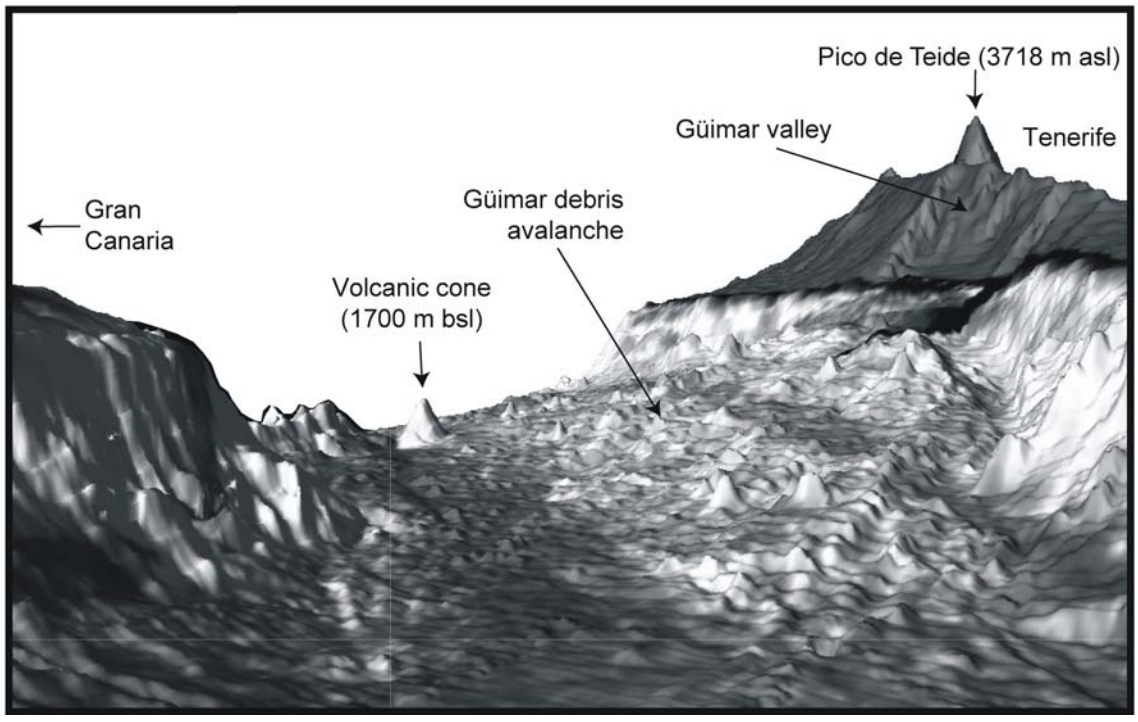

Figure 1.2 Example of seafloor topography in the Canary Islands region. Perspective view (direction WSW) of Güimar debris avalanche. Vertical exaggeration is 5. Shading is taken from GLORIA data. The lighter colour of the debris avalanche is due to stronger backscatter of the hummocky terrain (Krastel et al., 2001).

The bathymetry in the Canary Islands region is characterized by a broad shelf region of up to 150 m water depth, which extends between 25 and 100 km offshore (Summerhayes et al., 1976). The continental slope, that reaching depths of 3000 m, reflects various shapes, from steep with a complex morphology (eg. at Cape Ghir) to comparatively flat and continuous sloping (e.g. at Cape Yubi). An important structure off Cape Ghir is the Agadir Canyon, which consists of several channels cutting into the shelf and the slope (Uchupi et al., 1976; Ercilla et al., 1998; Wynn et al., 2000). Finally, a lot of different components, including organic-rich, carbonaceous, and volcanic materials (de Lange et al., 1987; Jarvis et al., 1998; Prahl et al., 2003) are transported by diverse event-like processes as turbidites, debris flows and debris avalanches and finally accumulate in the deep-sea plains (Masson et al., 1997; Weaver et al., 2000) (Fig. 1.3).

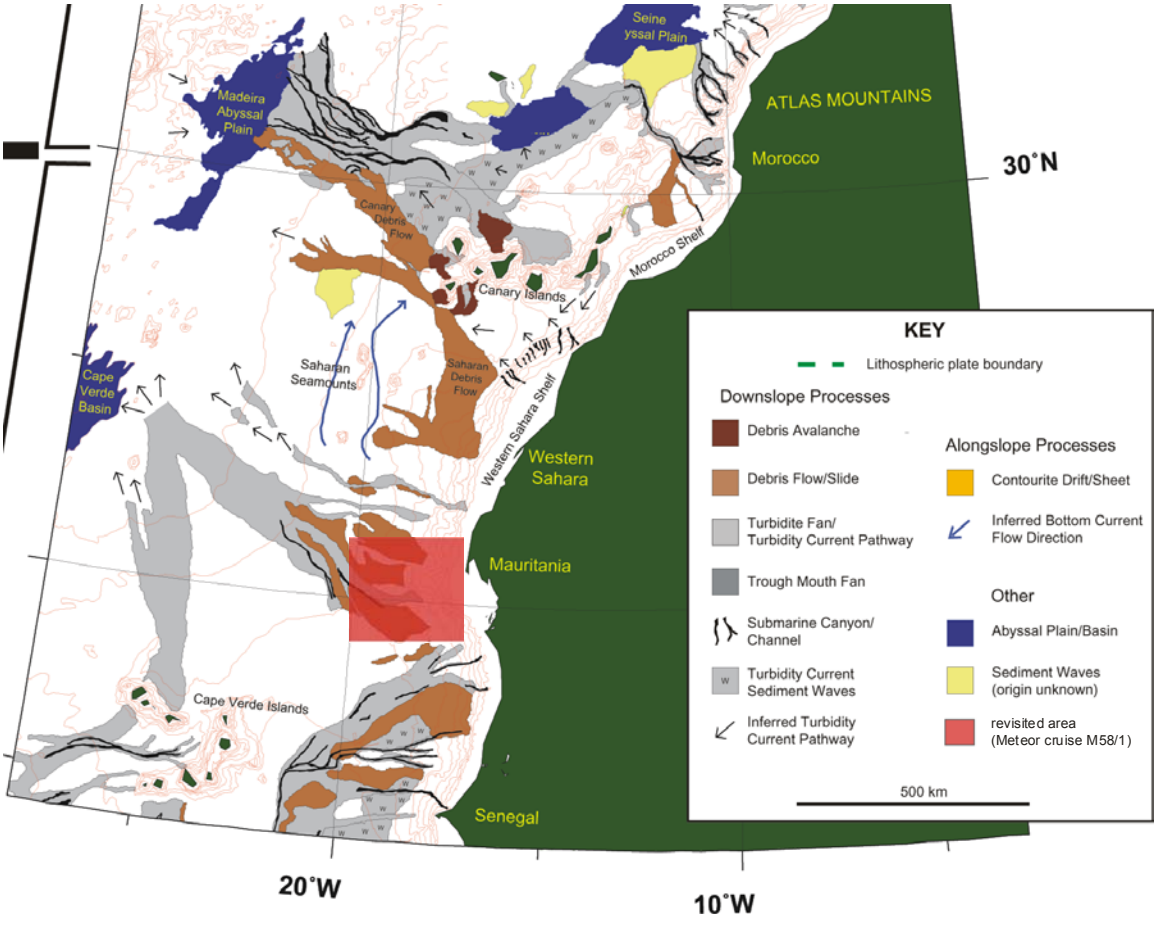

Figure 1.3 Sedimentation pattern along the NE Atlantic continental margin (modified from Weaver et al., 2000). The red square south of Cape Blanc marks a region that was revisited in 2003 during METEOR cruise M58/1. A canyon system named "Cape Timiris Canyon" was discovered and mapped using hydroacoustic systems (Cruise report, in prep.).

1.1.2 Atmospheric circulation

Two main wind systems characterize the NW African atmospheric circulation, the Saharan Air Layer (SAL) and the trade winds (Dubief, 1979; Tetzlaff and Wolter, 1980; Pye, 1987; Mayewski et al., 1997). The SAL is related to the African Easterly Jet, a mid-troposheric zonal wind system occurring at an altitude of 850 – 550 mb (1,500 – 5,500 m) (Prospero, 1990; Hastenrath, 1996). It is responsible for the long-range transport of dust originating mainly from Saharan and Sahelian sources (Prospero and Nees, 1986; Schütz et al., 1990; Middleton et al., 2001; Prospero et al., 2002; Colarco et al., 2003). A common feature of the SAL is the development of westward propagating waves. These easterly waves reach the African coast between 15 and 21° N (Fig. 1.4).

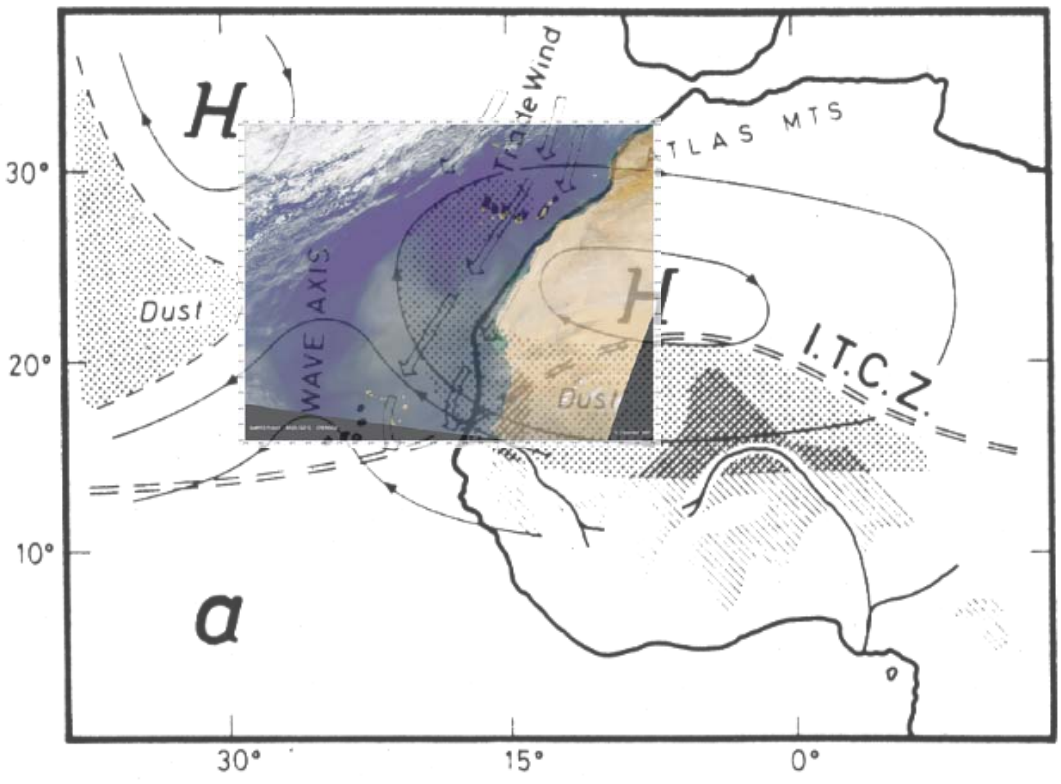

Figure 1.4 Schematic view (Sarnthein et al., 1981) of the lower mid tropospheric flow pattern and underlying trade winds associated with an easterly wave and a Saharan air dust outbreak along a hook-shaped branch turning towards the Canary Islands region. The average summer position of the Intertropical Convergence Zone (ITCZ) is indicated. Shaded areas illustrate some source areas of lateritic trace particles. The underlain satellite image reflects the situation described in the schematic view and was observed by the SeaWiFS sensor of the OrbView 2 satellite on Dec. 12th, 2000 provided by the SeaWiFS Project, NASA/Goddard Space Flight Center, and ORBIMAGE.

A hook-shaped branch directed to the northwest and later on to the north turning towards the Canary Islands region is frequently established in the lee of the waves (Fig. 1.4) (Tetzlaff and Wolter, 1980; Sarnthein et al., 1981).

The underlying wind system is dominated by the trade winds, blowing parallel to the coast in southwesterly direction. The seasonality of the trade winds decreases to the south, where at Cape Blanc (~ 21° N) they occur throughout the year (Schemainda et al., 1975; Nykjaer and Van Camp, 1994). The dust load of the trade winds originates from the northern Sahara and the Atlas mountains. It can be distinguished from the SAL-transported material using mineral (Schütz and Sebert, 1987; Bergametti et al., 1989; Chiapello et al., 1995; Torres-Padrón et al., 2002) and elemental ratios (Duce et al., 1991; Arimoto et al., 1995) as well as isotope data (Aléon et al., 2002). Recent studies emphasize the importance of dust and aerosols in the energy balance of the earth due to effects like absorption and scattering of the incoming solar radiation (Díaz et al., 2001; Goudie and Middleton, 2001; Perlwitz et al., 2001; Schollaert and Merrill, 2001; Kaufmann et al., 2002; Knutti et al., 2002; Mahowald and Kiehl, 2003; Sassen et al., 2003).

1.1.3 Oceanographic setting

The coastal upwelling of cold and nutrient-rich sub-surface waters is the most conspicuous response of the ocean to surface winds. By Ekman transport, trade winds force the upwelling of colder water at the continental shelf area (Schemainda et al., 1975; Hagen, 2001), which is well reflected in sea-surface temperature fields observed by remote sensing (Nykjaer and Van Camp, 1994; Barton et al., 1998). The upwelled water masses contain a higher nutrient concentration, which promotes enhanced marine productivity (Hughes, 1974; Sarnthein et al., 1982). Controlled by a combination of coastal morphology, wind stress and surface currents (Van Camp et al., 1991; Johnson and Stevens, 2000) large upwelling filaments develop, particularly at the cape locations (Hernández-Guerra et al., 1993; Helmke et.al., subm.). Upwelling water masses are transported in these filaments far offshore into the oligotrophic subtropical gyre region.

The general geostrophic transport of surface waters occurs within the Canary Current and is directed to the south (Klein and Siedler, 1989) (Fig. 4.1). The Canary Current is the easternmost branch of the North Atlantic subtropical gyre system, and receives its water mainly from the eastwardly directed Azores Current (Stramma, 1984; Mittelstaedt, 1991). Comparable to the wind system, the current system reflects strong

seasonal variations in direction and strength (Stramma and Siedler, 1988; Müller and Siedler, 1992; Knoll et al., 2002; Hernández-Guerra et al., 2003). A detailed description of small-scale oceanographic features in the Canary Islands region is given in chapter 4.2.1.

The water column is characterized by subtropical surface waters underlain down to 600 m depth by a mixture of North Atlantic Central Water (NACW) and South Atlantic Central Water (SACW), which is the source of the upwelled water masses. Below, derivates of the high-temperature and saline Mediterranean Outflow Water (MOW) propagate to the south up to a depth of 1500 m. North Atlantic Deep Water (NADW) occurs in the depth interval from 1500 to 4000 m, underlain only by the Antarctic Bottom Water (AABW) below 4000 m (Sarnthein et al., 1982).

1.1.4 Modern climate

The Saharan desert belt extends from about 17 to 28° N (Sarnthein et al., 1982) and is characterized by less than 100 mm annual precipitation (Weischert and Endlicher, 1999). To the south this region is separated from the monsoonal area by the Intertropical Convergence Zone (ITCZ). The ITCZ describes a band of low pressure characterized by the convergence of the Southeast and Northeast Trade Winds. The NW African monsoon, centered between 10 and 20° N, is characterized by intense summer precipitation and a long dry season in winter (Hsu and Wallace, 1976). North of the Saharan desert the precipitation shows a contrasting pattern, with a dry summer season and a winter rainfall maximum. This regime, extending down to 28° N in the coastal areas, is typical for the Mediterranean region and therefore called the "Mediterranean regime" (Hsu and Wallace, 1976; Andres, 1977).

The estimation of the extent of global change and the prediction of future environmental state or its stresses (desertification, greenhouse effect, etc.) largely depends on detection of the nature of the present and former environments. It remains very important to characterize the present climate conditions off NW Africa using parameters that offer the opportunity for a comparison with proxies of the climate history (Fischer and Wefer, 1999). One example from NW Africa is the palaeoecological atlas entitled: "The Holocene landscape and vegetation history of northern and western Africa" (Schulz et al., 2000), which is available from the homepage of the Department of Geography of the University of Würzburg (http://www.uni-wuerzburg.de/geographie/fachi/pal_atlas_afrika/index_atlas.htm). Vegetation maps (Fig. 6.1) indicate that under present conditions at about 28° N a

transitional floral composition is predominant between the northern more humid area and the Saharan desert to the south (Frankenberg, 1978; Dupont, 1993; Huang et al., 2000). These present pattern can be compared with paleo-pollen distributions analysed from climatic records like sediment cores and interpreted in terms of climate change.

1.1.5 Paleoclimate

The Holocene climate was comparatively stable as compared to the last glacial period. Nevertheless, significant variations are observed in climate reconstructions (Lamb et al., 1995). In the early-Holocene the NW African climate was already warm but significantly more humid than today. Therefore, this period has been called the "African humid period" (deMenocal et al., 2000a), and floral conditions reconstructed from modeling and palynological studies (Jolly et al., 1998), have resulted in its being called the "green Sahara" (Claussen et al., 1999). It has been inferred from investigations on lake levels (Yu and Harrison, 1996) and corroborated by recent modeling studies (Claussen et al., 2003) that the influence of the monsoonal system reached much further to the north than is the case today.

The climate at the last glacial maximum (LGM) has been characterized as colder and drier conditions than present, based on as results from a comparison of model results with pollen and lake-level data (Jolly et al., 1998). The suspected higher wind intensity during the LGM (Sarnthein et al., 1981; Hooghiemstra et al., 1987) should have caused more intense upwelling. These suggestions contrast local heterogeneities observed in productivity proxies (Bertrand et al., 1996; Martinez et al., 1999), reflecting highest productivity partly during the deglaciation or interglacial time intervals. Therefore, other processes have to be detected and localized to account for the observed local pattern.

A more detailed introduction to the wide field of investigations on the paleoclimate of N Africa is given in chapter 5.

1.2 Material

The diverse processes at the NW African Continental Margin have been the subject of an EU - MAST III Program (MAS3-CT96-0060) entitled: "Canary Islands Azores Gibraltar Observations" (CANIGO) (1996-1999). Within the subproject 3 "Particle Flux and Paleoceanography in the Eastern Boundary Current" two METEOR cruises (M 37/1 and M 42/4) were undertaken to retrieve sediment cores (gravity and piston cores) in the Canary Islands region with a high spatial resolution

(Wefer et al., 1997; Wefer et al., 1999). Timely results from initial investigations on these cores provided an overview of the investigation area and gave us the opportunity to retrieve very high-resolution cores on a further METEOR cruise (M45/5) in 2000 (Neuer et al., 2000). The aim for all these sites was to find sediment series that were undisturbed by turbidites, landslides, debris flows, volcanic gravel, and ash layers by using the onboard echo sounding systems. Summing up, a pool of 73 sediment cores with lengths from 1 to 12.5 m depth were retrieved within a comparatively small area comprising 6° of latitude and 8° of longitude, providing sediments covering the last 250,000 years for detailed analysis, particularly using core-logging methods.

2. MOTIVATION, OBJECTIVES, and RESEARCH

There is a popular trend in paleoceanography towards high-resolution analysis. Investigations on sediment archives with increasing temporal resolution have improved the detection and understanding of abrupt climate changes. To achieve climate proxy records from marine sediments at annual resolutions as provided by ice cores, or on seasonal scales comparable to sediment-trap data is the object of numerous recent investigations. Another common field of ongoing research is involved with the highly dynamic and heterogeneous regions of the oceans, including coastal upwelling areas, which require regional investigations with a high spatial resolution.

For obtaining both high temporal and high spatial resolution, methods are required that provide the ability to analyse the sediment cores within an acceptable amount of time. At the Department of Geosciences at the University of Bremen two core-logging systems, the Multi-Sensor Core Logger (MSCL) and the X-ray fluorescence (XRF) Core Scanner are available for multiple analyses. The application particularly of the XRF Core Scanner resulted in one task of this thesis, which was to investigate the accuracy of the system and to check the opportunity of calibrating the element intensity derived from the XRF Core Scanner into elemental concentrations.

2.1 XRF Core Scanner measurements

The XRF Core Scanner at the University of Bremen was developed and built at the Royal Netherlands Institute for Sea Research (NIOZ) and provides relatively quick and non-destructive measurements of element intensities on the surface of split sediment cores. Several experiments were carried out regarding the accuracy of the XRF Core Scanner (chapter 3). The XRF Scanner-derived element intensities were compared with standard (non-logging) geochemical methods, including ICP and XRF on discrete samples (chapter 5.5). As a result, the effects of physical properties such as porosity were shown to have little influence on the XRF scanner measurements. The precision of the XRF scanner measurements diminishes at low element concentrations, but the relative signal is reflected with a high accuracy.

2.2 Sediment accumulation

The Canary Islands region represents a key region with respect to biogeochemistry, reflecting both a zonal gradient from oligotrophic to nutrient-rich water masses and a high contribution of lithogenic material from adjacent African

continent. The main goal of this thesis is to determine the variable influence and interaction of coastal upwelling and terrigeneous supply on the marine sediments across an upwelling margin through the late-Quaternary. Previous single-core studies reported conflicting results regarding the incidence of most intense marine productivity on glacial-interglacial time scales (Sarnthein et al., 1988; Marret and Turon, 1994; Bertrand et al., 1996; Martinez et al., 2000; Zhao et al., 2000; Freudenthal et al., 2002; Moreno et al., 2002). The characterization and extent of areas reflecting varying behaviour of marine productivity within the Canary Islands region through time was determined to be the first step to an understanding of the NW African upwelling system.

The purpose of chapter 4 (manuscript 1) is to answer the frequently arising question in the literature about the regional and local aspects of marine productivity in the investigation area. An opportunity was developed to rapidly obtain age control for a huge pool of sediment cores using core-logging data. Local and regional processes in the Canary Islands region and their variation through time were inferred by the analysis of bulk sediment accumulation rates at a high spatial resolution. Contributions to the corresponding manuscript: "Reconstruction of paleoceanography off NW Africa for the last 40,000 years: influence of local and regional factors on sediment accumulation", by Kuhlmann, H., Freudenthal, T., Helmke, P., and Meggers, H. (submitted to Marine Geology) include density data for calculation of the accumulation rates and age models of the reference cores provided by Dr. T. Freudenthal and Dr. H. Meggers. SeaWiFS chlorophyll data were supplied by P. Helmke.

2.3 Supply of lithogenic material to the marine sediments

The complex interaction of lithogenic input with the marine productivity signal is subject to further investigation. The eolian input of African dust was studied in a variety of disciplines using aerosols (Chiapello et al., 2000; Formenti et al., 2003), material from ground-based dust samplers (Game, 1964; Chester and Johnson, 1971; Coude-Gaussen et al., 1987; Bergametti et al., 1989; Avila et al., 1997; Arimoto, 2001; Torres-Padrón et al., 2002), sediment traps (Kremling and Streu, 1993; Ratmeyer et al., 1999), and sediment records (Tetzlaff et al., 1989; Tiedemann et al., 1989; deMenocal et al., 2000a; Moreno et al., 2001; Bozzano et al., 2002). Only a few regional sediment studies with closer proximity to the coast also mentioned fluvial input of terrigeneous material (Koopmann, 1981; Sarnthein et al., 1981), which was regarded to be of minor importance off NW Africa. Therefore, another major aim of this thesis is to figure out

the interrelations of the different pathways of terrigeneous material with the marine production and sedimentation.

Manuscript 2 (chapter 5) focuses on the interaction of climatic systems in northern NW Africa and their impact on the terrigeneous contribution to the marine sediments. Although previous studies discussed eolian dust as the main contributor of lithogenic material, this study has determined that riverine input is also an important transport mechanism, particularly in coastal areas with a mountainous hinterland receiving significant precipitation. As a basis for this interpretation, high-resolution Fe distribution is presented as an indicator for terrigeneous input. To achieve the broadest basis for a calibration of the XRF Core Scanner data into elemental concentrations as much geochemical data as available were included. This is documented by the large number of co-authors of the corresponding manuscript: "Meridional shifts of the Mediterranean and monsoonal climate system off NW Africa during the last 130,000 years: implications from river discharge.", by Kuhlmann, H., Meggers, H., Moreno, A., Freudenthal, T., Kasten, S., Hensen, C., and von Oppen, C. (submitted to Quaternary Research). Dr. A. Moreno provided XRF data measured on discrete sediment samples. Dr. S. Kasten and Dr. C. Hensen supplied ICP-AES data and C. von Oppen provided AAS data. These data are used for the calibration of the XRF Scanner-derived cps into concentrations. Dr. T. Freudenthal and Dr. H. Meggers provided the age models of stratigraphic reference cores.

2.4 High-resolution Holocene implications

It is well established that the Holocene is not a period of constantly warm climatic conditions (Keigwin, 1996; Bond et al., 1997; deMenocal et al., 2000b; Thompson et al., 2002; Friddell et al., 2003). Several millennial-scale climate changes have been reported from various regions (Lamb et al., 1995; Alley et al., 1997; deMenocal et al., 2000a; Bond et al., 2001; Haug et al., 2001). The aim of the study presented in chapter 5 is to compare the high-resolution data of the terrigeneous signal recorded off Cape Ghir with other climate systems to relate possible mechanisms and climatic interactions.

Based on the knowledge of the initial studies of this thesis, it was possible to select the site with the highest sediment accumulation rate of all GeoB sediment cores in the region. The investigation of the potassium record with spectral and wavelet analysis reflects strong similarities to the oxygen-isotope data of the GISP 2 ice core. The connecting link is suggested to be part of the NAO mechanism influencing the modern

Northern Hemisphere climate. The manuscript: "Holocene climatic changes in NW Africa - Timing and regional extent", by Kuhlmann, H., Meggers, H., Freudenthal, T., and Wefer, G. (submitted to Geophysical Research Letters) is supported by oxygen-isotope data and radiocarbon analysis that are the basis for the age model of core GeoB 6007 contributed by Dr. Helge Meggers and Dr. Tim Freudenthal.

2.5 Further articles

The research is supplemented by some additional articles that are not included in this thesis but form part of the research carried out during my PhD work. Contributions to the upwelling and productivity pattern in the Canary Islands region are provided by the articles of Dr. A. Moreno and Dr. T. Freudenthal.

Moreno, A., Nave, S., Kuhlmann, H., Canals, M., Targarona, J., Freudenthal, F., Abrantes, F. (2002): Productivity response in the North Canary Basin to climate changes during the last 250,000 years: a multi-proxy approach. Earth and Planetary Science Letters, 196/3-4, 147-159.

My contribution to the article of Dr. A. Moreno was initiated during a two-month scholarship from the DAAD (Deutscher Akademischer Austauschdienst) in 2001 at the University of Barcelona. The contributions contain core-logging data and suggestions for their interpretation.

Freudenthal, T., Meggers, H., Hendericks, J., Kuhlmann, H., Moreno, A., and Wefer, G. (2002): Upwelling intensity and filament activity off Morocco during the last 250,000 years. Deep-Sea Research II, 49/17, 3655-3674.

Magnetic susceptibility data providing information on the age control were contributed to the paper of Dr. T. Freudenthal.

Two further articles focus on investigations of the atmospheric circulation in terms of its relation to the record of eolian dust (G. Bozzano) and present pattern of the upwelling filament at Cape Ghir (P. Helmke).

Bozzano, G., Kuhlmann, H., Alonso, B. (2002): Storminess control over African dust input to the Moroccan Atlantic Margin, (NW Africa) at the time of maxima boreal summer insolation: A record of the last 220 kyr. Paleogeography, Paleoclimatology, Paleoecology, 183/1-2, 155-168.

My contribution to the article of G. Bozzano was also initiated during the two-month scholarship from the DAAD at the University of Barcelona. The contributions contain core-logging data of core GeoB 4205 and suggestions for their interpretation.

Helmke, P., Davenport, R., and Kuhlmann, H.: Wind stress-related filament structures off Cape Ghir, NW Africa. (subm. to Deep-Sea Research)

The article of P. Helmke was supported by paleo data (Holocene accumulation rates) regarding the interpretation of modern upwelling pattern.

3. EVALUATION OF XRF CORE SCANNER MEASUREMENTS

Kuhlmann, H., Westerhold, T., Röhl, U.

3.1 Introduction

Various types of automated core-logging systems have been developed in the last decade in response to the increasing requirements of high-resolution analysis in paleoceanography and paleoclimatology. These instruments operate either on whole-round or split sediment cores, or both. They provide information on variations in sediment composition and properties related to climate and environmental changes (Ortiz and Rack, 1999). In this chapter, which is presented as a preface to the further application of data we provide background information on two core-logging systems, the Multi-Sensor Core Logger (MSCL) and the X-ray fluorescence (XRF) Core Scanner. We also discuss the accuracy and limitations of the XRF Core Scanner.

By comparing high-resolution data of physical properties obtained by the MSCL with XRF scanner-derived element intensities, we detected several parameters, which are affecting the XRF measurements. The effects of physical sediment properties such as porosity and water content are evaluated by measuring the same sample material both, under wet and dry conditions. A detailed comparison of XRF Core Scanner data with standard geochemical analysis as calibration issues is discussed in chapter 5.5 (manuscript 2).

3.2 Methods

3.2.1 Multi-Sensor-Core-Logger and GEOSCAN II camera

The GEOTEK™ **M**ulti-**S**ensor-**C**ore-**L**ogger (MSCL) is capable of producing rapid and non-destructive magnetic susceptibility, gamma-ray density and porosity, p-wave velocity, and electrical resistivity measurements on either split or unsplit sediment cores (Weaver and Schultheiss, 1990; Gunn and Best, 1998). Additionally, the system is equipped with the GEOTEK™ GEOSCAN II calibrated core imaging system, which provides images and colour measurements (Fig. 3.1). The camera incorporates 3 linescan **C**harge **c**oupled **d**evices (CCD´s) with 1024 pixels each behind an interference filter to create RGB (red green blue) images. The maximum image resolution is 1200 dpi on a 2 cm-wide strip of core. All MSCL data presented in this study were obtained on split sediment cores. The magnetic susceptibility measurements were carried out

using the BARTINGTON™ point sensor MS2F. The calibration of the gamma-ray density was carried out using an aluminium standard following Weber et al. (1997).

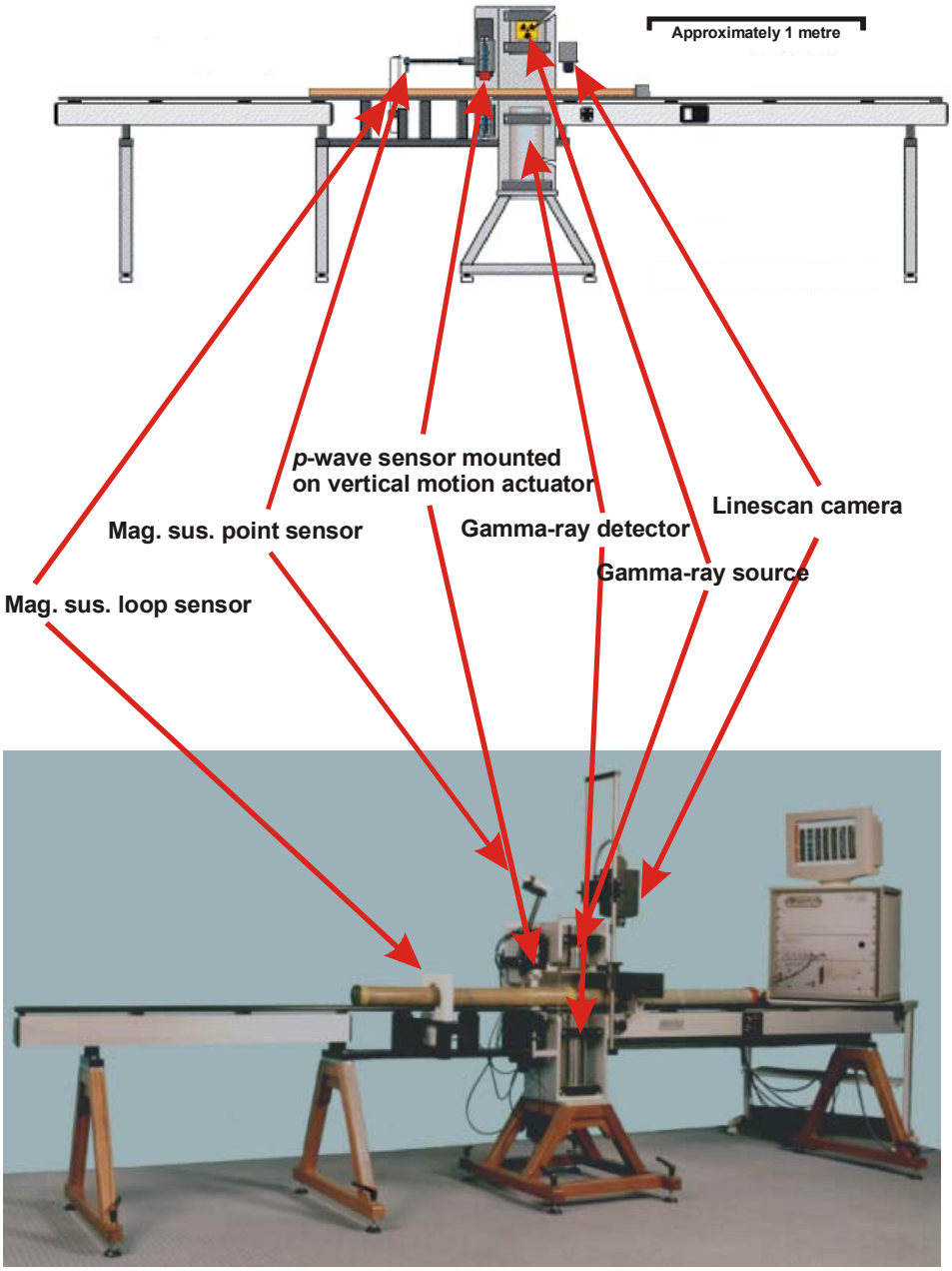

Figure 3.1 Multi-Sensor Core Logger (MSCL)

3.2.2 X-ray fluorescence Core Scanner

Incident X-rays increase the energy level in an atom and as result an electron from the inner shell is emitted. This vacancy is filled by an electron from an outer shell (higher energy level), which moves into the position of the emitted electron. The

surplus energy detected in the fluorescent radiation, reflecting the energy difference between the shells, is element specific (Potts, 1987).

The XRF Core Scanner was developed at the Royal Netherlands Institute for Sea Research (NIOZ) (Fig. 3.2) and makes use of the XRF technique directly at the surface of split sediment cores (Jansen et al., 1998). This non-destructive scanning tool performs relatively rapid semi-quantitative analyses of major elemental composition. XRF data used in these studies were collected at the very top of the surface of sediment cores over a 1 cm^2 area, typically using a 30-second count time, 20 kV X-ray voltage, and an X-ray current of 0.087 mA to obtain statistically significant data for the

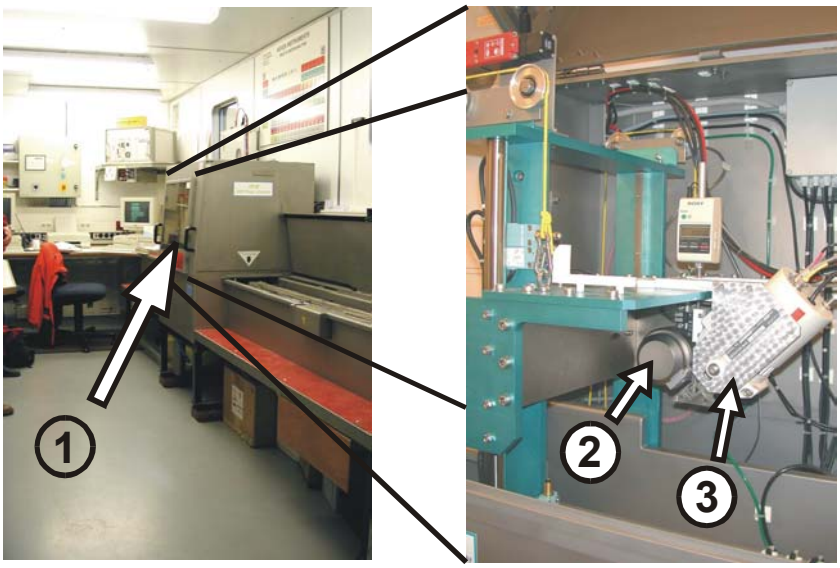

Figure 3.2 X-Ray Fluorescence (XRF) Core Scanner. 1: central sensor unit; 2: X-ray source; 3. detector.

elements K, Ca, Fe, Ti, Mn, and Sr. The resulting data are element intensities in counts per second (cps). The response depths of different elements vary from a few μm for lighter elements to several 100 μm for heavier elements, due to the differing wavelengths of the emitted fluorescence radiation. Element concentrations (e.g., in percent or parts per million) are not provided directly by the XRF measurements and the used processing software. But element intensities (in cps) can be converted from XRF scans by calibration with data derived from standard analytical methods on selected samples as initially shown by Jansen et al. (1998). This approach has been applied and extended in this thesis, chapter 5.5 (manuscript 2). XRF Core Scanner data has led to improved opportunities in the analysis of sediments and to new prospects in

paleoceanography and climatology over the last few years (Röhl and Abrams, 2000). The high-resolution data sets have been successfully used for stratigraphic and paleoceanographic applications, e.g., in the Maastrichtian (MacLeod et al., 2001), the Paleogene (Norris and Röhl, 1999; Röhl et al., 2000, 2001; Pälike et al., 2001), and the Neogene (Vidal et al., 2002; Jahn et al., 2003). Further applications have provided high-resolution insights regarding millennial-scale changes in ocean currents systems and the hydrologic cycle during the last Glacial (e.g., Arz et al., 1998; Peterson et al., 2000), and the Holocene, (Arz et al., 2001; Haug et al., 2001; Lamy et al., 2001; Arz et al., 2003). The combined application of both scanner systems (XRF and MSCL) also provided a very successful tool in detecting unconformities in the sediment records, such as turbidites and volcanic ash layers (Fig. 3.3).

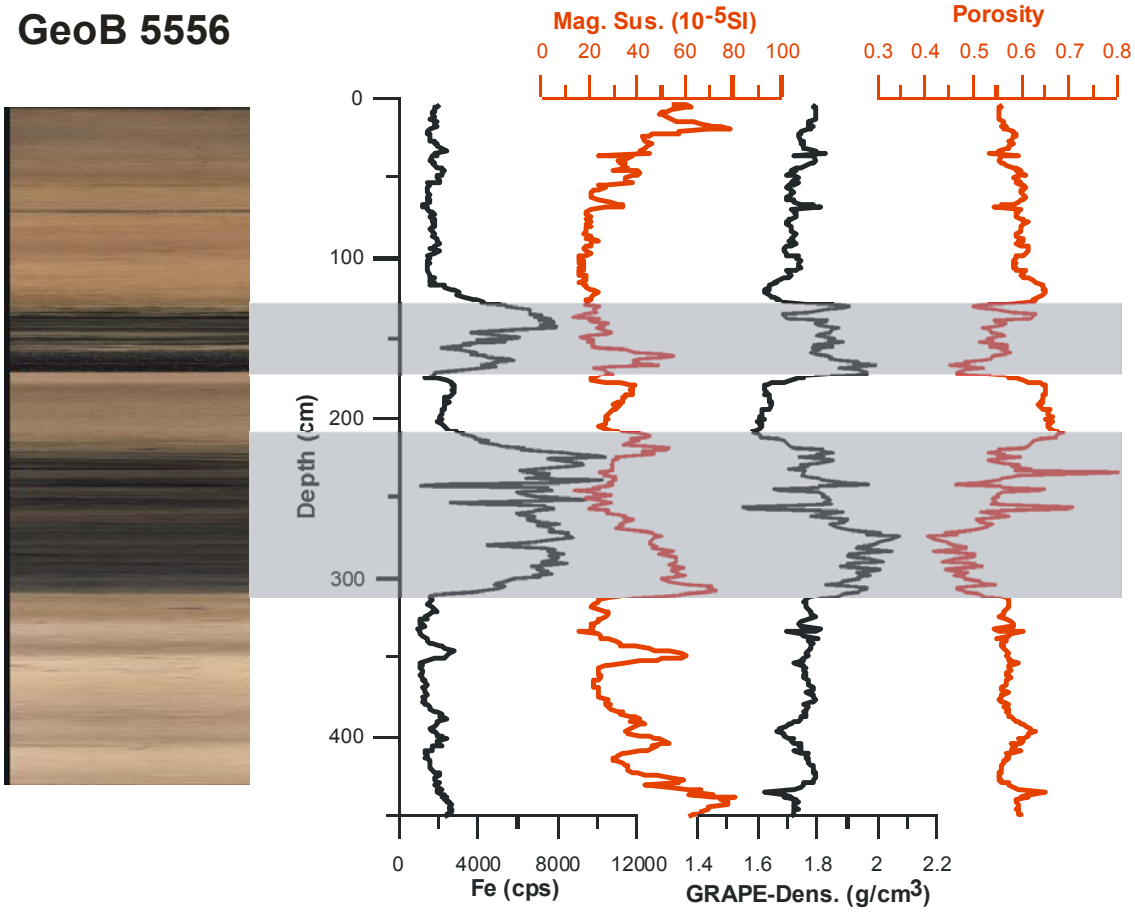

Figure 3.3 Determination of unconformities in core GeoB 5556 located west of Lanzarote. The photo image, magnetic susceptibility (Mag. Sus.), density, and porosity are obtained with the MSCL, the Fe intensities result from the XRF Scanner. The volcanic ash layers are already visible in the photo image. But for the exact determination of their extent in the core record the other parameters like Fe content or porosity are needed. This is particularly valid for the detection of turbidites, which are often not detectable by the visual inspection.

3.3 Effects of physical sediment properties on XRF Core Scanner data accuracy

A characteristic feature of ODP cores drilled with an extended core barrel is the occurrence of core biscuits surrounded by softer drilling mud. The ODP core section, 175-1085A-34X-4 mainly consists of drilling biscuits ranging in thickness between 2 and 4 cm (Wefer et al., 1998). Colour measurements obtained with the GEOSCAN II calibrated colour core imaging system clearly reflect the alternation of biscuits and drilling mud. The abrupt changes from core biscuits to drilling mud are also pronounced in the porosity record due to the reduced pore space in the material rinsed by drilling fluids whereas higher porosity is observed in the biscuits. The XRF Core Scanner measurements of Fe and Ca (Westerhold, 2003) show a correlation with the porosity and colour measurements on a very fine scale (Fig. 3.4). The element intensities are lower in the drill biscuit intervals than between them. It seems that the relatively higher porosity in the drill biscuits influences the element intensity as it is reduced by stronger scattering in the pore space.

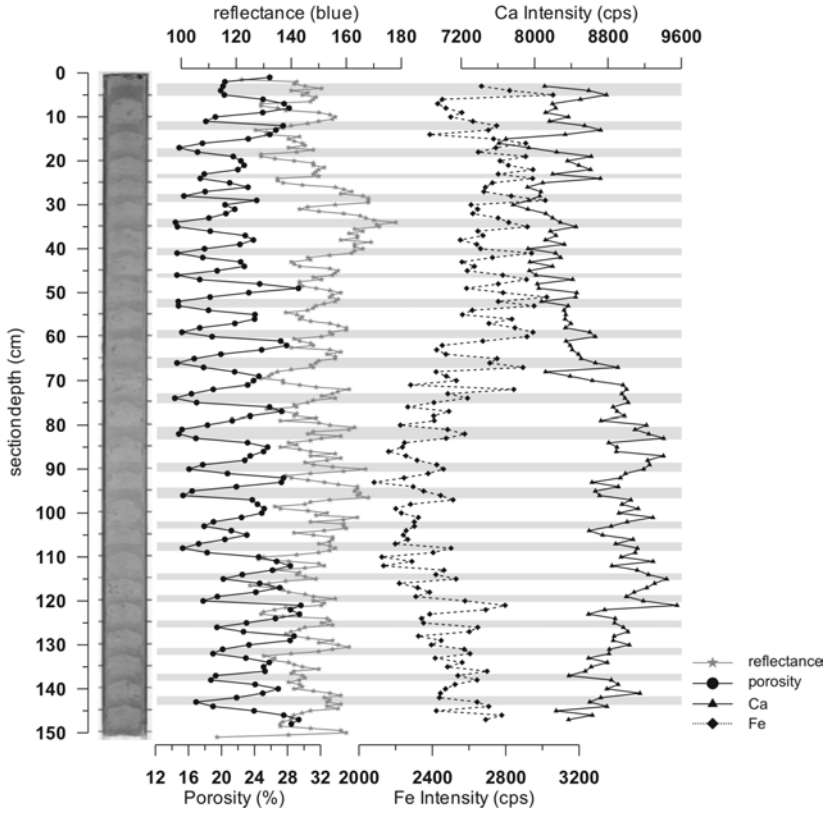

Figure 3.4 Porosity (%) (solid line with circles), photo image, reflectance (grey line), and Fe- (dotted line) and Ca intensities (solid line with triangles) for ODP Leg 175, Site 1085-53X-4. The grey bands are the so-called drilling mud intervals, the lighter sections are the drill biscuits.

In addition to these small-scale variations, the overlying signal with a general typical anticorrelation is visible in the Fe and Ca intensities (Fig. 3.4).

3.4 Influence of different pore space filling

To determine the effects of physical sediment properties on the XRF scanner data accuracy, discrete samples from different sediment types (e.g., foraminifera turbidite, nannofossil ooze) with varying $CaCO_3$, terrigeneous, and siliceous contents were filled into Nunc cup cabs. These were mounted on a sample tablet for carrying out "wet" (as derived from the sediment core) and "dry" (after drying for 24h in an oven at 40°C) measurements. The samples were weighed before and after dehumidification to determine the water content and porosity. The dried samples were then scanned with the XRF core scanner. The porosity was determined according to Ruddiman (1989).

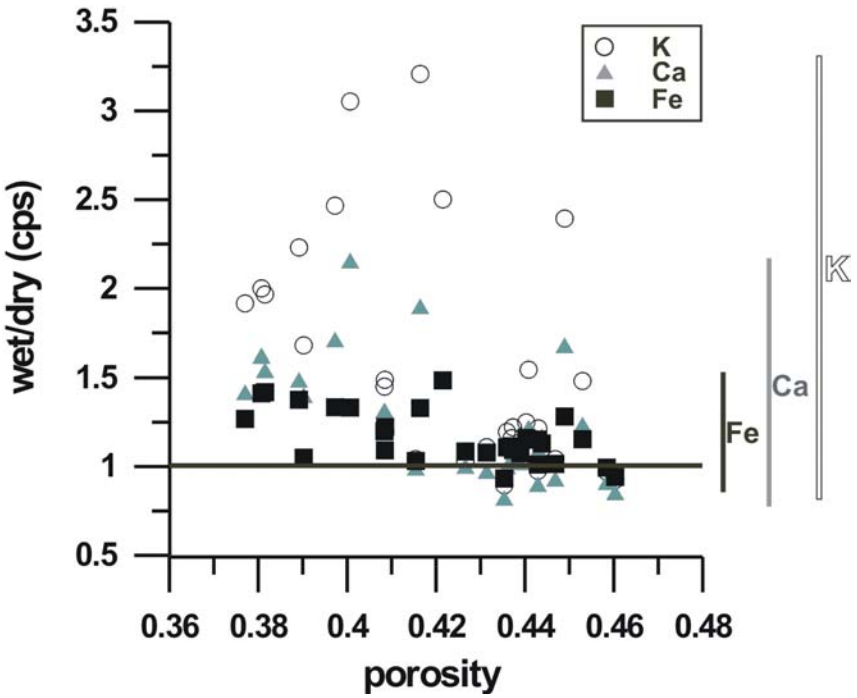

Figure 3.5 Wet/dry condition measurement ratios calculated for K (open circles), Fe (black squares), and Ca (grey triangles) versus the porosity of the sample. The vertical bars at the right show the variation of the wet/dry ratio for K, Fe and Ca.

The measurements under wet conditions delivered element intensities that were generally higher than those under dry conditions due to the increased porosity and

enhanced attenuation of the radiation in air. The drying of the samples results in reduced porosity of the dried material and is detectable by visual inspection after the drying procedure. Additionally, the surface tension of the water forces the particles to stick closer together, in the pore space as well as at the plastic foil covering the core, which is very important due to the thin surface layer that is measured. The smallest differences between wet and dry measurements were detected for Fe intensities, followed by Ca, and then K intensities. Due to its higher atomic weight iron behaves more robustly regarding changes on the porosity than do Ca and K. There is no obvious trend of the differences between wet and dry measurements for Fe, Ca and K in relation to the porosity of the samples (Fig. 3.5).

3.5 Conclusion

The XRF Core Scanner is capable of providing high-resolution, rapid, and non-destructive element intensity measurements, with the major advantages being rapid and non-destructive analysis. It is important to take into account that the XRF Core Scanner measurements are taken on the surface of split sediment cores, on a material that is not homogenized or otherwise prepared for optimal measurement conditions. Therefore the quality of the sediment surface as physical sediment property has an important influence on the XRF data and accuracy. It has been shown that most of the small scale variability in the XRF data of core section 53X-4 is related to porosity changes produced by the drilling technique. The overall, lower frequency signal, however, was recorded properly. Additionally the pore space filling has little imprint on the XRF Core Scanner measurements as shown by the comparison of measurements of sediment samples under "wet" and "dry" conditions. All of these possible imprints have to be considered, especially if there are strong changes in the physical properties of an analysed record. Additionally, the alteration of sediment cores during their storage (loss of humidity) should be considered when the same core is measured again after a couple of years. It is essential to respect that the absolute counts for a given element at a certain time also depends on the hardware configuration of the instrument at that time.

The comparison of data from standard geochemical methods with data from XRF Core Scanner measurements are shown in chapter 5.5 (manuscript 2). These reveal that the general elemental signal is represented very well, at high accuracy, and at a very high resolution. All these are enormous advantages compared to relatively expensive and time-consuming standard analytical methods.

Acknowledgements

The authors thank the crews on board RV METEOR and JOIDES RESOLUTION. This research used samples and data provided by the Ocean Drilling Program (ODP). The ODP is sponsored by the U.S. National Science Foundation (NSF) and participating countries under management of Joint Oceanographic Institutions (JOI) Inc.. All data will be made available in the WDC PANGAEA: www.pangaea/home/kuhlmann. This research was funded by the "Deutsche Forschungsgemeinschaft" (DFG Grant no. WE 922/31-1).

4. Reconstruction of paleoceanography off NW Africa during the last 40,000 years: influence of local and regional factors on sediment accumulation

H. Kuhlmann*, T. Freudenthal, P. Helmke and H. Meggers

University of Bremen, Department of Geosciences, PO Box 330440, 28334 Bremen, Germany

submitted for publication in **Marine Geology**

4.1 Abstract

A set of 43 sediment cores from around the Canary Islands is used to characterize this region, which intersects meridional climatic regimes and zonal productivity gradients with a high spatial resolution. Using rapid and non-destructive core logging techniques we carried out Fe intensity and magnetic susceptibility (MS) measurements and created a stack on the basis of five stratigraphic reference cores, for which a stratigraphic age model was available from $\delta^{18}O$ and ^{14}C analyses on planktic foraminifera. By correlation of the stack with the Fe and MS records of the other cores we were able to develop age depth models at all investigated sites of the region. We present the bulk sediment accumulation rates (AR) of the Canary Islands region as an indicator of shifts in the upwelling-influenced areas for the Holocene (0-12 kyr), the deglaciation (12-18 kyr), and the last glacial (18-40 kyr). As a general observation it can be said that productivity was enhanced during glacial times with highest values during the deglaciation. The main differences between the analysed time intervals we interpret to be the result of the sea-level effects, changes in the geographical extent of high productivity areas, and variations in current intensity.

Keywords: Canary Islands; Sediment accumulation rates; Coastal upwelling; Sea-level; Holocene; Last glacial

* Corresponding author. phone: ++49-421-2182886; fax: ++49-421-2183116; E-mail: kuhlma@uni-bremen.de.

4.2 Introduction

High flux rates between the various atmospheric, oceanic and sedimentary element pools focus research on the climate-relevant carbon cycle in high productivity areas like coastal upwelling regions. The high nutrient content of the upwelled water masses results in enhanced primary productivity in these areas and, depending on the favoured organisms exploiting the high nutrient conditions, accounts for the role as source or sink for carbon. Changes in the upwelling intensity and primary productivity are presumed to have major impact on the variability of the oceanic and atmospheric CO_2 concentrations at glacial/interglacial time scales (Berger and Keir, 1984). In glacial time intervals the atmospheric circulation was enhanced, which is interpreted to have caused generally higher productivity in subtropical eastern boundary-current regions. Higher productivity in combination with increased dust input is presumed to have caused higher sediment accumulation rates (AR) in glacial continental margin sediments off NW Africa (Sarnthein et al., 1988). Recent research indicates that the assumption of enhanced glacial sediment accumulation off NW Africa has to be modified. Various studies point to strong differences in the upwelling-related productivity pattern, with highest productivity partly during glacial times, partly during deglaciation times, and partly during wet intervals like the early Holocene, although the driving force of the upwelling, the seasonal trade winds, are supposed to be of regional significance (Bertrand et al., 1996; Marret and Turon, 1994; Martinez et al., 2000; Zhao et al., 2000). A variety of factors influencing productivity and the sediment accumulation records were identified. Changes of climatic conditions, atmospheric circulation, and sea-level changes act as regional factors influencing environmental conditions, whereas displacement of upwelling cells, sediment transport and seafloor morphology result in local differences. In single-core studies it is not possible to distinguish between these influencing factors, and only regional studies can provide the opportunity to separate these factors and the resulting features in the sediment accumulation.

The modern patterns of upwelling and related primary productivity in the Canary Islands region are manifold, including zonal gradients from the near-coast upwelling areas to oligotrophic conditions further off the coast, as well as coastal morphology-induced filament formation. The upwelling pattern, as recognized from satellite-derived chlorophyll-a concentrations, is known to be an indicator of primary productivity. This pattern, characterizing sea-surface conditions, is mirrored in the underlying sediments by the AR. Regional studies with a high spatial resolution are necessary to distinguish the various local and regional factors in order to get a better

impression of changes in the NW African climate and related upwelling systems (Bertrand et al., 1996). Correlations of the records of 43 sediment cores in the Canary Islands region were made to resolve a detailed picture of even mesoscale processes that affect the sedimentation. We address the question of the sensitivity of sediment accumulation pattern to various oceanographic features such as coastal upwelling, filament structures off the cape locations and more oligotrophic conditions in the Canary Islands region. Our data set will also provide insights into the changes of the upwelling processes and the sedimentary environment over time, i.e. through the last glacial, the deglaciation, and the Holocene. We focus on the causes for shifts and changes in the intensity of upwelling processes mirrored by AR during the last 40 kyr.

4.2.1 Oceanographic setting

The investigation area, located at the NW African continental margin between 27°N and 32°N is shown in Fig. 4.1 with the surface-current direction and chlorophyll-a concentration. The sea-floor morphology is characterized by a shallow (< 150 m) continental shelf that extends offshore to about 25 km at Cape Ghir and up to 75 km north of Cape Yubi (Summerhayes et al., 1976). An important structure on the narrow continental slope at Cape Ghir is the Agadir Canyon system, which consists of several channels draining into the Agadir Basin. By contrast the continental slope at Cape Yubi is comparatively regular and plain (Uchupi et al., 1976; Weaver et al., 2000).

The water column in the region is characterised by subtropical water at the surface, underlain by southward-directed North Atlantic Central Water, with increments of South Atlantic Central Water increasing to the south down to a depth of 600 m, which is the main source of the upwelling water masses. Below this the Mediterranean Outflow Water, with southward-increasing imprints of South Atlantic Intermediate Water, occurs in water depths down to 1700 m, and this is underlain by southward-directed North Atlantic Deep Water (Knoll et al., 2002; Llinás et al., 2002; Sarnthein et al., 1982). The surface water is influenced by the southward-directed Canary Current, which is fed by the eastern branch of the subtropical North Atlantic gyre (Knoll et al., 2002; Mittelstaedt, 1991). During the last glacial the Canary Current is presumedd to have intensified due to the generally enhanced atmospheric and oceanic circulation (Sarnthein et al., 1982). Sea level was lower by 120 m during the last glacial maximum compared to modern values (Fairbanks, 1989) and rose during the deglaciation up to the present level in several steps (Bard et al., 1989; Bard et al., 1996). These changes caused the exposure of large areas of the continental shelf during the

glacial and therefore altered coastal morphology. These changes are believed to have a strong influence on the sediment accumulation, particularly at sites located near the coastline (Bertrand et al., 2000; Martinez et al., 1999).

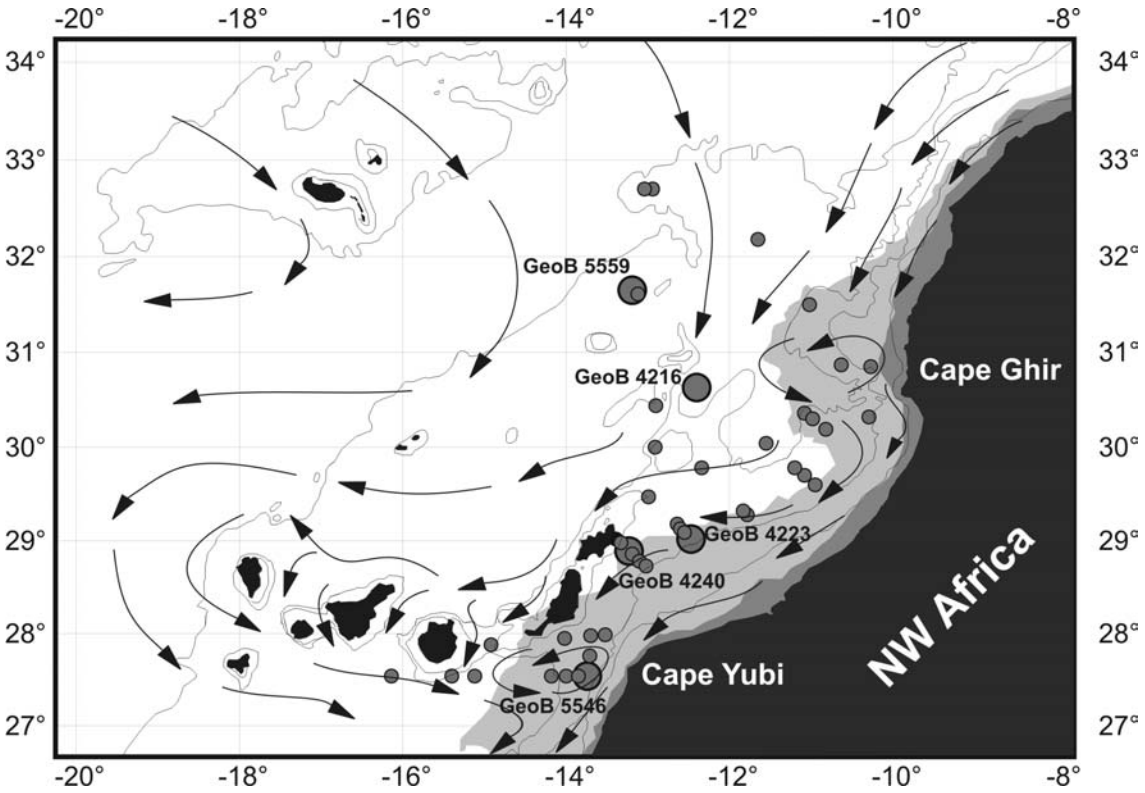

Figure 4.1 Bathymetric map of the investigation area with 100, 1000, 2000 and 4000 m depth contour lines. SeaWiFS derived chlorophyll-a concentrations averaged from 1997 – 2000; areas with > 1 mg m^{-3} are shaded dark grey, 0.25 – 1 mg m^{-3} light grey, < 0.25 mg m^{-3} not shaded. The surface currents are indicated by arrows (after Mittelstaedt, 1991). The filled circles indicate core locations, the larger circles show stratigraphic reference cores GeoB 5559, GeoB 4216, GeoB 4223, GeoB 4240 and GeoB 5546.

Trade-wind-induced coastal upwelling occurs mostly in a narrow 5-km band on the shelf (Mittelstaedt, 1991), while oligotrophic conditions prevail further offshore. In the northern part of the working area, at Cape Ghir (~ 30°N) a strong seasonal upwelling dominates in the summer, whereas at Cape Yubi (~ 27°N) the trend of upwelling conditions throughout the whole year is observed as is also the case further to the south at Cape Blanc (Nykjaer and Van Camp, 1994). Upwelling features deduced from satellite-derived chlorophyll-a concentrations are closely connected to high primary productivity (Antoine et al., 1996; Behrenfeld and Falkowski, 1997; Davenport et al., 1999). The water masses from the upwelling areas are transported far offshore in

filaments (Davenport et al., 2002; Hagen, 2001; Van Camp et al., 1991), which are generated by interaction of the current system and the coastal morphology (cape locations) (Johnson and Stevens, 2000).

S to SW of the Canary Islands a small-scale formation of cyclonic and anticyclonic eddies is reported, which results from the lee-side hydrographic and atmospheric conditions (Arístegui et al., 1994; Barton et al., 1998). The associated up- and downwelling at these sites impacts the ecosystem development in these areas (Arístegui et al., 1997; Basterretxea et al., 2002).

In the northern part of the region, modern oceanography is influenced by river input from the Souss River draining the Atlas Mountains. There has been no significant recent fluvial input south of 30°N, with activity limited to sporadic active wadi systems. During the climate optimum in the early Holocene, the adjacent African continent received more humidity from the monsoon system (Gasse, 2000; Gasse et al., 1990). This may have resulted in a drainage via wadi systems into the ocean. During the glacial time period, dry conditions comparable to the present situation prevailed in NW Africa.

4.3 Material and Methods

4.3.1 Material

This study benefits from a pool of 73 sediment cores recovered during METEOR cruises M37/1 (Wefer et al., 1997), M42/4 (Wefer et al., 1999) and M45/5 (Neuer et al., 2000), all located in the Canary Islands region off NW Africa. From this set 43 cores were selected, for which a confident stratigraphic interpretation was possible. We excluded all cores where turbidites, volcanic gravel and ash layers extended over long intervals of the cores. Additionally, cores where the extent of these layers were uncertain had to be omitted because of the resulting uncertainties in the age control. The cores used in this study are from 800 - 4,000 m waterdepth (Tab. 4.1), representing different areas of enhanced productivity near the coast of Morocco, especially at the cape locations and more oligotrophic conditions further offshore (Fig.4.1).

Core logging methods provide the opportunity to work on a large number of cores with a sufficient resolution in an acceptable length of time. We used two rapid and non-destructive core logging facilities at the University of Bremen: the Multi-Sensor Core Logger (MSCL) and the X-Ray Fluorescence (XRF) Core Scanner.

4.3.2 Multi-Sensor Core Logger (MSCL)

Physical properties (GRAPE-density, p-wave velocity and magnetic susceptibility) were measured non-destructively on the archive halves of the cores using a GEOTEK™ (Surrey, UK) MSCL (Gunn and Best, 1998; Weaver and Schultheiss, 1990) at the Department of Geosciences at the University of Bremen. Here we present the magnetic susceptibility (MS) measurements, carried out using a BARTINGTON™

Table 4.1 Cruise and core number, geographic position, water depth, gear type and recovery of the investigated sediment cores from the Canary Islands Region. (GC = gravity corer, PC = piston corer)

Cruise Meteor	Station GeoB	Latitude (°N)	Longitude (°W)	Geartype	Waterdepth (m)	Recovery (cm)
M37/1	4205-2	32°10.9	11°38.9	GC	3272	501
M37/1	4206-1	31°30.0	11°01.3	GC	1855	571
M37/1	4209-2	30°21.4	11°05.0	GC	2150	970
M37/1	4210-1	30°18.0	10°58.8	GC	1959	424
M37/1	4211-2	30°11.6	10°49.3	GC	1773	650
M37/1	4212-2	29°36.2	10°57.0	GC	1256	857
M37/1	4213-2	29°41.8	11°04.7	GC	1547	754
M37/1	4214-1	29°46.9	11°11.8	GC	1788	952
M37/1	4215-2	30°02.2	11°33.2	GC	2106	766
M37/1	4216-2	30°37.9	12°23.8	GC	2325	1117
M37/1	4217-5	30°26.1	12°53.7	GC	2504	716
M37/1	4218-1	29°57.3	12°54.7	GC	2723	619
M37/1	4221-1	29°46.5	12°20.3	GC	1826	843
M37/1	4223-2	29°01.1	12°28.0	GC	777	779
M37/1	4225-1	29°16.5	11°46.9	GC	1281	725
M37/1	4226-3	29°19.2	11°50.0	GC	1400	907
M37/1	4228-3	29°28.2	12°59.4	PC	1633	1188
M37/1	4229-1	29°10.9	12°38.3	GC	1422	663
M37/1	4230-2	29°07.7	12°35.8	GC	1316	993
M37/1	4231-1	29°05.2	12°33.1	GC	1197	726
M37/1	4232-2	29°01.3	13°23.2	GC	1161	991
M37/1	4233-1	28°58.5	13°19.8	GC	1303	1076
M37/1	4235-2	28°51.4	13°11.4	GC	1247	777
M37/1	4236-1	28°47.0	13°05.7	GC	1030	1084
M37/1	4237-2	28°43.7	13°01.0	GC	800	966
M37/1	4240-2	28°53.3	13°13.5	GC	1358	688
M42/4	5536-2	27°32.2	16°08.1	GC	3456	880
M42/4	5537-3	27°32.1	15°24.1	GC	2362	784
M42/4	5538-1	27°32.2	15°07.0	GC	2537	1080
M42/4	5540-2	27°32.1	14°10.5	GC	2035	920
M42/4	5541-4	27°32.2	13°59.7	PC	1748	1252
M42/4	5545-1	27°32.2'	13°50.8	PC	1431	1156
M42/4	5546-2	27°32.2	13°44.2	PC	1071	851
M42/4	5547-3	27°45.6	13°42.6	GC	1310	1066
M42/4	5548-2	27°59.5	13°31.1	GC	1162	755
M42/4	5549-3	27°58.7	13°41.7	GC	1454	890
M42/4	5550-2	27°57.1	14°00.9	GC	1738	1056
M42/4	5551-3	27°52.6	14°54.9	GC	1885	1027
M42/4	5559-2	31°38.7	13°11.2	GC	3178	585
M42/4	5560-1	31°36.6	13°07.1	GC	3944	469
M42/4	5561-2	32°42.2	12°56.1	GC	3500	434
M45/5	6006-1	30°52.1	10°37.8	GC	1275	908
M45/5	6011-1	30°18.9	10°17.3	GC	993	477

point-sensor. The measurements were made in 1-cm steps over an area of 1 cm^2. The resulting data are the volume specific magnetic susceptibilities in 10^{-5} SI units.

4.3.3 X-Ray Fluorescence (XRF) Core Scanner analysis

The XRF Core Scanner at the University of Bremen is a non-destructive analysis system for scanning the surface of archive halves of sediment cores. It was developed and built at the Royal Netherlands Institute for Sea Research (NIOZ), Texel, Netherlands (Jansen et al., 1998). The central sensor unit consists of a molybdenum X-ray source (3-50kV), a Peltier-cooled PSI detector (KEVEX™) with 125 µm beryllium window, and a multichannel analyser with a 20 eV spectral resolution. The system configuration (X-ray tube energy, detector sensibility) at the University of Bremen allows the analyses of elements from K (atomic no. 19) to Sr (atomic no. 38) (X-ray tube voltage: 20 kV). We analysed element intensities at 1-cm intervals, each measurement over an area of 1 cm^2. In this study we present the elements Fe and Ti, using 30-s count time and an X-ray current of 0.087 mA. The acquired XRF spectrum for each measurement was processed by the KEVEX™ software Toolbox©. The resulting data are element intensities in counts per second (cps). Detection limits of the device as well as accuracy experiments were carried out by Jansen et al., 1998.

4.3.4 Density measurements and accumulation rates

Density calculations were carried out following Weber et al., (1997). We measured wet weight (WW) and dry weight (DW) of discrete samples of 10 cm^3 volume at 5-cm spacing for all cores used in this study. The salt weight (SW) was calculated assuming 35 ‰ pore water salinity.

$$SW\ (g) = WW\ (g) - DW\ (g) \times 0.035) \times (1 - 0.035)^{-1}. \quad (1)$$

The dry bulk density (DBD) was calculated following the equation:

$$DBD\ (g \times cm^{-3}) = (DW\ (g) - SW\ (g) \times volume^{-1}\ (cm^3), \quad (2)$$

DBD was used to calculate average AR in combination with sedimentation rates (SR) that were inferred from stratigraphic investigations following the equation:

$$AR\ (g \times cm^{-2} \times kyr^{-1}) = SR\ (cm \times kyr^{-1}) \times DBD\ (g \times cm^{-3}). \quad (3)$$

4.4 Stratigraphy

The well established but time and cost intensive oxygen isotope stratigraphy technique is not appropriate for the investigation of a large number of sediment cores as were used in this study. Therefore we used Fe intensities and MS records, obtained by rapid and non-destructive core logging tools to transfer the age models of five reference cores with reasonable age control to the remainder of the cores. These reference cores cover the various environmental and sedimentary conditions representing offshore and nearshore locations as well as northern and southern locations in the Canary Islands region. Their age-depth relationships (Fig. 4.2) were established by correlating the $\delta^{18}O$ records of planktic foraminifera with the SPECMAP stack (Imbrie et al., 1984) and the higher-resolution records of Martinson et al. (1987) and Raymo (1997) in combination with ^{14}C measurements. The age models of the cores GeoB 4216, GeoB 4223, and GeoB 4240 were adopted from Freudenthal et al. (2002), the age model of core GeoB 5559 from Moreno et al. (2001). These age models were slightly modified within oxygen isotope stage (OIS) 3 based on six additional ^{14}C-AMS dates (Freudenthal, et al. subm.). The age model of core GeoB 5546 will be published elsewhere (Meggers et al., in prep.).

MS and Fe intensity of the five reference cores are shown versus age in Fig. 4.2. Generally we observe a rough coincidence of the two parameters, with higher values during interglacial periods as compared to glacial conditions. The change from the penultimate glacial to the following interglacial period is characterised by a strong increase from minimum glacial values to higher values during OIS 5.5. The high values at OIS 5.3 (represented by a characteristic double peak) and 5.1 are interrupted by significantly lower values during the interstadials 5.2 and 5.4. The following glacial time interval is characterised by relatively low values of both parameters with minimum values in OIS 3 at about 40 kyr and during OIS 2 at 18 and 12 kyr.

Comparing the Fe intensity and MS records of the different stratigraphic reference cores, we see that the pattern is time equivalent at all sites as demonstrated in the Fe and MS stacks (Fig. 4.2).

4.4.1 Canary Stacks (CAFE, CAMS)

The iron intensity (CAFE Stack) and MS (CAMS Stack) records of the stratigraphic reference cores GeoB 4216, GeoB 4223, GeoB 4240, GeoB 5546 and GeoB 5559 were used to create a stack following Imbrie et al. (1984) and von Dobeneck and Schmieder (1999)(Fig. 4.2). After the removal of a few turbidite,

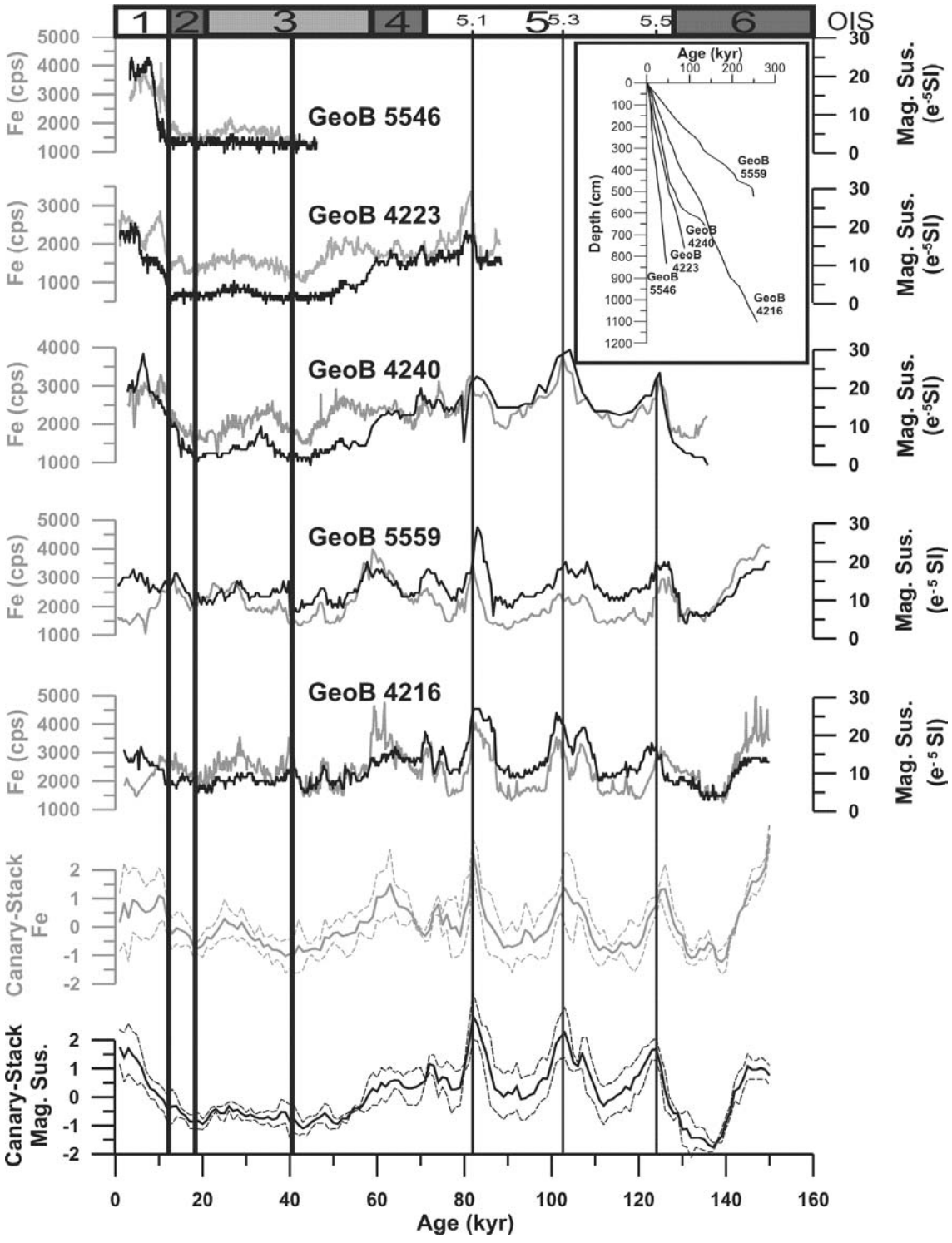

Figure 4.2 Canary **Fe** (CAFE) (grey) and **Ca**nary **m**agnetic **s**usceptibility (CAMS) (black) records (arithmetic mean with standard deviation band) resulting from the records of the stratigraphic reference cores. Vertical lines indicate the tie points at 12, 18, 40 kyr (bold lines) and 80, 100, 122 kyr. Oxygen isotope stages are indicated at the top and in the upper right edge the age versus depth plots of the five reference cores are shown.

volcanic gravel and ash layers (all < 10 cm that were identified by visual core description), MS and density records of the stacked curves show the characteristic pattern observed in the reference cores. To compensate for different amplitudes, each record was subtracted by its mean, divided by the standard deviation and resampled in 1 kyr intervals (Imbrie et al., 1984). The resulting stack records exhibit the similarities to the five reference cores, in particular, relative minima during glacial and deglacial times at 12, 18, and 40 kyr and well-pronounced maxima during the last interglacial at 80, 100 and 122 kyr.

Diagenetic processes may have a significant influence on the Fe and MS data. The MS record is partly altered during glacial times at sites influenced by upwelling and enhanced primary productivity. This effect is documented in Fig. 4.2 for the cores GeoB 5546 and GeoB 4223. This is interpreted to be caused by dissolution of fine grained magnetite as a result of carbon oxidation (Bloemendal et al., 1992; Haag, 2000). Therefore, where available we chose the Fe-intensity record for the age transfer, especially at the near-coast sites. The iron intensity records are quite robust against diagenesis, because the X-ray fluorescence analysis detects Fe atoms irrespective of their oxidation state. To ensure that the diagenetic transport of iron does not affect the records significantly we compared the Fe records with those for Ti, which is known to be much less subject to diagenetic alteration than iron. We found that the Ti records show a pattern that is nearly identical to the Fe records, and the Fe/Ti ratio is quite constant throughout the cores, giving no obvious indication for a diagenetic displacement of iron (Kuhlmann et al., subm.). Summing up the influence of diagenetic effects, we decided to use the CAFE stack preferentially for stratigraphic correlation. In cases where Fe data were not available we used the CAMS stack.

We successfully transferred the age model of the stacks to the other cores in the region by correlation. Even detailed characteristics like the double peak at about 100 kyr could be detected in most records. For the comparison of AR at different time intervals we have chosen three tie points that were easily detected in most of the cores. These selected tie points are 12, 18 and 40 kyr, enabling us to define three time intervals representing full glacial conditions (18 – 40 kyr), the deglaciation (12 – 18 kyr) and the Holocene starting at 12 kyr. Now we are able to calculate the average SR for the time intervals. We used the AR, where SR and DBD are included to avoid the influences of density changes through the cores, for the comparison of different time intervals. To obtain the average Holocene AR, we assumed that the core top is the sediment surface and has an age of 0 kyr. It should be mentioned that the core tops

generally do not reflect the sediment surface, because of the sampling procedure using gravity corer. This effect is more pronounced in cores with lower sedimentation rates but from the reference cores it is obvious that the maximum loss is 3 kyr (Fig. 4.2). Therefore, the Holocene accumulation rates may be slightly overestimated, but do not significantly change the results.

4.5 Holocene sediment accumulation rates

The most prominent feature of the Holocene time interval is the wide range of AR from the lowest values (1.65 g cm^{-2} kyr^{-1}) at offshore sites to the highest values (17.17 g cm^{-2} kyr^{-1}) at nearshore sites. Among the near coastal sites we observe the highest AR at Cape Yubi. This is less pronounced at Cape Ghir except for an exceptional result at site GeoB 6007, which is excluded from Figures 4.3-4.5. This site is located in a small sedimentation trough, where sediment focusing results in a SR of about 80 cm kyr^{-1}. The lowest nearshore values are observed between these two cape locations (Fig. 4.3). The zonal productivity gradient, as a major feature in the region, is slightly modified on the transect off Cape Yubi (27°32´N). Here we observe a higher sediment accumulation rate at the site GeoB 5536 than at the two adjacent sites GeoB 5537 and GeoB 5538, which are located nearer to the coast (SE of Gran Canaria).

The scenario depicted by the Holocene AR reflects the pattern observed in satellite derived chlorophyll-a concentrations in surface waters of the area (Fig. 4.3), which is known to be an indicator of primary productivity (Antoine et al., 1996; Behrenfeld and Falkowski, 1997; Hoepffner et al., 1999). The relationship of AR and productivity is expressed by a linear regression between AR and chlorophyll-a concentrations at the core locations with a coefficient of determination of $r^2 = 0.41$. The calculated *F* of the statistical correspondence test exceeds the critical *F* (Swan and Sandilands, 1995). This tendency is additionally supported by analyses of productivity proxies in surface sediments of the Canary Islands region, which show a highly comparable distribution with the AR reported in this study (Meggers et al., 2002).

The particle export from surface waters includes eolian dust, which is known to be an important particle source in this area (Ratmeyer et al., 1999; Sarnthein et al., 1981; Schütz et al., 1981). The results of sediment-trap studies indicate that the particle flux of lithogenic material is strongly related to biological processes by scavenging and incorporation into faecal pellets (Neuer et al., 1997; Wefer and Fischer, 1993). This could explain the close relationship between primary production and AR even if a similar atmospheric dust input into high and low productivity regions is assumed.

Sediment trap studies indicate that lateral particle transport exists in the Canary Islands region (Freudenthal et al., 2001). However, the good correlation of chlorophyll-a concentration in surface water with the AR indicates that lateral particle transport as reported from trap studies in this area may shift and smooth the filament pattern known from the sea surface, but does not disturb the general signal (Freudenthal et al., 2002). We therefore conclude that particle export to the sediment in the Canary Islands region is strongly influenced by processes that are closely connected to the primary productivity.

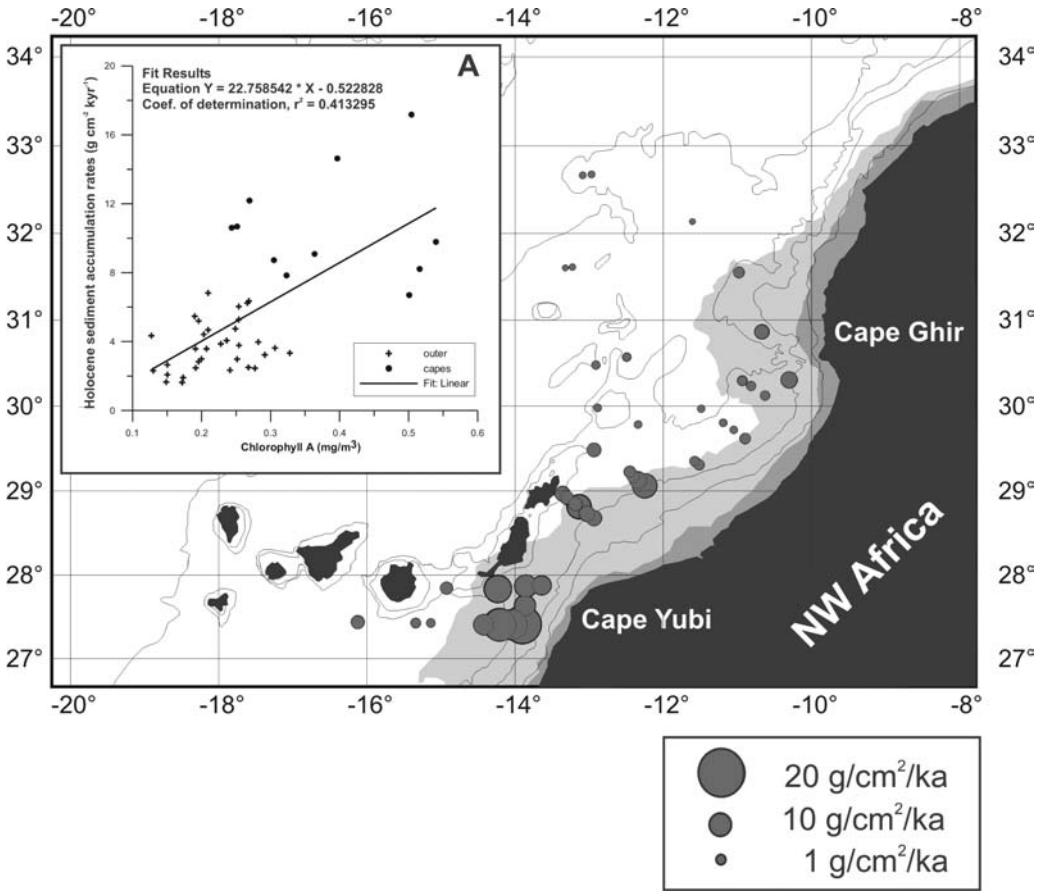

Figure 4.3 Holocene (0-12 kyr) bulk sediment accumulation rates (g cm^{-2} kyr^{-1}) for each investigation site. Chlorophyll-a concentrations are indicated as in Fig. 4.1. **A**: Linear regression of Holocene bulk sediment accumulation rates and chlorophyll-a (same source as Fig. 4.1) resulting in a coefficient of determination $r^2 = 0.41$.

We interpret the higher AR at Cape Yubi compared to Cape Ghir to be the result of sediment transport influenced by differences in sea-floor morphology. The Agadir Canyon is known to be an important pathway of sediment to the Agadir Basin and the Madeira Abyssal Plain (de Lange et al., 1987; Ercilla et al., 1998; Weaver et al.,

1992). The narrow shelf area and relatively steep continental slope at Cape Ghir as compared to Cape Yubi may also sustain the transport of material to the deep sea plains further off the coast. Another reason for the differences between the two cape locations may be the seasonality of the upwelling at Cape Ghir as detected by the Ekman upwelling index, whereas at Cape Yubi the duration of the upwelling season lasts three times as long as at Cape Ghir (Nykjaer and Van Camp, 1994). This would result in enhanced primary productivity values averaged over a year, but it is not reflected in the average chlorophyll-a concentration shown in Fig. 4.3b.

In contrast to the zonal pattern of decreasing AR further off the coast, the outermost core of the Cape Yubi transect (GeoB 5536) shows higher values. This site is influenced by a mesoscale stationary cyclonic and anticyclonic eddy system, which is caused by the location of the Canary Islands in the atmospheric and oceanic current systems. Lee-side effects on the SW side of Gran Canaria cause a stationary cyclonic and anticyclonic eddy system, which induces up- and downwelling with the associated impacts on productivity (Arístegui et al., 1994; Arístegui et al., 1997; Barton et al., 1998; Basterretxea et al., 2002). These sea-surface conditions might also have influenced also the surface sediment (Meggers et al., 2002). We may speculate that the observed Holocene AR pattern is a result of these island-generated eddies on the lee side of the Canary Islands, which caused upwelling, enhanced primary productivity and, therefore, higher AR at site GeoB 5536. At any rate, this high-spatial-resolution study indicates that the Holocene AR pattern is compatible with present oceanographic characteristics of the Canary Islands region. With this actualistic assessment we will now focus on the differences of AR between Holocene, deglaciation and the last glacial.

4.6 Variability of sediment accumulation through time

The general scenario in the Canary Islands region during all the investigated time intervals is characterized by low AR offshore and high AR nearshore, with pronounced high accumulation at the cape locations (Fig. 4.3, 4.4a, 4.4b). Another common effect seen in all the time intervals is the higher AR at Cape Yubi when compared to Cape Ghir. In contrast to these findings, strong differences in the intensity, size and position of high-accumulation areas are shown in Figures 4a-c. The time interval of the deglaciation (12 – 18 kyr) generally shows the highest AR (max. 22.6 g cm^{-2} kyr^{-1}), except for a small area north of Cape Yubi, where the AR during the glacial time interval is higher (Fig. 4.5a, c). The high-accumulation area at Cape Ghir is expanded to the southwest during deglaciation (Fig. 4.5a). In contrast, the high-

accumulation area of Cape Yubi is extended in a northerly direction (Fig. 4.5a). The pattern of enhanced accumulation SW of Cape Ghir is less pronounced, but also present in the time interval representing full glacial conditions (18 – 40 kyr) (Fig. 4.5b).

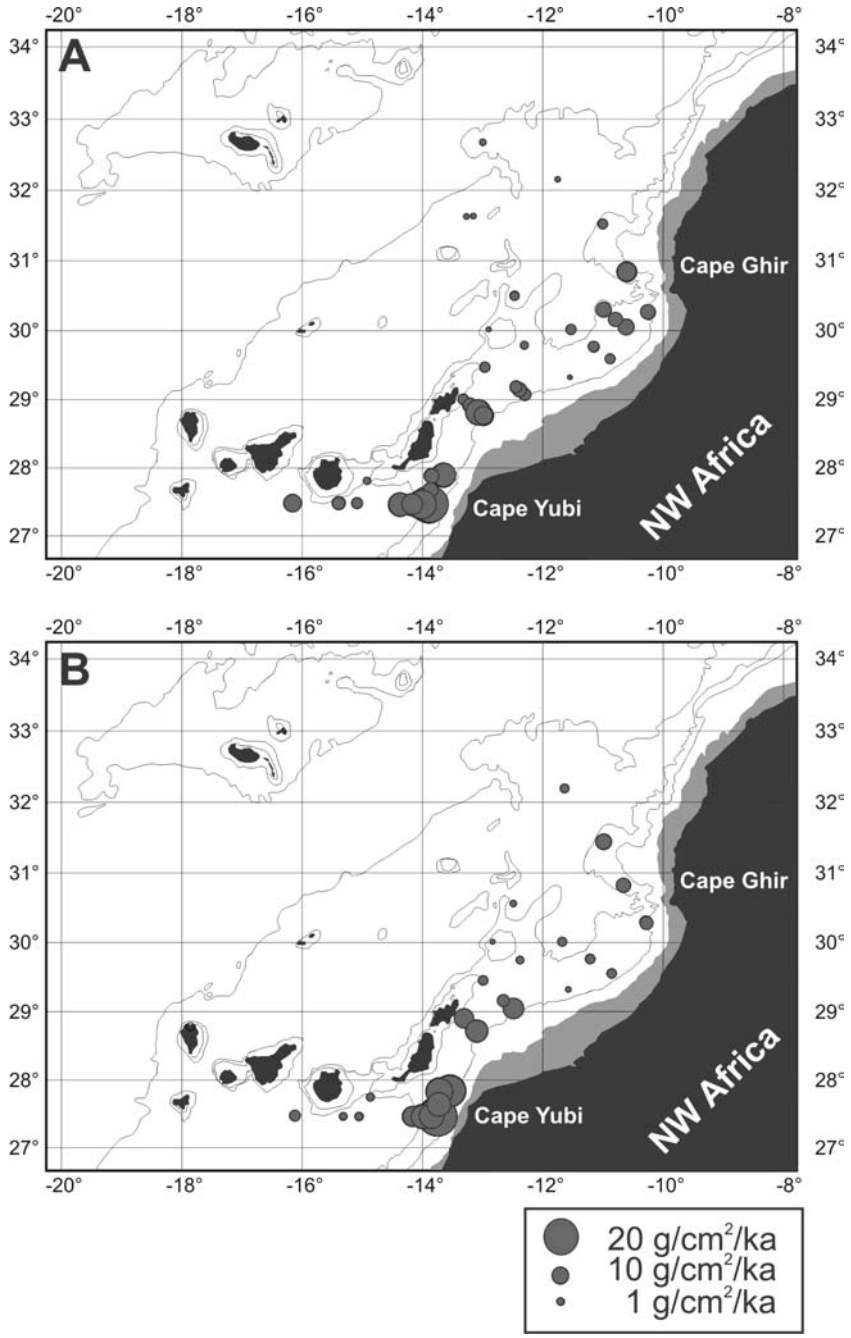

Figure 4.4 Bulk sediment accumulation rates (g cm^{-2} kyr^{-1}) for the time intervals of (**a**) deglaciation (12 – 18 kyr) and (**b**) the last glacial (18 – 40 kyr). The depth interval 0 – 100 m is shaded grey to indicate the coastline during sea-level lowstand.

The most prominent differences in the AR during the glacial period compared to the other time intervals are observed in the area between Fuerteventura and the coast of Morocco. This area of high sediment accumulation adjacent to Cape Yubi shows its widest extent and reaches up to 50 km further to the north during the glacial period (Fig. 4.5b, c).

The general trend of enhanced accumulation during the last glacial and deglaciation may result from higher productivity of the Atlantic Ocean during glacials, which is frequently described and discussed in the literature (e.g., Mix, 1989). For the region off NW Africa Sarnthein et al. (1988) report the same trend of enhanced primary productivity. The enhanced atmospheric circulation with stronger trade winds during glacial times may have intensified coastal upwelling and therefore caused higher productivity in the upwelling-influenced parts of the working area. This would explain the generally higher AR in the Canary Islands region during deglaciation and the glacial as compared to the Holocene.

The current system is an important factor influencing the filament formation (Johnson and Stevens, 2000) independent of the upwelling intensity. The intensity of the Canary Current is assumed to have been stronger during the glacial and deglaciation intervals (Sarnthein et al., 1982; Zahn et al., 1997). This corresponds with findings of an intensified filament activity detected by total organic carbon (TOC) measurements at specific sites off NW Africa (Freudenthal et al., 2002; Moreno et al., 2002). We conclude that the enhanced accumulation in the filament-influenced area off Cape Ghir result from the even more intensified filament formation during the deglaciation. The differences in AR indicate that the direction of the Cape Ghir filament during the Holocene (westerly) was different during glacial (south-westerly) and even more pronounced during deglaciation, as is illustrated in Fig. 4.5a, b. In recent descriptions of filament structures off Cape Ghir, Helmke et al. (subm.) report a comparable pattern. In general they describe filaments directed to the west, but also a south-westerly filament direction prevails at times of very strong wind intensities. Therefore, we conclude that the enhanced atmospheric circulation during deglaciation and the last glacial caused a south-westerly shift of the high-accumulation area of Cape Ghir. The pattern of increased AR described for the three easternmost cores on the transect south of Gran Canaria is pronounced, and may be an effect of the enhanced surface circulation (Sarnthein et al., 1982) and stronger throughflow through the Canary Islands.

The larger extension of the high-accumulation area north of Cape Yubi we interpret to result from sea-level changes. In the working area ,the continental shelf lies, for the most part under less than 150 m of water and was therefore widely exposed during sea-level lowstands at the last glacial (Bard et al., 1989; Bard et al., 1996; Fairbanks, 1989). The morphological cape characteristics, which cause the upwelling and especially the formation of filaments were situated about 50 km to the N during sea-level lowstand.

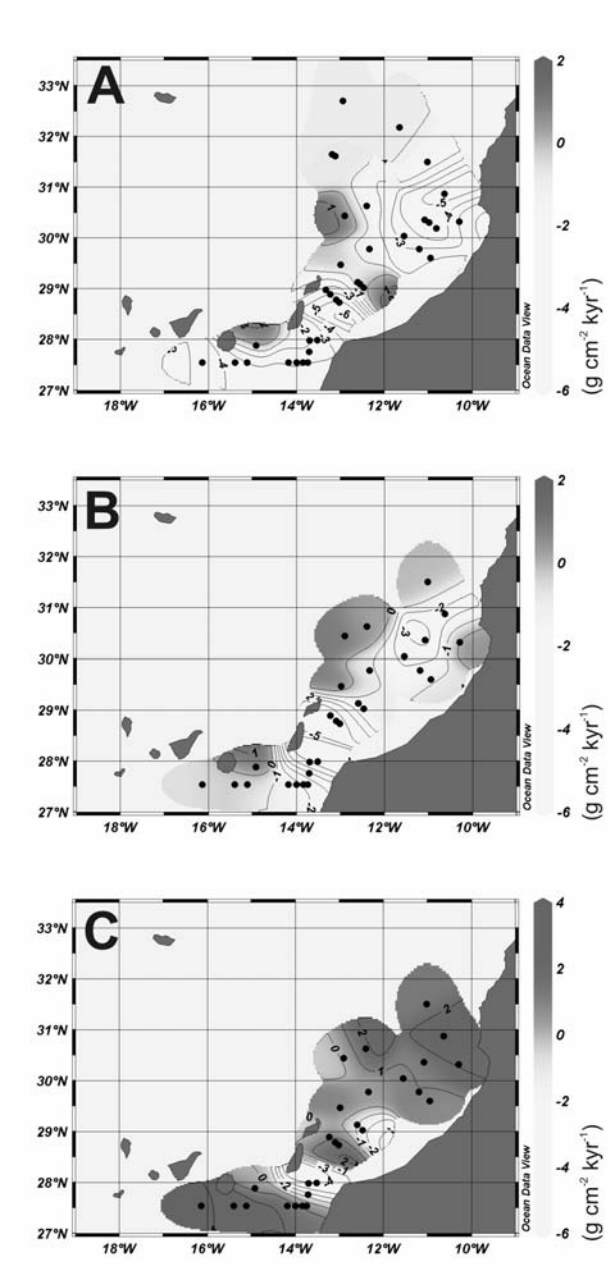

Figure 4.5 Differences (g cm^{-2} kyr^{-1}) in bulk sediment accumulation rates of the time intervals between (**a**) Holocene and deglaciation, (**b**) Holocene and glacial and (**c**) deglaciation and glacial (negative values indicate higher AR in the Holocene (a, b) and the deglaciation (c)). The interpolated contour line maps were generated with Ocean Data View (Schlitzer, 2002).

We conclude that as a consequence, the upwelling area extended further to the N at times of sea-level lowstand. The size of this upwelling area decreased with rising sea-level. The time interval of the deglaciation represents an intermediate state on the way to Holocene conditions.

The possible influence of temporal variations in river discharge on the AR is not clearly reflected. During the glacial and deglaciation based on paleohydrological data, the adjacent African continent has been characterized as dominated by dry conditions. At the boundary to the Holocene a generally wet climate was established. This persisted until the mid-Holocene transition at about 5 kyr, after which dry conditions again prevailed (Gasse, 2000; Gasse et al., 1990). An interval of more humid conditions within the Holocene, including enhanced river discharge to the ocean is not reflected in the AR, possibly because these are averaged over the entire Holocene.

It has been suggested that eolian dust input was enhanced during glacial and deglacial times due to greater wind stress (Bozzano et al., 2002; Moreno et al., 2001; Tiedemann et al., 1989). The transport mechanism to the sediments is assumed to be closely connected to scavenging effects as discussed in the previous chapter. Assuming the same close relationship between primary production and AR as for the Holocene, we think that enhanced eolian dust input may have strengthened the AR pattern, but not significantly modified its distribution.

The regional features as claimed by Bertrand et al. (1996) in the Canary Islands region resulting from the AR of the last 40 kyr exhibit higher values during the glacial and deglaciation as compared to the Holocene. But we observed additional local features such as enhanced differences in the AR between different time intervals in areas influenced by upwelling filaments, and effects of varying coastal morphology due to sea-level changes, which modify the general pattern locally.

4.7 Conclusion

The comparison of Holocene AR and satellite-derived chlorophyll-a concentrations representing present-day primary productivity revealed strong similarities. The features of coastal upwelling and filament formation pattern are well mirrored in the underlying sediment by the AR. Even small-scale features such as an eddy system at the lee-side of Gran Canaria have left their imprint on the sediment accumulation pattern.

We conclude that the higher sediment accumulation rates at Cape Yubi, as compared to the northern area at Cape Ghir, primarily reflect the topographic conditions, which favour sediment transport to the open ocean at the northern site. Additionally, the duration of intense upwelling in the seasonal cycle is much shorter at Cape Ghir, which is interpreted to be the reason for lower particle production.

In comparing the Holocene with the deglaciation time interval the most prominent enhancement of sediment accumulation is observed at the outer filament-influenced area of Cape Ghir. These findings are interpreted to indicate a stronger filament activity due to enhanced oceanic circulation during the glacial and especially the deglaciation.

The differences in AR between the glacial time interval and the Holocene are greatest to the north of Cape Yubi, where the continental shelf is very wide. We conclude that lower sea-level is responsible for the northward enlargement of the upwelling-influenced area of Cape Yubi, where the highest AR occur during the glacial time interval.

The results of this study show that the heterogeneity of even a small scale region like the Canary Islands region indicates the need for studies with high spatial resolution to detect and understand the processes responsible for the observed regional pattern in contrast to local features and their related processes.

Acknowledgements

We thank the captains and crews of R.V. Meteor for their help at sea on cruises M37/1, M42/4 and M45/1. Astrid Eberwein, Jana Koester and Julia Thiele conducted the laboratory analysis of DBD. We are grateful to Ana Moreno for helpful suggestions on an earlier version of the manuscript. We acknowledge the valuable comments of two anonymous reviewers. SeaWiFS data were supplied by the SeaWiFS Project and the Distributed Active Archive Center, Goddard Space Flight Center, Greenbelt, MD, USA. Data presented in this study will be made available at the World Data Center for Marine and Environmental Sciences: www.pangaea.de/home/kuhlmann. This research was funded by the "Deutsche Forschungsgemeinschaft" (DFG Grant no. WE 922/41-1).

5. Meridional shifts of the Mediterranean and monsoonal climate system off NW Africa during the last 130,000 years: implications from river discharge

Holger Kuhlmann[*a], Helge Meggers[a], Ana Moreno[b], Tim Freudenthal[a], Sabine Kasten[a], Christian Hensen[a], and Caroline von Oppen[c]

[a] *University of Bremen, Department of Geosciences, PO Box 330440, 28334 Bremen, Germany*
[b] *Grup de Recerca Consolidat en Geosciències Marines, Departament d´Estratigrafia, Paleontologia i Geosciéncies Marines, Universitat de Barcelona, Campus de Pedralbes, E-08028 Barcelona, Spain*
present address: Pyrenean Institute of Ecology, CSIC, Apdo. 202, 50080 Zaragoza, Spain
[c] *University of Bremen, Department of Marine Chemistry, PO Box 330400, 28334 Bremen, Germany*

submitted to **Quaternary Research**

5.1 Abstract

For the NW African region the eolian dust is widely accepted to be the most important contributor of lithogenic material to the marine sediments, reflecting environmental conditions in the source areas as well as properties of the atmospheric circulation. Here we present river discharge as a second important vehicle for the transport of lithogenic material to the NE Atlantic Ocean, which has been previously so far underestimated. We show, that the iron concentration of marine sediment cores from the Moroccan coast investigated with the X-ray fluorescence Core Scanner in high spatial and temporal resolution can be used as an indicator of fluvial input. From our results we conclude that the northern part of the investigation area (> 30° N) has received humidity throughout the last 130,000 yr, which is mainly forced by the Mediterranean winter rain. In contrast, the southern part (< 30° N) reflects humid conditions only during the early-Holocene and the oxygen-isotope stage 5. These findings are interpreted to result from the northward propagation of humid conditions induced by the monsoonal climate system during wet phases of interglacial periods up to 30°N.

Keywords: Canary Islands; River discharge; Eolian dust; African monsoon; Holocene; Last glacial; African humid period

[*] Corresponding author. phone: ++49-421-2182886; fax: ++49-421-2183116; E-mail: kuhlma@uni-bremen.de.

5.2 Introduction

Changes of late-Quaternary climate in NW Africa are documented by archeological, geomorphological and hydrological records. These studies often suffer from gaps in the records. In this study we present a reconstruction of paleoclimate using continuous records from marine sediments of the adjacent NE Atlantic Ocean. The varying composition of the marine sediment combines many influencing factors. The marine portion of the sediment reflects signals from coastal upwelling and related primary productivity. The eolian dust portion of the sediments represents a part of the lithogenic material delivered from the NW African continent. Here, land climate and especially the wind systems have made their imprint on the material. Another part of the lithogenic fraction results from river discharge. It reflects preferentially the humidity and precipitation as an important aspect of climate. All these contributions to the sediments are possibly influenced secondarily by sediment transport in the ocean. The obvious complexity of paleoclimatic reconstruction on the basis of marine sediment records off NW Africa is revealed by regional investigations as already claimed by Bertrand (1996). For our investigation we use more than 43 sediment cores to cover a region located at the transition of the Mediterranean climate system and the African monsoonal system in order to detect meridional delineations and their shifts throughout the last 130,000 yr.

5.3 Investigation area

The NW African region is one of the most important source areas of lithogenic material transported to the NE Atlantic Ocean. Additionally, intense marine productivity in a coastal upwelling system attaches importance to the NW African continental margin in terms of biogeochemical cycles. Both parameters have been investigated intensively during the last decades for their implications on the climatic and environmental conditions in the past (Sarnthein et al., 1988; Tiedemann et al., 1989; Dupont, 1993; deMenocal et al., 2000a; Zhao et al., 2003). The enormous intensity of lithogenic input and primary productivity build the basis for very high accumulation of sediment in the adjacent Atlantic Ocean (Sarnthein et al., 1981; Schütz et al., 1981; Prospero, 1996; Ratmeyer et al., 1999). The dust portion of the lithogenic material is the target of manifold investigations (Andreae, 1996; Myhre and Stordal, 2001; Schollaert and Merrill, 2001; Bozzano et al., 2002; Claustre et al., 2002; Saydam and Senyuva, 2002; Mahowald et al., 2003; Sassen et al., 2003). Until now the fluvial input has been interpreted as negligible and paleoceanographic work between 20 and

30° N has concentrated on dust input. In this study we will stress fluvial input as another climate-sensitive indicator, especially of the humidity on the continent. We will analyze the meridional shifts of the monsoonal and Mediterranean climate system on the basis of Fe concentrations in the sediments as an indicator for fluvial input. Regarding the drainage of rivers in NW Africa, there are only a few studies available (Andres, 1977; Dupont and Hooghiemstra, 1989), maybe because of the present arid conditions, maybe because of the insufficient spatial resolution for the investigation of river influence on the sediment composition. We present data at a very high spatial resolution from the Canary Islands Region, which indicate varying river input at two locations (Cape Ghir and Cape Yubi) for the last 130,000 yr. The resulting pattern reflects the dominance of dust input to the NE Atlantic Ocean, but also the local importance of river discharge providing valuable paleoclimatic implications.

5.3.1 Present environmental conditions

The lithogenic material is delivered to the adjacent North Atlantic Ocean as eolian dust transported by the wind systems and as fluvial input carried by rivers. The eolian input originates from central African sources, as well as from near-coastal sources and is transported within two major wind systems (Glaccum and Prospero, 1980; Coude-Gaussen et al., 1987; Herrmann et al., 1997; Falkovich et al., 2001; Goudie and Middleton, 2001; Aléon et al., 2002; Guieu et al., 2002; Prospero et al., 2002). The Saharan Air Layer (SAL) is related to the African Easterly Jet, a mid-tropospheric zonal wind system, which occurs a an altitude between 1500 and 5000 m (Prospero, 1990). The underlying wind system is dominated by the meridional trade winds blowing mostly parallel to the coast of NW Africa in a southwesterly direction. The trade winds generally account for dust transport from Moroccan sources (Hooghiemstra et al., 1987; Bergametti et al., 1989; Duce et al., 1991; Chiapello et al., 1995; Torres-Padrón et al., 2002; Zhao et al., 2003). The mobilization and the transport of dust particles are very efficient at present arid climatic conditions.

However, another potential transport mechanism for lithogenic material is the input via river and wadi systems. There are several river systems developed at the coast of Morocco and Mauretania (Fig. 5.1). Most of them are non-discharging under the present climate, but some of them drain episodically depending on the seasonal precipitation, like the Souss river draining the Atlas Mountains (Olivera, 1996) (Fig. 5.1). Some of the dried river systems such as the Tamanrasett in the area of Cape Blanc have been identified by modelling studies (Vörösmarty et al., 2000).

The NW African continental margin is one of the most important upwelling regions in the oceans (Mittelstaedt, 1991; Nykjaer and Van Camp, 1994; Freudenthal et al., 2002). Cold and nutrient-rich water masses are brought to the surface by the offshore movement of surface waters, induced by the northeastern trade winds and the

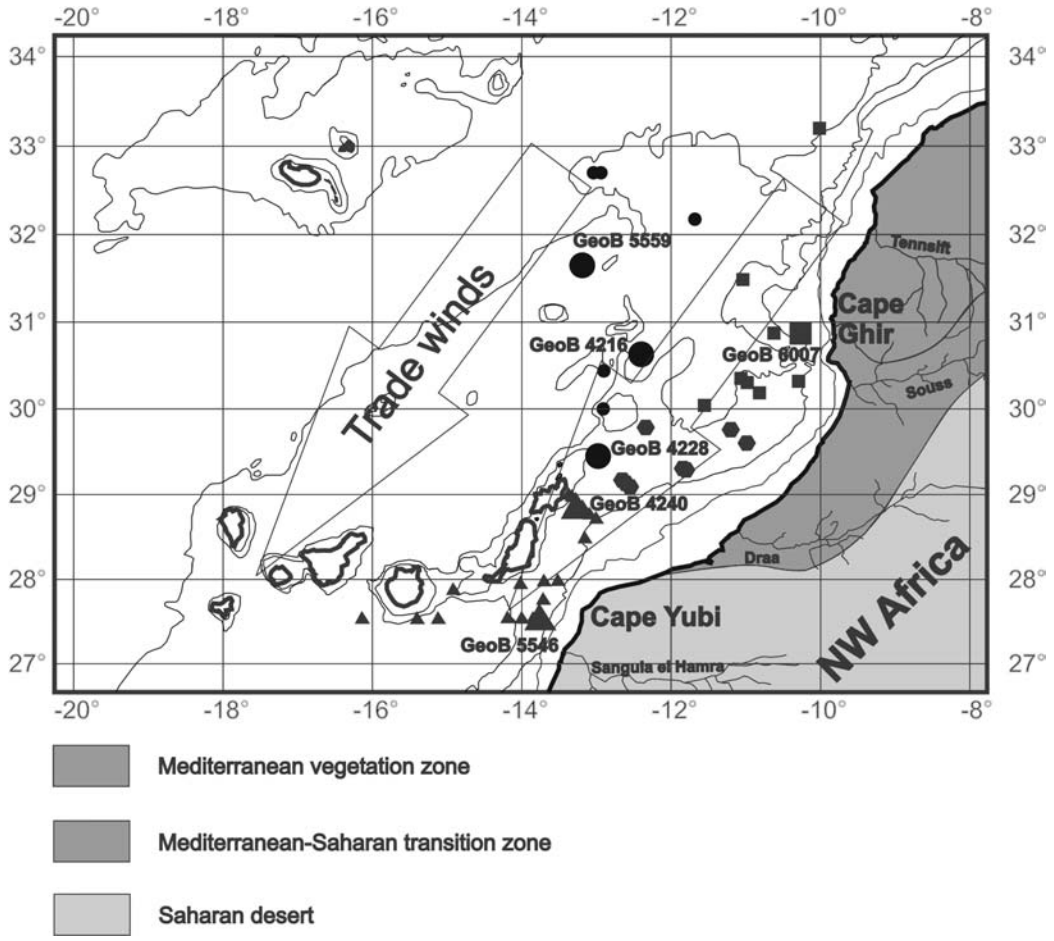

Figure 5.1 Bathymetric map of the investigation area situated in the Canary Islands Region with 100, 1000, 2000 and 4000 m depth contour lines. The symbols indicate core locations separated in three main areas: area 1: Cape Ghir (squares), area 2: Cape Yubi (triangles), area 3: northwestern offshore cores (circles) and a transition between the two cape locations (hexagons). The larger symbols indicate reference sites GeoB 5559, GeoB 4216, GeoB 4223, GeoB 4228, GeoB 4240, and GeoB 5546. On the African continent the main river systems are shown and the zonal vegetation following White (1983).

coastal morphology (Johnson and Stevens, 2000). The signal from the coastal upwelling is transported further into the ocean with frequently developed filaments, which occur especially at cape locations (Van Camp et al., 1991; Hagen, 2001; Davenport et al.,

2002). The pattern of enhanced primary productivity at the cape locations is mirrored by the underlying sediment (Meggers et al., 2002; Kuhlmann et al., subm.).

5.3.2 Early-Holocene environmental conditions

In the early-Holocene, also called the "African humid period" (deMenocal et al., 2000a), the climatic conditions in NW Africa were significantly different from the present as the results from model studies indicate (Claussen et al., 1999). Dust transport was reduced due to weaker wind intensities. The expansion of the monsoonal climate system delivering humidity into previously arid desert areas resulted in less mobilization of lithogenic material for eolian transport (Petit-Maire, 1989; Petit-Maire et al., 1990; Damnati et al., 1996; Damnati, 2000; deMenocal et al., 2000a; Zhao et al., 2003). In contrast, fluvial transport became more important; hence, the monsoonal humidity was delivered to the continent (Gasse, 2000).

5.3.3 Glacial environmental conditions

As a result of the stronger temperature and pressure gradients, glacial environmental conditions of NW Africa were characterized by stronger wind intensity (Sarnthein et al., 1982; McIntyre et al., 1989; deMenocal and Rind, 1993; Bertrand et al., 1996; Martinez et al., 1999). The African continent was dominated by dry climatic conditions, as inferred from pollen and hydrological data (Hooghiemstra, 1989; Dupont, 1999; Gasse, 2000). As a consequence of the enhanced trade winds, stronger upwelling intensity has been reported by Sarnthein (1982). Regarding the upwelling pattern through time various studies point to strong differences, reflecting the most intense primary productivity during glaciation, deglaciation or during humid intervals of the interglacial periods (Marret and Turon, 1994; Bertrand et al., 1996; Martinez et al., 2000; Zhao et al., 2000). To understand these differing results studies with a high spatial resolution have been carried out (Kuhlmann et al., subm.) reporting, e.g., sea-level changes and coastal morphology as factors of regional importance to the upwelling-related primary productivity. This kind of high-resolution study enables us to detect in great detail the shift of environmental conditions and related climate systems.

5.4 Material and Methods

This study benefits from a pool of 73 sediment cores located in the Canary Islands Region off NW Africa recovered during METEOR cruises M37/1 (Wefer et al., 1997),

M42/4 (Wefer et al., 1999) and M45/5 (Neuer et al., 2000). We selected data from 43 sites where confident stratigraphic interpretations of the records are possible.

Table 5.1 Cruise and core number, geographic position, water depth, gear type and recovery of the investigated sediment cores from the Canary Islands region.

Cruise Meteor	Site GeoB	Latitude (°N)	Longitude (°W)	Geartype *	Waterdepth (m)	Recovery (cm)
M37/1	4205-2	32°10.9	11°38.9	GC	3272	501
M37/1	4206-1	31°30.0	11°01.3	GC	1855	571
M37/1	4209-2	30°21.4	11°05.0	GC	2150	970
M37/1	4210-1	30°18.0	10°58.8	GC	1959	424
M37/1	4211-2	30°11.6	10°49.3	GC	1773	650
M37/1	4212-2	29°36.2	10°57.0	GC	1256	857
M37/1	4213-2	29°41.8	11°04.7	GC	1547	754
M37/1	4214-1	29°46.9	11°11.8	GC	1788	952
M37/1	4215-2	30°02.2	11°33.2	GC	2106	766
M37/1	4216-2	30°37.9	12°23.8	GC	2325	1117
M37/1	4217-5	30°26.1	12°53.7	GC	2504	716
M37/1	4218-1	29°57.3	12°54.7	GC	2723	619
M37/1	4221-1	29°46.5	12°20.3	GC	1826	843
M37/1	4223-2	29°01.1	12°28.0	GC	777	779
M37/1	4225-1	29°16.5	11°46.9	GC	1281	725
M37/1	4226-3	29°19.2	11°50.0	GC	1400	907
M37/1	4228-3	29°28.2	12°59.4	PC	1633	1188
M37/1	4229-1	29°10.9	12°38.3	GC	1422	663
M37/1	4230-2	29°07.7	12°35.8	GC	1316	993
M37/1	4231-1	29°05.2	12°33.1	GC	1197	726
M37/1	4232-2	29°01.3	13°23.2	GC	1161	991
M37/1	4233-1	28°58.5	13°19.8	GC	1303	1076
M37/1	4235-2	28°51.4	13°11.4	GC	1247	777
M37/1	4236-1	28°47.0	13°05.7	GC	1030	1084
M37/1	4237-2	28°43.7	13°01.0	GC	800	966
M37/1	4240-2	28°53.3	13°13.5	GC	1358	688
M42/4	5536-2	27°32.2	16°08.1	GC	3456	880
M42/4	5537-3	27°32.1	15°24.1	GC	2362	784
M42/4	5538-1	27°32.2	15°07.0	GC	2537	1080
M42/4	5540-2	27°32.1	14°10.5	GC	2035	920
M42/4	5541-4	27°32.2	13°59.7	PC	1748	1252
M42/4	5545-1	27°32.2'	13°50.8	PC	1431	1156
M42/4	5546-2	27°32.2	13°44.2	PC	1071	851
M42/4	5547-3	27°45.6	13°42.6	GC	1310	1066
M42/4	5548-2	27°59.5	13°31.1	GC	1162	755
M42/4	5549-3	27°58.7	13°41.7	GC	1454	890
M42/4	5550-2	27°57.1	14°00.9	GC	1738	1056
M42/4	5551-3	27°52.6	14°54.9	GC	1885	1027
M42/4	5559-2	31°38.7	13°11.2	GC	3178	585
M42/4	5560-1	31°36.6	13°07.1	GC	3944	469
M42/4	5561-2	32°42.2	12°56.1	GC	3500	434
M45/5	6006-1	30°52.1	10°37.8	GC	1275	908
M45/5	6011-1	30°18.9	10°17.3	GC	993	477

* GC = gravity corer; PC = piston corer

The cores are located in a waterdepth from 800 to 4,000 m (Tab. 5.1), representing three different areas: Cape Ghir, Cape Yubi and a third group of sites located further offshore in the northwestern part of the investigation area.

5.4.1 Core-scanning

Core-logging methods provide a good opportunity to work on such a high number of sediment cores with a sufficient resolution in an acceptable amount of time. We present data obtained with the quick and non-destructive X-Ray Fluorescence (XRF) Core Scanner at the University of Bremen. A detailed description of the applied XRF analysis and the system configuration of the XRF Core Scanner at the University of Bremen is given by Jansen, et al. (1998) and Röhl, et al. (2000).

XRF data used in this study were collected on the surface of split sediment cores over a 1 cm^2 area using a 30-second count time, 20 kV X-ray voltage and an X-ray current of 0.087 mA to obtain statistically significant data for the elements K, Ca, Fe, Ti, Mn, and Sr. The resulting data are element intensities in counts per second (cps). Element concentrations are not directly available from the XRF scanner measurements and the installed processing software, but they can be converted from XRF scans by calibration with standard analytical methods on selected samples as initially shown by Jansen et al. (1998).

5.4.2 Element analysis on discrete samples

To calibrate the scanner-derived element intensities into concentrations, we analyzed element concentrations on discrete samples of selected sediment cores with XRF, **i**nductively **c**oupled **p**lasma **a**tomic **e**mission **s**pectrometry (ICP-AES) and flame **a**tomic **a**bsorption **s**pectrometry (AAS).

5.4.2.1 XRF

Sediment samples from the cores GeoB 4216, GeoB 5559, and GeoB 6007 were ground and homogenized in an agate mortar for XRF analyses. For major element determination, glass discs were prepared by melting about 0.3 g of ground bulk sediment with a Li tetraborate flux. Bulk-sediment geochemistry of the samples was determined in a Philips PW 2.400 sequential wavelength dispersive X-ray spectrometer. After calibration with international standards (GSS-1 to GSS-7), the analytical precision was checked by replicate analyses of samples and was found to be better than 0.8 % for

major elements. Finally, all standard X-ray fluorescence results were corrected for the contribution and dilution effect of the sea-salt content in the dried sediment.

5.4.2.2 ICP-AES, Flame-AAS

Sediment samples of the cores GeoB 4228, GeoB 4240 and GeoB 5546 were taken for 5-cm intervals, freeze-dried, and ground in an agate mortar prior to further processing. For bulk solid-phase analysis, 50 mg of dry sediment were digested in a microwave system (MLS-MEGA II, MLS-1200 MEGA, and MLS-ETHOS 1600) with a mixture of concentrated nitric (3 ml), hydrofluoric (2 ml) and hydrochloric (2 ml) acids of supra-pure quality at a temperature of ~200° C and a pressure of 30 bar. The digestion solutions were evaporated to dryness, redissolved in 0.5 ml of concentrated nitric acid and 4.5 ml deionized water (MilliQ) and homogenized, resulting in a final volume of 50 ml.

The concentrations of Fe and Al were determined by ICP-AES using a Perkin Elmer Optima 3300RL (GeoB 4228, GeoB 5546), or flame-AAS using PERKIN ELMER PE/1100B (GeoB 4240). The precision of the ICP-AES analyses (three consecutive measurements on the same sample solution) was better than 1 %. The accuracy of the analytical procedure was checked using standard reference material SDO-8. The concurrently determined element contents were within the certified ranges. The reliability of certified MESS-1 standard sediment (National Research Council of Canada) checked for flame AAS measurements was within the certified range.

5.5 Calibration of scanning results

We have chosen six reference cores from the data set (GeoB 4216, GeoB 4228, GeoB 4240, GeoB 5546, GeoB 5559, GeoB 6007) representing characteristic areas of the region (Fig. 5.1). In addition to high-resolution XRF scans, we carried out geochemical analysis (ICP-AES and XRF) on discrete samples and compared the datasets for each core. As we found an overall excellent correlation between the data sets, even at high-resolution (Fig. 5.2) we used the data to define a mathematical relationship for calibrating the XRF element intensities. We plotted the element concentrations for discrete samples from five reference cores versus the XRF scanner measurements and calculated the linear regression (Fig. 5.3). We achieved a high coefficient of determination ($r^2 = 0.907$; $p < 0.01 n$). The resulting equation as used for the conversion of element intensities to concentrations is: ($x = (y + 314.81) / 139.83$),

where x is the concentration and y the measured element intensity. The differences in the data from the standard analytical methods on discrete samples compared to the XRF scanner measurements can be partly assigned to different preparation methods and therefore different basic physical conditions. Samples used for standard analytical methods were dried and ground before analysis, while XRF scans take place on the surface of the original sediment with its natural porosity and water content. The observed minor differences between element concentrations obtained by XRF measurements on discrete samples, ICP-OES, AAS analysis, and the XRF core scanner measurements can be also explained by the fact that for discrete sample analysis a special sample volume is taken

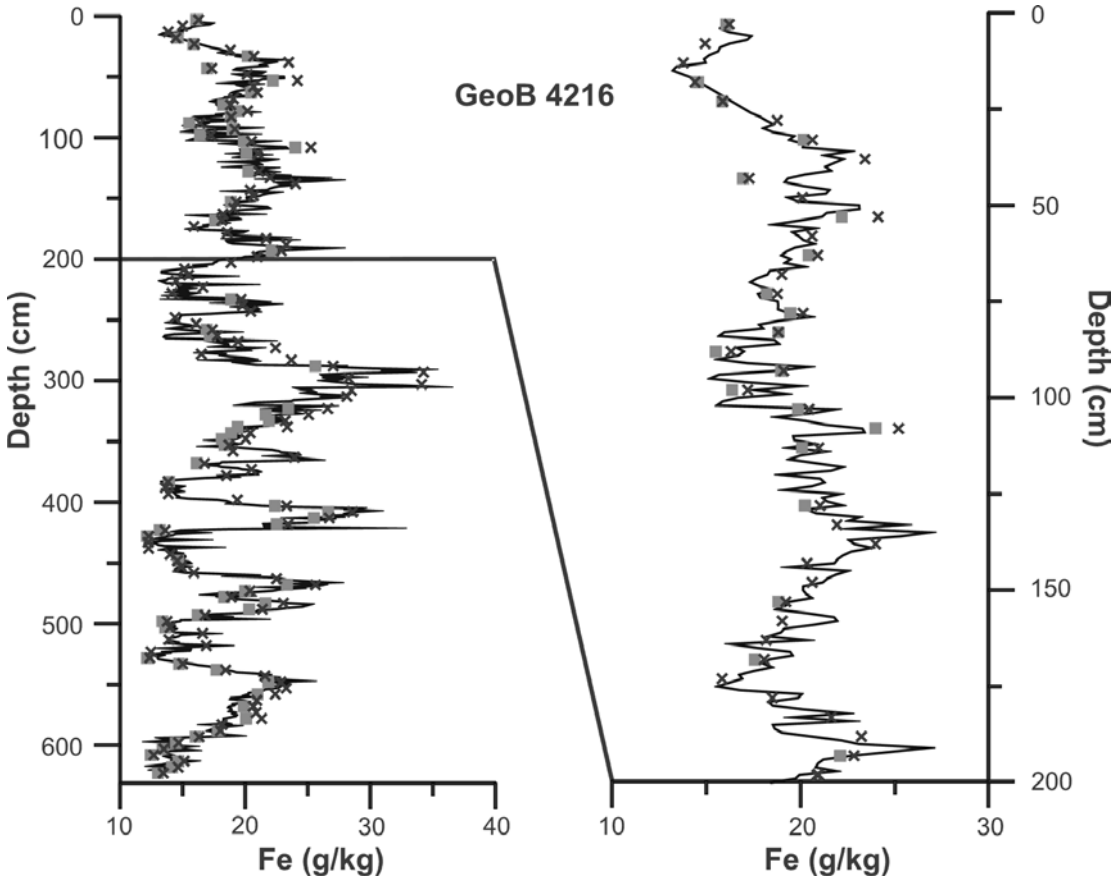

Figure 5.2 Comparison of three methods analyzing the Fe concentration of the sediment core GeoB 4216 from the Canary Islands Region (for position see Fig. 5.1). XRF scanning (thin solid line) was done in 1 cm resolution. ICP-OES measurements (crosses) were carried out in 5 cm resolution and XRF analysis on discrete samples (squares) was applied to samples with an irregular distribution throughout the core. The scanner derived Fe intensity is converted into (g/kg) following the procedure described in the text. The first two meters of core GeoB 4216 are shown enlarged in the right graph.

and homogenized, whereas the XRF scanning at the surface of the sediment core just measures a very thin layer of tenth to hundreds of microns, which is determined by the element specific wave length of the fluorescent radiation (Jansen et al., 1998). It is notable, that the linear regression curve does not pass through the origin (zero) of the axis. We conclude that this is also due to the influence of other factors on the XRF core scanner measurements, e.g. porosity. By applying the formula we calculated element concentrations from the XRF scanner derived element intensities. To test whether this

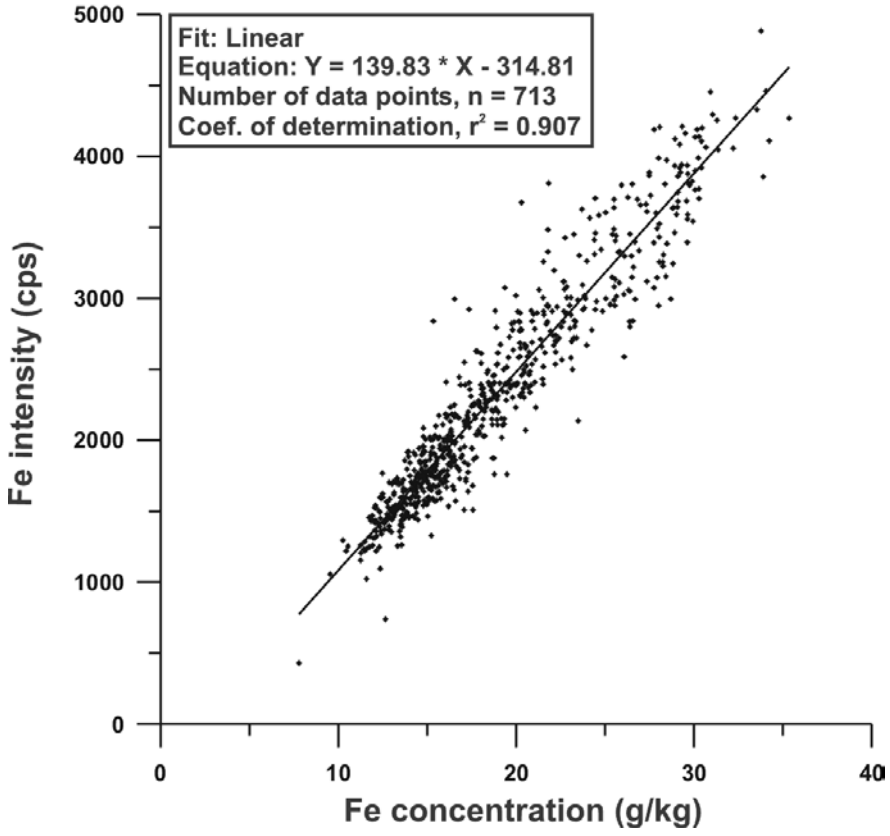

Figure 5.3 Scatter plot of Fe intensity (XRF Core Scanner) versus standard measurements (ICP-OES, XRF) from cores GeoB 4216, GeoB 6007, GeoB 4228, GeoB 4240, and GeoB 5546. The equation derived from linear regression y = 139.83 * x - 314.81 shows a coefficient of determination $r^2 = 0.907$ ($p < 0.01$*n*).

is a appropriate approach we calculated the linear regression of the reference cores, excluding site GeoB 5559. With the resulting relationship we calculated the Fe concentration of core GeoB 5559 and compared them with the measured Fe concentrations. The results, presented in Fig. 5.4, exhibit a very high accuracy throughout the core and the XY scatterplot shows a very high accuracy ($r^2 = 0.913$; $p <$

0.01*n*). Therefore it is indeed possible to obtain absolute element concentrations from XRF core scanner measurements with a very high accuracy, as shown in this study for sediments off NW Africa up to 300,000 yr in age. Further work needs to be done to test whether this calibration can be extended to a wider variety of sediment types, larger areas, different regions and ages, and the related limiting factors.

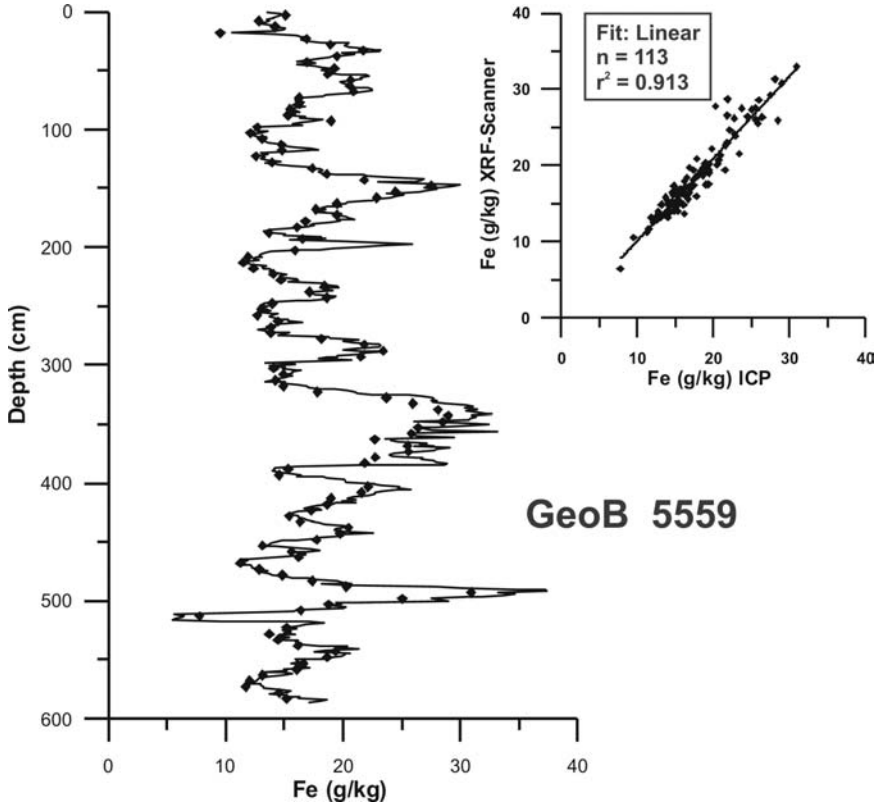

Figure 5.4 Conversion of semiquantitative XRF scanner data (cps) into concentrations (g/kg) for GeoB 5559 (for position see Fig. 5.1). Fe concentration was calculated from scanner data (solid line) and compared with separately measured XRF standard method (dots). Additionally, the scatterplot of the calculated and measured Fe concentrations including linear regression and coefficient of determination $r^2 = 0.913$ ($p < 0.01n$) is shown.

5.6 Stratigraphy

In a previous study we have shown that changes in Fe intensity exhibit similar variations at all investigated sites, and that these can be used for stratigraphic correlation (Kuhlmann et al., subm.). A Canary Islands Fe stack was calculated following Imbrie (1984), based on the Fe records of 6 reference cores with reasonable age control. The resulting characteristic tie points representing Fe minima at 12,000, 18,000, and 40,000 yr, and Fe maxima at 80,000, 99,000, and 122,000 yr (Fig. 5.5) have

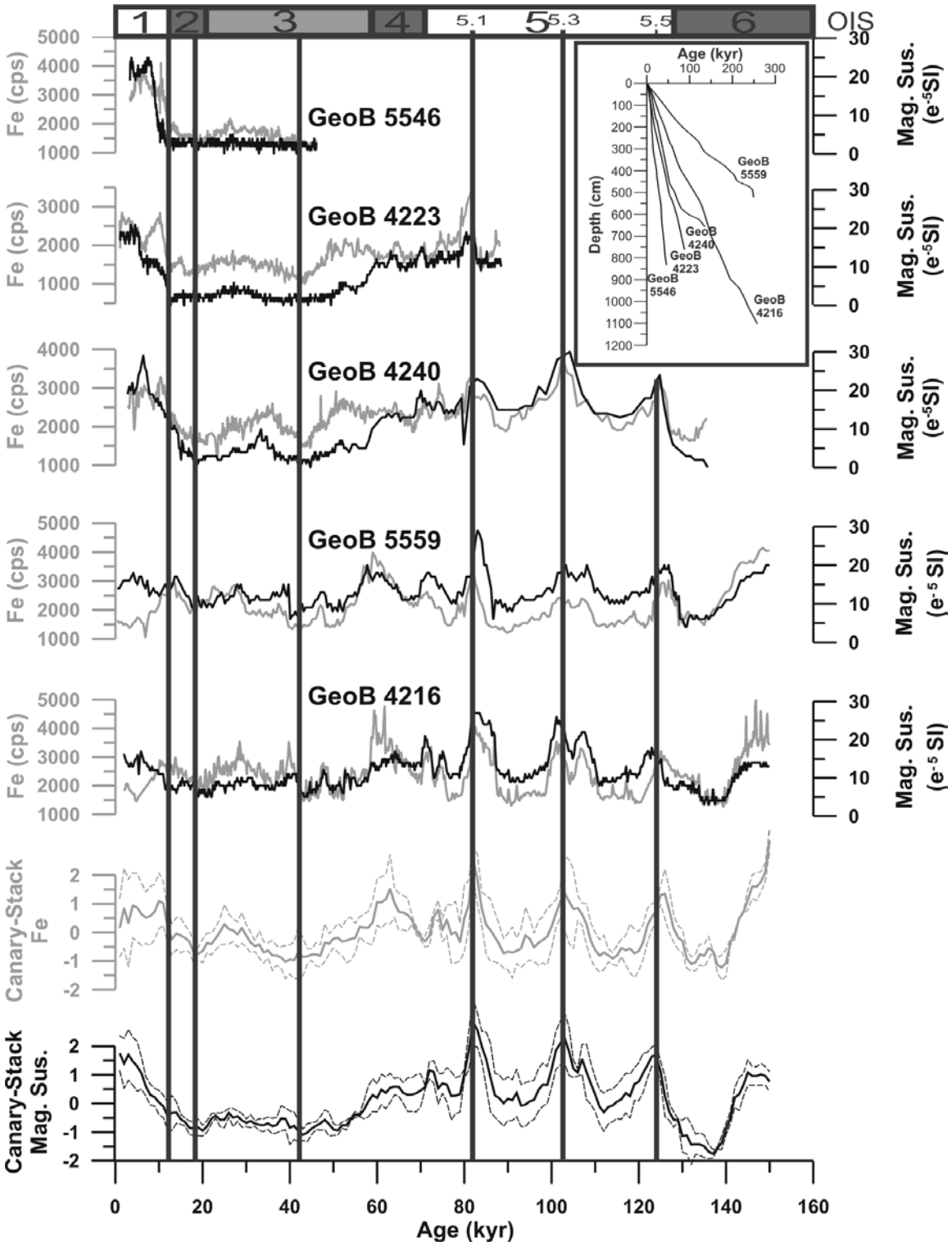

Figure 5.5 Canary **Fe** (CAFE) (grey) and **Ca**nary **m**agnetic **s**usceptibility (CAMS) (black) records (arithmetic mean with standard deviation band) resulting from the records of the stratigraphic reference cores (after Kuhlmann et al. subm.). Vertical lines indicate the tie points at 12,000, 18,000, and 40,000 yr (bold lines) and at 80,000, 99,000, and 122,000 yr. Oxygen isotope stages are indicated at the top and in the upper right edge the age-versus-depth plots of the five reference cores are shown.

been successfully transferred to the other sediment cores in the Canary Islands Region. In addition to the overall similarity of Fe records used for stratigraphic purposes in this study, we also focus on the regional differences in the absolute amounts of Fe concentrations for paleoclimatic reconstruction. It should be mentioned that the core tops generally do not reflect the sediment surface, because of the sampling procedure using gravity corer. Depending on the sedimentation rate the last 3,000 to 5,000 yr are missing. In Fig. 5.6a we present the age model of GeoB 5546, which has a high sedimentation rate (24 cm/kyr), showing that the top section of the core predominantly represents the early-Holocene. These findings are more pronounced in cores with lower sedimentation rates but all cores still reflect part of the early-Holocene.

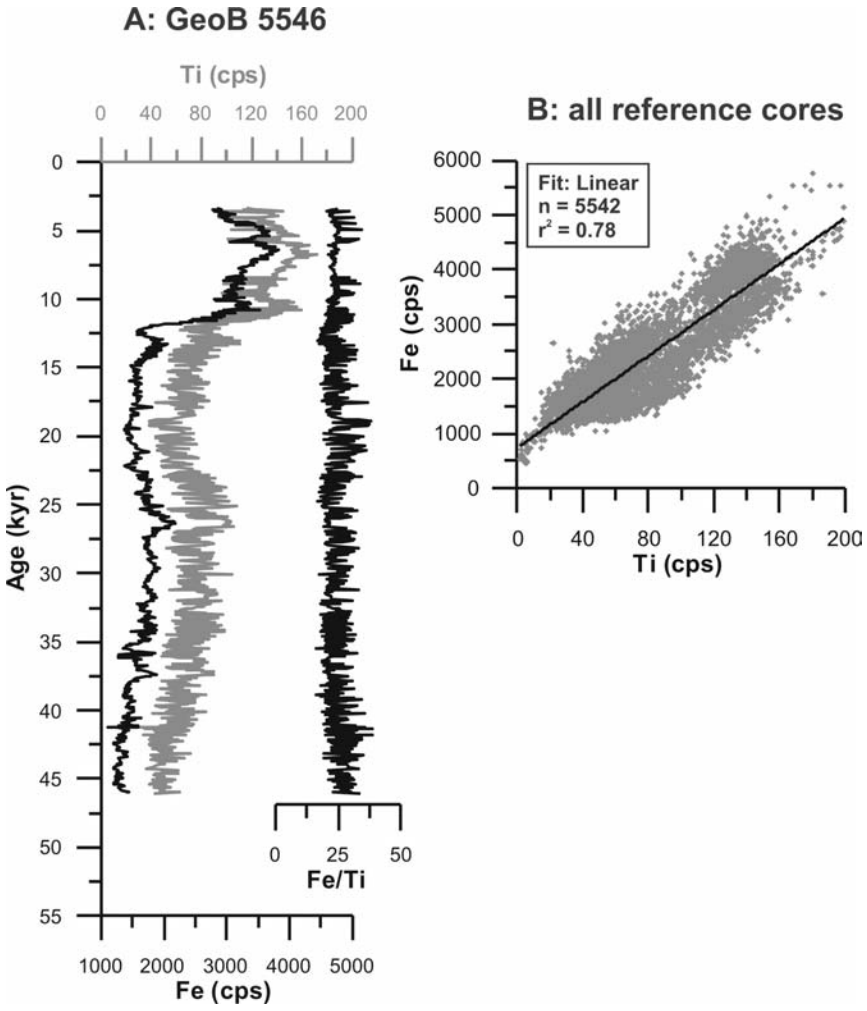

Figure 5.6 A: Fe and Ti intensities as well as Fe/Ti ratios (mean ~34) of core GeoB 5546 off Cape Yubi (for position see Fig. 5.1) are shown versus age. Note that the core top has an age of 3,300 yr, younger sediments were lost due to the coring procedure. **B:** XRF Core Scanner-derived Fe and Ti intensity scatterplot of all reference cores (5542 data points) resulting in coefficient of determination of $r^2 = 0.78$ ($p < 0.01n$).

5.7 Results

The pattern of the Ti records are similar to the Fe concentrations as shown for the reference core GeoB 5546 (Fig. 5.6a) and as in the scatterplot for the values of all reference cores (Fig. 5.6b). The Fe/Ti ratio is quite constant with a mean value of 34. Al concentrations are available for the reference cores. We calculated the Fe /Al ratios (Tab. 5.2) for comparison with studies investigating the sources of eolian dust.

The pattern of average Fe concentration and accumulation in the Canary Islands Region for five time intervals covering the last 130,000 yr is shown in Fig. 5.7. The Fe accumulation rates are strongly dominated by the bulk sediment accumulation (Kuhlmann et al., subm.). Therefore we present additionally the Fe concentration to elucidate the Fe signal of the Fe accumulation rates. The Fe concentrations exhibit a wide range from 12 g/kg up to 25 g/kg. The early-Holocene period (Fig, 5.7a,f) is characterized by low Fe concentration and accumulation in the northwestern offshore part of the investigation area. In contrast, both cape locations reflect maximum Fe concentrations. This pattern becomes more complicated when looking at the glacial time intervals (Fig. 5.7b-d, g-i). Here we observe slightly higher Fe accumulation and concentration in the northwestern offshore area compared to the early-Holocene. At Cape Ghir Fe concentrations decreased, but remain above 20 g/kg. In contrast at Cape Yubi we observe a drastic decrease of the Fe concentration to a level that is comparable to northwestern offshore sites (< 20 g/kg). In a comparison between the early Holocene and the last glacial, Cape Yubi undergoes the most remarkable changes, whereas the Fe content Cape Ghir remains at a comparable level. To compare the early-Holocene with **O**xygen **I**sotope **S**tage (OIS) 5 we compensated for the effect of a different number of sites available for the two time intervals by only using sites containing values in both data sets (Fig. 5.8). The general Fe pattern is quite comparable even though the coastal records of Cape Yubi are not long enough to reach OIS 5. These different scenarios with respect to Fe concentrations lead us to separate characteristic areas within the Canary Islands Region as indicated by different symbols in Fig. 5.1, highlighting the differences between the two capes.

Area 1: sites located near the Moroccan coast at Cape Ghir representing generally high Fe concentrations with maxima during interglacial periods.

Area 2: sites located off Cape Yubi representing the most significant differences between high Fe concentrations during interglacial time intervals and low values during glacial time intervals.

Area 3: sites located at the northwestern offshore area, representing generally low Fe concentrations with minimum values during interglacial periods.

5.8 Discussion

To interpret the pattern and changes of Fe content in the marine sediments of NW Africa for the last 130,000 yr, highlighting the extraordinarily different situation at Cape Yubi between the early-Holocene and last glaciation, we have to consider many influencing factors, which may act also in different combinations with each other.

5.8.1 Transport through the water column

Diverse transport processes have left their imprint on the particle and aggregate distribution during their settling through the water column. The results of sediment-trap studies indicate that the particle flux of lithogenic material is influenced by scavenging and incorporation into faecal pellets (Ramaswamy et al., 1991; Wefer and Fischer, 1993; Neuer et al., 1997; Ratmeyer et al., 1999). This may cause zonal gradients of parameters indicating terrigeneous material, because the coastal areas are influenced by high productivity due to upwelling and filament formation. But these upwelling-related influences on the particle distribution should be similar at both cape locations in the investigation area, because the environmental conditions are comparable (Barton, 1998; Barton et al., 1998; Hagen, 2001). Although local differences in glacial paleoproductivity are known (Bertrand et al., 1996), differences in the paleoproductivity between the two cape locations seem to be improbable (Sarnthein et al., 1982; Henderiks et al., 2002). However, we observe a significant difference in the Fe distribution pattern between the two cape locations during glacial time intervals (Fig. 5.7b-d). If we assume that the upwelling conditions were comparable at both cape locations also during glacial periods, another mechanism must be responsible for the differences. The transport mechanisms are interpreted to be more effective during glacial times due to the enhanced productivity. Nevertheless, we observe the highest Fe concentration during interglacial time intervals. At any rate, the Fe concentrations should not be influenced by scavenging processes, because also material associated with primary productivity should accumulate in higher numbers, which should not significantly affect the concentration.

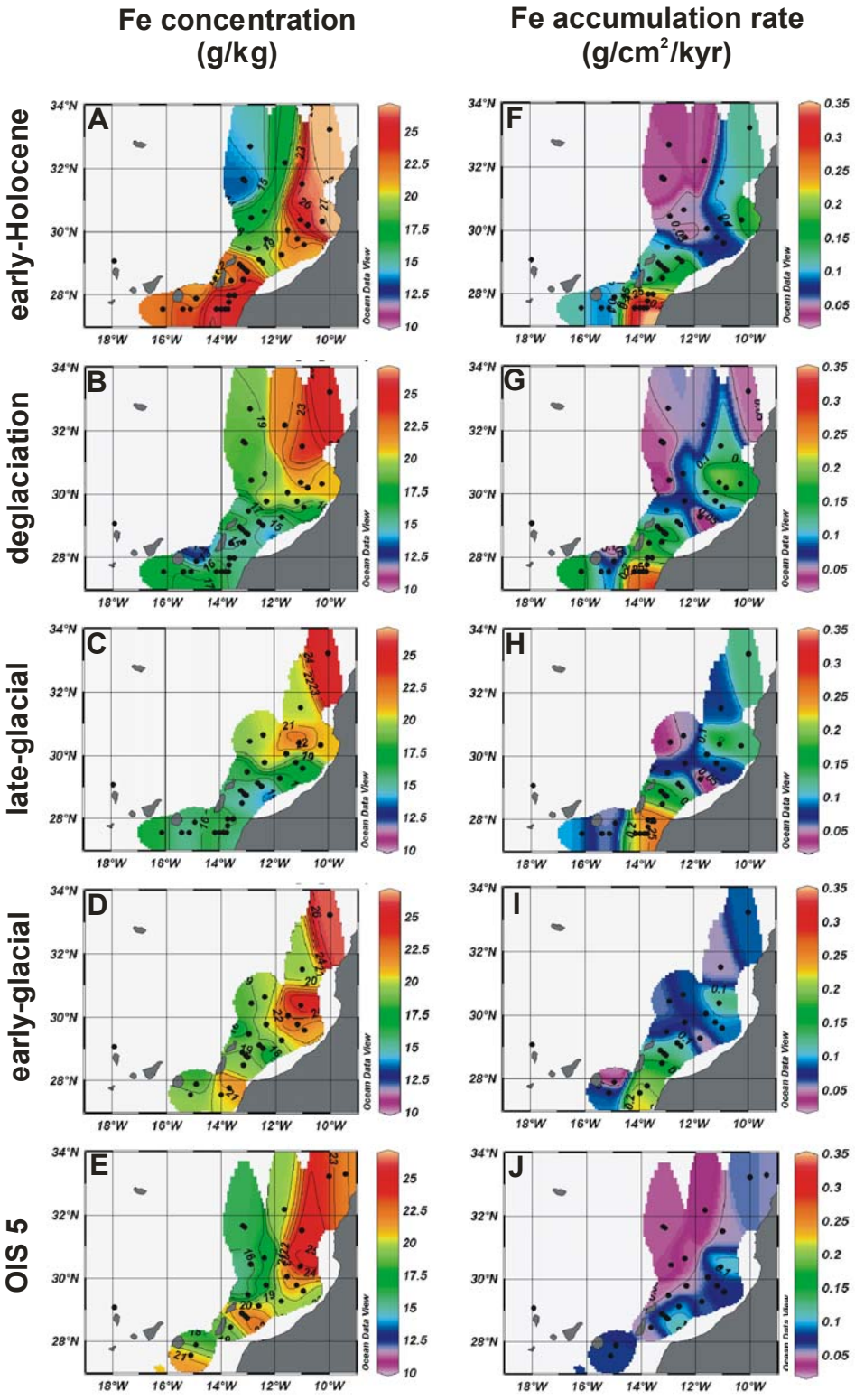

Figure 5.7 Fe concentrations (**A-E**) and Fe accumulation rates (**F-J**) are plotted for all sites available for the time intervals of **A, F** the early-Holocene (- 12,000 yr), **B, G** the deglaciation (12,000 - 18,000 yr), **C, H** and **D, I** the last glaciation (18,000 – 40,000 and 40,000 – 80,000 yr) and **E, J** the oxygen isotope stage (OIS) 5 (80,000 – 124,000 yr). Black dots indicate core locations used for the interpolation. The interpolated maps are generated with Ocean Data View (Schlitzer, 2002).

Therefore, we conclude that transport mechanisms are not the main factor to explain the distribution of Fe concentrations.

5.8.2 Diagenesis

Diagenetic processes may have a significant influence on the Fe distribution in the sediment. The Fe-intensity records are quite robust against diagenesis, because the X-ray fluorescence analysis detects Fe atoms irrespective of their oxidation state. To make sure that the diagenetic transport of Fe does not significantly affect the records we compared them to Ti, which is known to be much less sensitive to diagenesis than iron. We found that the Ti records show a nearly identical pattern to the Fe records. The Fe/Ti ratio is quite constant (mean ~34) throughout the cores (Fig. 5.6) and gives no obvious hints for a diagenetic displacement of iron.

The dissolution of carbonate, which is the main component in the investigated sediments could cause an increase in Fe concentration (Henderiks et al., 2002; Meggers et al., 2002). This process should affect Cape Yubi during the early-Holocene and even more strongly during the last glaciation because of the enhanced productivity. For the Fe concentration we would expect the opposite trend of the carbonate concentration. We found the highest Fe concentrations during the early-Holocene. These findings we interpret as indicative that carbonate dissolution has no dominant influence on the Fe distribution pattern.

5.8.3 Eolian input

The lithogenic material off NW Africa is frequently described as predominantly delivered in form of dust input from the arid desert areas on the adjacent African continent, namely the Saharan and Sahelian Region (Schütz et al., 1981; Sarnthein et al., 1982). The investigation area is located near these source regions of the dust, and all investigated sites receive lithogenic material via eolian input. It is widely accepted that eolian input during glacial times was stronger due to the enhanced atmospheric circulation (Sarnthein et al., 1981; McIntyre et al., 1989; Tiedemann et al., 1989; Balsam et al., 1995). This pattern is well reflected only at the sites located at the northwestern offshore region of the investigation area (area 3). Fe concentration and accumulation here are higher compared to early-Holocene values, whereas the bulk sediment accumulation remains constant. Therefore, we explain our findings with higher Fe input in glacial time intervals. The Fe /Al ratios of the reference cores located in this area are similar to many values that were obtained from dust sampling, sediment trap

studies, and from sediment core analysis (Tab. 5.2). Therefore we conclude that this region receives lithogenic material that is exclusively delivered by eolian transport. Comparable results of Fe concentrations (Fig. 5.7b, c) and Fe/Al ratios (Tab. 5.2) off Cape Yubi occurring under arid conditions during glacial time intervals let us conclude that they also result from dominant eolian input. The atmospheric dust transport is a relatively constant mechanism of dust input into the ocean over long distances compared to oceanographic features, which are often of small scale origin (Windom, 1976). To explain the differences between Cape Yubi and Cape Ghir we have to keep in mind that the distance between these two cape locations is only 3° of latitude. The observed meridional heterogeneity cannot be explained by variable dust input in the investigation area. The fact that the maxima in Fe concentration occur during interglacial periods, whereas the eolian input is known to reach its maximum influences in glacial times supports our interpretation of another transport process being responsible for the observed distribution of Fe concentrations.

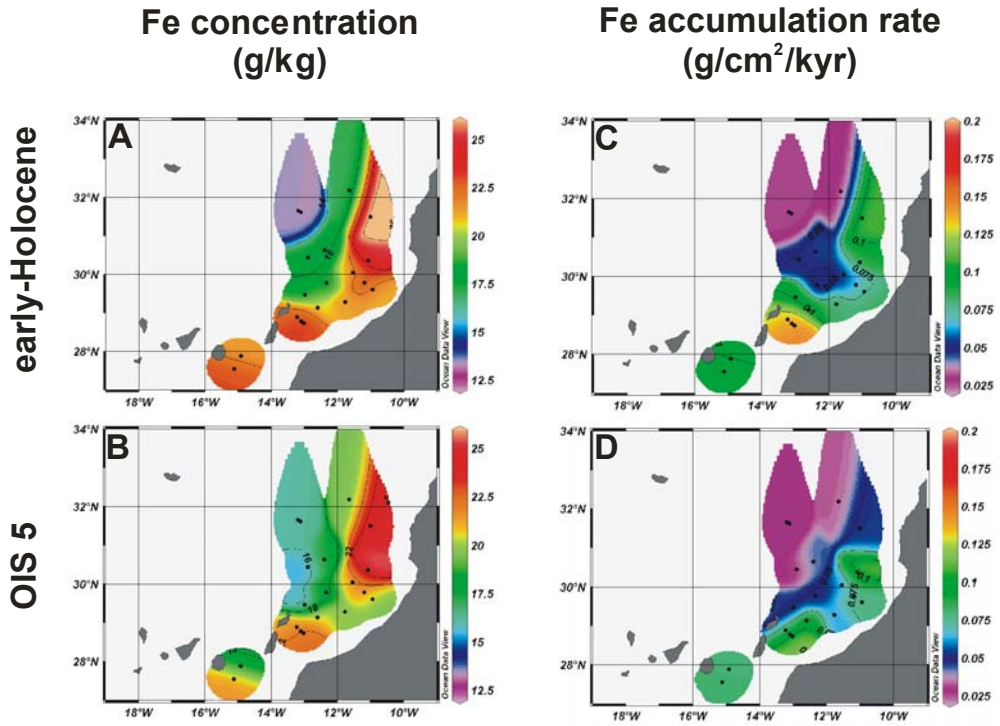

Figure 5.8 Fe concentration (**A, B**) and Fe accumulation rates (**C, D**) are plotted for **A, C** the early-Holocene (- 12,000 yr) and **B, D** the oxygen isotope stage (OIS) 5 (80,000 – 124,000 yr). Note that only sites were used where data from both time intervals were available. Black dots indicate core locations used for the interpolation. The interpolated maps are generated with Ocean Data View (Schlitzer, 2002).

5.8.4 Fluvial input

The recent annual river discharge of suspended material at the NW African continental margin is conservatively estimated by Milliman (1983) to reach 110×10^6 t. This material originates mainly from river and wadi systems draining the Atlas mountains e.g. the Souss river, flowing into the North Atlantic Ocean at Cape Ghir. The Souss River drainage area and the seasonal runoff (Olivera, 1996) are presumed to be induced mainly by Mediterranean winter precipitation (Hsu and Wallace, 1976). South of 30° N no significant river discharge is documented under the present arid conditions. This is reflected by grain-size analysis on surface samples and applied end-member modeling, resulting in the distribution of the end-member representing fluvial input (Holz, et al., subm.). This is also in agreement with results from the distribution

Table 5.2 Fe/Al ratios originating from lithogenic material of NW African origin.

Source	Location	Fe/Al	Reference
Soils			
	Morocco	0,64	Guieu`02
	Sahara	0,69	Guieu`02
Dust			
	Israel	0,7	Falkovich`01
	24° N, 24° W	0,54	Game`64
	Korsika	0,63	Guieu`02
	Catalonia	0,5	Avila`97
	Barbados	0,51	Arimoto`95
	Bermuda	0,61	Arimoto`95
	Tenerife	0,7	Arimoto`95
	Cape Verde	0,542	Chiapello`97
Sediment traps			
	22° N, 25° W	0,53	Kremling`93
Marine sediments			
	24° N, 20° W	0,44	Game`64
	GeoB 4216	0,52	this study
	GeoB 4228	0,53	this study
	GeoB 4240	0,51	this study
	GeoB 5546	0,49	this study
	GeoB 5559	0,5	Moreno`01
	GeoB 6007	0,38	this study

of $\delta^{13}C_{org}$ in surface sediments, which indicate an increase of terrigeneous organic matter from Cape Yubi towards Cape Ghir (Meggers et al., 2002). The same

distribution pattern is reflected in the Fe concentrations under arid conditions prevailing during glacial time intervals (Fig. 5.7b, c). Additionally, the Fe/Al ratios of the reference core GeoB 6007 located near the coast off Cape Ghir show exceptionally low values that are not in accordance with values reported from eolian dust (Tab. 5.2), reflecting the general N-S trend of lower Al concentrations due to lower kaolinite concentration in the north (Chester and Johnson, 1971; Measures and Brown, 1996; Chiapello et al., 1997; Caquineau et al., 1998). Therefore we conclude that this may point to a different origin and transport path of Fe- and Al-containing material. This lets us conclude that under arid conditions the sediments near the coast north of 30° N are influenced by river input, whereas south of 30° N no significant river input is observed. In contrast to the situation under arid climate conditions, there are indications from palynology, geomorphological investigations, and grain-size analyses, that, during humid climate phases in the past, significant river runoff has been established (Andres, 1977; Koopmann, 1981; Dupont and Hooghiemstra, 1989). The high Fe concentrations off Cape Yubi (area 3) during the early-Holocene and OIS 5 (25 g/kg) are in contrast to the very low concentrations observed during glacial time intervals (14 g/kg). The high values are comparable to those off Cape Ghir indicating river discharge; the lower ones are similar to the values found further off the coast where eolian dust is the only contributor of lithogenic material. We conclude that high Fe concentrations (> 20 g/kg) near the coast can be used as indicator of river input, in the Canary Islands Region. That means for the different areas:

Area 1: sites located near the Moroccan coast at Cape Ghir have received a significant portion of the terrigeneous matter from river discharge throughout the last 130,000 yr.

Area 2: sites located off Cape Yubi are influenced by river input under humid conditions during interglacial time intervals, whereas under arid conditions dust input dominates the terrigeneous fraction.

Area 3: sites located at the northwestern offshore area receive lithogenic material exclusively via eolian transport.

5.8.5 Climatic implications

Higher Fe concentrations during glacial time intervals at sites influenced exclusively by eolian input (area 3) support the interpretation that stronger wind intensities due to stronger temperature gradients caused higher dust input in glacial times (Sarnthein et al., 1981; Tiedemann et al., 1989).

The permanent river activity north of 30° N during the last 130,000 yr lets us conclude that river discharge from the Atlas mountains is a permanent feature of the region. This area is favoured to receive the humidity from the Mediterranean climate system dominated by winter rain (Hsu and Wallace, 1976) because of its exposed morphology. This is also mirrored in phytogeographical maps of NW Africa (White, 1983; Dupont, 1999) and palynological studies of the sediments off NW Africa (Hooghiemstra, 1989; Dupont, 1999).

In contrast, at Cape Yubi, river input as reflected by the Fe concentration occurs only during interglacial time intervals. There are numerous hints from the marine environment that the northward extension of the West African monsoonal climate system was reduced during dry episodes like the last glaciation (Rossignol-Strick and Duzer, 1979; Hooghiemstra et al., 1987; Dupont and Hooghiemstra, 1989; Overpeck et al., 1989; Tiedemann et al., 1989; Street-Perrot and Perrot, 1990; Kutzbach and Liu, 1997; Hoelzmann et al., 1998). As a result, the area of Cape Yubi did not receive a significant input of humidity and therefore no river discharge is reflected. These findings are supported by geomorphological investigations of the river valleys south of the Atlas Mountains. The sedimentation and erosion of mud terraces provide hints of significant river activity only in the early-Holocene (Andres, 1977), induced by strong rain events, like those that occur within the monsoon (Hsu and Wallace, 1976; Milliman and Meade, 1983). Modeling studies come up with the same trend of strengthening and expanded northward extent of the monsoonal climate system during interglacial time periods (Kutzbach and Liu, 1997; Hoelzmann et al., 1998; Geb, 2000; Tuenter et al., 2003). In comparison to lake-level and palynological studies, the northward extent was often underestimated. This is a result of vegetation and soil feedback mechanisms, which are presumed to lead to an amplification of the monsoonal climate system and its northward extent (Yu and Harrison, 1996; Jolly et al., 1998; Joussaume et al., 1999; Claussen et al., 2003). Our results support the findings that the northward extent of the influence of the monsoonal climate system of NW Africa during interglacial time intervals can reach as far as 30° N.

5.9. Conclusion

We have shown that XRF scanner-derived element intensities can be converted to absolute concentrations with the help of geochemical reference measurements. We introduced a calibration for sediments off NW Africa up to 300,000 yr in age. It has to

be checked in future whether and how this calibration can be transferred to other sediment types of different age from different regions.

The Fe concentrations are identified as a useful signal for interpreting fluvial input at the near-coastal sites and eolian input at sites further off the continent in the Canary Islands Region. At a high spatial resolution we showed that the northern part of the investigation area (> 30° N) has received river input throughout the last 130,000 yr, with indications of enhanced river activity during interglacial time intervals. In contrast, the southern part (< 30° N) reflects fluvial input only during wet phases of interglacial periods. This results in the interpretation that the Atlas Mountains generally have received humidity of northern (Mediterranean) origin throughout the investigated period, whereas, further to the south, the northern Saharan region receives humidity only during the humid phases of interglacial time intervals, such as the early-Holocene and the warm substages of OIS 5 from the enlarged northward propagation of the W African monsoonal climate system.

Acknowledgement

The authors thank the crews on board RV METEOR during various cruises. We thank E. Segui and J.M. Socias (XRF laboratory, Universitat de Barcelona) for laboratory analysis. Data presented in this study will be stored in the WDC PANGAEA under www.pangaea/home/kuhlmann. A.M. acknowledges funding from Generalitat de Catalunya autonomic government (grant 1998FI00655). This research was funded by the "Deutsche Forschungsgemeinschaft" (DFG Grant no. We 992/31-1 and We 992/41-1).

6. The transition of the monsoonal and N Atlantic climate system off NW Africa during the Holocene

H. Kuhlmann*, H. Meggers, T. Freudenthal, and G. Wefer

Department of Geosciences, University of Bremen, Klagenfurter Str., D-28359 Bremen, Germany

submitted to **Geophysical Research Letters**

6.1 Abstract

We present a very high-resolution Holocene sediment record off NW Africa (30°51.0´N; 10°16.1´W) indicating that the major change in sedimentation rate and periodicity of the terrigeneous signal occurred in this region at 8,500 years before present. Spectral and wavelet analyses reveal a 300-year periodicity of the terrigeneous input for the early-Holocene and a 900-year periodicity for the later Holocene. From comparison with further regional pattern we conclude that the early-Holocene at the core location reflects influence of the NW African monsoonal system, whereas the later Holocene is dominantly driven by the North Atlantic climate system.

Keywords: NW Africa; Holocene; wavelet analyses; terrigeneous material; Potassium; river discharge; NAO

* Corresponding author. Phone: ++49-421-2182886; fax: ++49-421-2183116; E-mail: kuhlmaquni-bremen.de

6.2 Introduction

Holocene climate as interpreted from arctic ice core projects was thought to be quite constant compared to abrupt events and millennial-scale cyclicities during the foregoing glacial period (Grootes and Stuiver, 1997). Recent investigations on the GISP 2 ice core record reveal an intensively oscillating signal for the Holocene time period although less in amplitude compared to the last glacial (Schulz and Paul, 2002). The analyses of sediment cores from the North Atlantic realm point to comparable signals (Bond et al., 1997; Bianchi and McCave, 1999). Climate reconstructions and modeling studies carried out at lower latitudes reflect a differing signal indicating a significant climate change in the mid-Holocene at about 5,000 yr before present (B.P.; all ages are reported as calendar years) (Ganopolski et al., 1998; Claussen et al., 1999; Arz et al., 2001), separating the so-called "African Humid Period" (deMenocal et al., 2000a) in the early-Holocene from the arid late-Holocene. We present a marine sediment record from 31°N off NW Africa indicating a major environmental change at about 8,500 yr B.P..

6.3 Regional settings

The NW African region is mainly influenced by two climate systems. The so-called "Mediterranean regime" (Hsu and Wallace, 1976) provides winter rain in the northern part. The mechanisms are closely connected to North Atlantic Oscillation (NAO) by the position and strength of the subtropical high-pressure system and the related trade wind intensity. Further to the south, separated by a transition zone centered at ~ 30° N the NW African monsoonal system plays a major role in providing monsoonal summer precipitation. This pattern is well reflected by vegetation and pollen distribution in NW Africa (White, 1983; Dupont, 1993). The two major related wind systems occur at different altitudes. The Saharan Air Layer at an altitude between 1,500 and 5,000 m accounts for the transport of eolian dust of Saharan and Sahelian origin (Bergametti et al., 1989; Tetzlaff et al., 1989; Torres-Padrón et al., 2002). The lower altitudes are dominated by the seasonal NE trade winds, blowing parallel to the coast, which account for the delivery of lithogenic material from northerly sources like the Atlas mountains (Coude-Gaussen et al., 1987; Chiapello et al., 1995).

Another part of the terrigeneous material transported into the North Atlantic Ocean originates from fluvial input. Recent river discharge at the NW Africa north of 15° N is restricted to river systems draining the Atlas mountains (Milliman and Meade,

1983) (Holz et al., subm.). Olivera (1996) investigated the seasonal runoff of the Souss river, which reaches the N Atlantic Ocean near the investigated site GeoB 6007. Another major component of the sedimentation at NW African continental margin is material originating from the intense marine productivity. The trade-wind-induced Ekman transport causes intense coastal upwelling (Hagen, 2001). Due to the higher nutrient concentration resulting from the upwelling we observe high primary productivity near the coast (Davenport et al., 2002), which is transported by filaments several 100 km into the ocean at the cape locations (Johnson and Stevens, 2000). This pattern is reflected by the chlorophyll-a concentration in the surface waters, as observed by satellites (Nykjaer and Van Camp, 1994; Davenport et al., 2002; Helmke et al., subm.) and mirrored within the underlying sediments (Meggers et al., 2002; Kuhlmann et al., subm.).

6.4 Investigation site GeoB 6007

The high-resolution site GeoB 6007 (30°51.0´N; 10°16.1´W) is located on the slope of the NW African continental margin within the transition zone between the "Mediterranean regime" and the NW African monsoonal climate system. The gravity core was retrieved in 900 m water depth during METEOR cruise M 45/5 (Neuer et al., 2000). The visual core description as well as colour measurements point to a homogeneous sedimentation with no disturbances of the lithology or significant diagenetic overprint. The 11.05 m record covers the last 13,000 years resulting in an average sedimentation rate of 85 cm/kyr. The high terrigenous input combined with the large amount of material originating from the intense marine productivity lead to very high sedimentation rates in the underlying sediments.

6.5 Stratigraphy

Nineteen Accelerator Mass Spectrometry (AMS) radiocarbon dates provide the age control for the sediment core GeoB 6007 (Tab.6.1). We converted the ^{14}C ages into calendar ages using the program CALIB 4.1 (Stuiver and Braziunas, 1993) and the INTCAL data set for marine carbonates, assuming 402 years reservoir age (Stuiver et al., 1998). Ages between the dates were obtained by linear interpolation. The core covers a time interval from ~ 250 – 13,500 yr B.P.. Thus, a sampling interval of 1 cm results in an average resolution of 12 years. In Fig. 6.1a we present the age model plotted versus depth and the resulting sedimentation rates.

Except for two spikes in the late Holocene (3,000 to 3,500 and 1,000 yr B.P.), we can divide the core into two sections separated by a significant drop in the sedimentation rate at about 8,500 yr B.P.. The average sedimentation rate for the earlier part reaches 160 cm/kyr and decreases abruptly to an average of 70 cm/kyr for the later Holocene. Additionally, we carried out $\delta^{18}O$ analyses on the planktic foraminifera, *Globigerina bulloides*, using a Finnigan MAT 251 mass spectrometer. Precision for repeated measurements was $\pm$ 0.07 ‰. The laboratory standard was calibrated to PDB using the international standards NBS 18, 19, and 20. The values vary between -0.4 and 0.2 ‰ during the Holocene and represent very well the change to values above 1 ‰ for the Younger Dryas period (Fig. 6.1b).

Table 6.1 AMS radiocarbon dating of Site GeoB 6007 planktonic foraminifera. All values were measured at the Leibnitz-Labor AMS facility in Kiel, Germany. The calibration was performed using the program CALIB 4.1 (Stuiver and Braziunas, 1993) and the INTCAL data set for marine carbonates, assuming 402 years reservoir age (Stuiver et al., 1998).

Lab.-ID	Core depth (cm)	Species *	^{14}C AMS Age (yr B.P.)	+/- error	Calibrated age (cal. yr B.P.)	Calibrated age range (cal. yr B.P.)
KIA20537	3	planktic forams	285	35		
KIA16978	53	*G. bulloides*	1525	35	1063	1040-1123
KIA20536	78	planktic forams	1695	25	1257	1236-1274
KIA16976	148	*G. bulloides*	2840	30	2660	2545-2691
KIA16984	208	*G. bulloides*	3470	25	3348	3327-3369
KIA20535	248	planktic forams	3720	40	3631	3581-3682
KIA16983	308	*G. bulloides*	4590	35	4814	4796-4830
KIA20533	328	planktic forams	4985	45	5307	5284-5394
KIA16982	408	*G. bulloides*	6125	35	6548	6493-6611
KIA20532	453	planktic forams	6660	45	7202	7154-7240
KIA20531	493	planktic forams	7560	45	7999	7951-8038
KIA20530	518	planktic forams	8160	50	8615	8558-8791
KIA16975	558	*G. bulloides*	8630	40	9028	8982-9301
KIA16974	608	*G. bulloides*	8855	45	9434	9100-9744
KIA20508	668	planktic forams	8980	55	9606	9450-9806
KIA16980	733	*G. bulloides*	9660	45	10312	10279-10579
KIA16979	838	*G. bulloides*	9920	60	10682	10371-11118
KIA16986	978	*G. bulloides*	10635	60	11844	11493-12264
KIA20528	1048	planktic forams	11095	60	12735	12325-12859

* mixed planktic foraminifera containing surface species: *G. bulloides, G. sacculifer, G. calida, G. ruber, G. falconensis, G. rubescens, T. quinqueloba, O. universa*

6.6 Decadally resolved terrigeneous input

Potassium (K) and its main mineralogical carrier illite are frequently used as an indicator of terrigeneous supply to marine sediments and have a long tradition in the investigation of source regions of eolian dust (Delany et al., 1967; Chester and Johnson, 1971; Glaccum and Prospero, 1980; Caquineau et al., 2002). At the investigated site near the coast of Morocco we also have to consider river discharge as process of terrigeneous input (Olivera, 1996), Holz, et al. subm.). The K record (Fig. 6.1c) was determined using the X-ray fluorescence (XRF) Core Scanner at the University of Bremen. This non-destructive analysis system for scanning the surface of archive of cores was developed and built at the Royal Netherlands Institute for Sea Research (NIOZ), Texel, Netherlands (Jansen et al., 1998; Röhl and Abrams, 2000). The measurements were carried out at 1-cm intervals, corresponding to an average sampling interval of 12 years. To obtain statistically significant data of K we used 30 s count time and an X-ray current of 0.087 mA. The acquired XRF spectrum for each measurement was processed by the KEVEX^{TM} software Toolbox$^{©}$. The resulting data are element intensities in counts per second (cps). The K intensities presented in Fig. 6.1c range over the entire core from 200 to 450 cps. We observe a significant increase in the K counts from about 250 cps characterizing the Younger Dryas period to 450 cps at the start of the Holocene. The following 7,500 years (from ~11,000 – 3,500 yr B.P.) are characterized by periodic oscillations occurring at different frequencies with an amplitude between 300 and 400 cps. Between 3,500 and 2,500 yr B.P. we observe an abrupt decrease in the K intensity followed by an increase in the amplitude of the fluctuations, as has also been noted for Cariaco Basin sediments (Haug et al., 2001).

6.7 Spectral and wavelet analyses

Spectral analyses confirm the visual recognition of the centennial cyclicities of the K record (Fig. 6.2). We used the AnalySeries 1.1 software package (Paillard et al., 1996) applying the Blackman-Tukey method (Blackman and Tukey, 1958) for spectral analyses of the K record from core GeoB 6007. Prior to the spectral analyses the time series were detrended and normalized to unit variance. With respect to the significant changes in the sedimentation rate and the frequency of the K record we divided the record at 8,500 yr B.P. into two sections and carried out spectral analyses separately. The results show an 80 % confidence level for the early-Holocene with a period of about 300 years (Fig. 6.2b), whereas the younger part is dominated by a period of about 900 years (Fig. 6.2a).

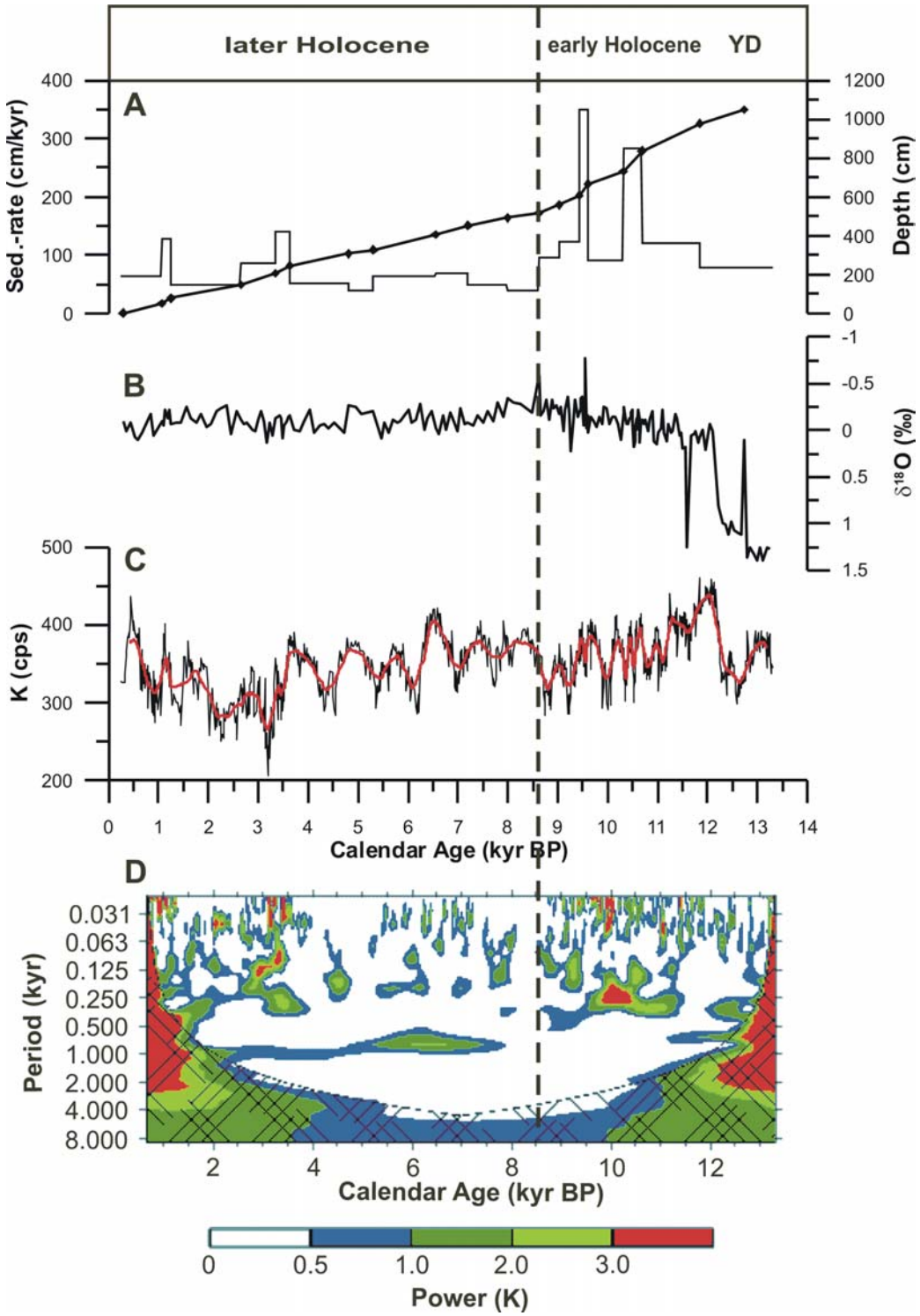

Figure 6.1 Analyses of sediment record site GeoB 6007. **A:** Age control and sedimentation rate, dots indicate the ^{14}C AMS dates. **B:** $\delta^{18}O$ record of the planktic foraminifera *G. bulloides*. **C:** Potassium (K) intensity obtained with the XRF core scanner is presented below (black line) with running average of 21 points (red line). The major environmental change at 8,500 yr is indicated by the grey vertical line. **D:** Wavelet analysis of the unsmoothed K record performed by using the online facility of the Program in Atmospheric and Oceanographic Science at the University of Colorado at Boulder (http://paos.colorado.edu/research/wavelets/) (Torrence and Compo, 1998). Red colours represent the 80% confidence level.

Wavelet analysis of the K record from core GeoB 6007 was carried out using the online facility of the Program in Atmospheric and Oceanographic Science at the University of Colorado at Boulder (http://paos.colorado.edu/research/wavelets/) (Torrence and Compo, 1998). The application of the wavelet analyses on the normalized K record reveals the shift from 300 year to 900 year periodicity at about 8,500 yr B.P.. These results, shown in Fig. 6.1d, confirm the findings of visual inspection as well as spectral analyses of the K record and give us confidence in interpreting the wavelet power.

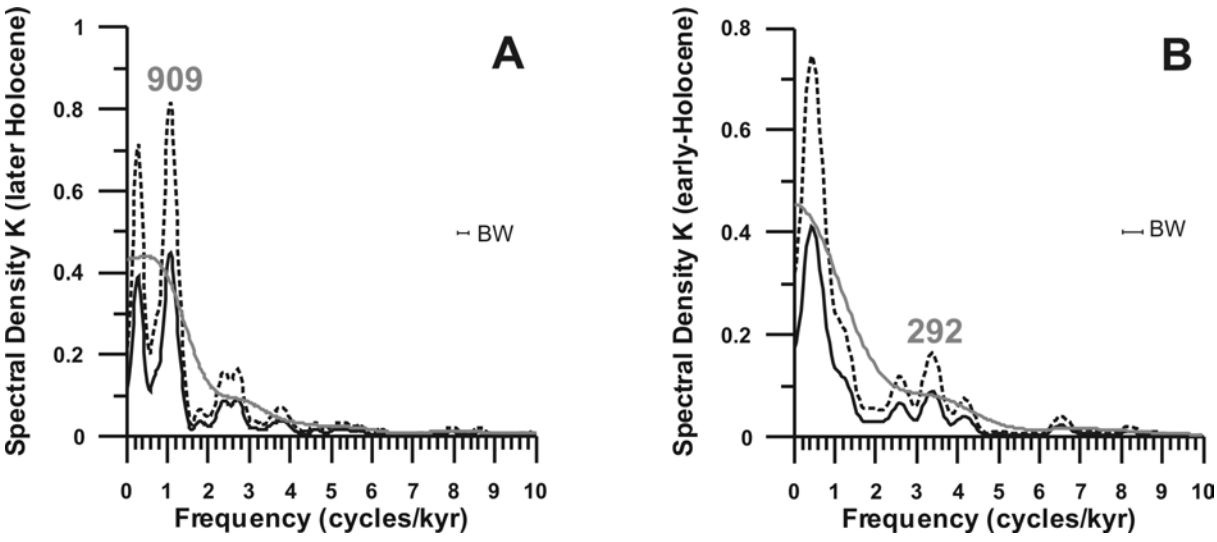

Figure 6.2 Spectral analyses of the unsmoothed K record of site GeoB 6007 was carried out for the later Holocene (- 8,500 yr B.P.) **A** and the early-Holocene (8,500 – 13,300 yr B.P.) **B**. We applied the Blackman-Tukey method using Analyseries 1.1 software (Paillard et al., 1996). Shown is the high and low power spectrum in high resolution mode (black and red line) and the low resolution mode (blue line). Points of intersection represent the 80% confidence level. (BW: band width, cps: counts per second).

6.8 Climatic implications

The significant change in sedimentation rate and periodicity of the K record at site GeoB 6007 occurs in the early-Holocene at about 8,500 yr B.P.. From southern Europe the age of 8,500 yr B.P. is interpreted to mark the beginning of the establishment of modern conditions, as indicated by pollen data (Davis et al., 2003). Also around 8,500 yr B.P. climate changes were described off Morocco on the basis of pollen and dinoflagellate records, which are indicators for land and oceanic climate

signals, respectively (Marret and Turon, 1994). In contrast, further to the south the major climate shift is reported from the mid-Holocene (6,000 – 4,000 yr B.P.) from terrigeneous as well as from oceanic climate proxies (Lézine et al., 1990; deMenocal et al., 2000a) and modeling studies (Kutzbach and Liu, 1997; Ganopolski et al., 1998; Claussen et al., 1999). We suggest that the mid-Holocene climate change is pronounced in the NW African region of monsoonal influence, whereas north of 30° N the North Atlantic climate system including the subtropical high pressure system and the related trade winds are dominating the climate records reflecting the drastic change at about 8,500 yr B.P..

A 300-year period, as we observe in the early-Holocene, was also reported both in modeling studies (Renssen et al., 2003) and lake-level fluctuations (Lézine et al., 1990) from a more southern origin in NW Africa. These similarities indicate a pronounced monsoonal influence of the investigation area at this time. This frequency became detached by a period of 900 years after 8,500 yr B.P. at the investigated site GeoB 6007. This period is well known from the $\delta\,^{18}O$ record of the GISP2 ice core (Schulz and Paul, 2002). The origin of this frequency may result from eccentricity variations of the Earth´s orbit (Loutre et al., 1992) or from internal feedback mechanisms (Schulz and Paul, 2002). However, the frequencies of the two records are in the same order of magnitude. As results from spectral analyses of the unsmoothed data sets indicate, the differences between the GISP2 (Schulz and Paul, 2002) and the GeoB 6007 (this study) periods (890 and 909 years, respectively) are within the uncertainty of the age control of the records. There is evidence that the mechanism of the decadal NAO signature may play a role for millennial-scale oscillation (Keigwin and Pickard, 1999; Rimbu et al., 2003). We suggest that the terrigeneous signal off the NW African region is linked to the Greenland temperature signal through the North Atlantic climate system (Fig. 6.3). A strong Icelandic Low located between Iceland and Greenland brings cold polar temperatures to Greenland (Barlow et al., 1997). At present, this situation is connected with a positive phase of the North Atlantic Oscillation (NAO+) (Kushnir, 1999). In this phase the related strong Subtropical High is located at its westernmost position. This influences the NW African terrigeneous signal via the trade winds and the westerlies, which regulate the eolian input and moisture-related fluvial transport of lithogenic material at the investigated site, respectively.

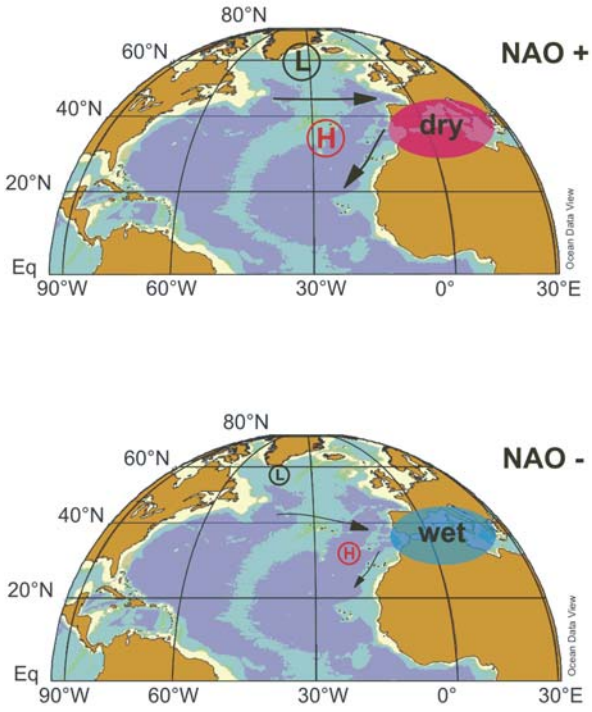

Figure 6.3 Model of the influence of NAO mechanisms on the NW African terrigeneous input.

6.9 Conclusion

From the sedimentation rate and the frequency of the terrigeneous record reported in this study we suggest that the major environmental change in the investigation area occurs at 8,500 yr B.P.. The timing of this event in comparison with other climate records from Northern Africa and Southern Europe indicate that the investigation area at this time is mainly influenced by the Mediterranean regime, coupled to the mechanisms of the NAO.

The observed 300 y periodicity in the terrigeneous proxy record during the early-Holocene provides hints of the influence of the NW African monsoonal system on the investigation area until 8,500 yr B.P., where modern conditions became established in the study area.

The periodicity of 900 years is very comparable to the GISP2 $\delta\ ^{18}O$ record reflecting temperature variation in Greenland. The possible link may be that Greenland temperatures are connected via NAO mechanisms with the subtropical high pressure system. The related trade winds and westerlies have placed their imprint on the eolian and fluvial input of lithogenic material. Therefore we conclude that the terrigeneous signal observed off NW Africa (~31° N) is characterized during last 8,500 years by the North Atlantic climate system.

Acknowledgement

The authors thank the crew and captain onboard RV METEOR during cruise M 45/5. Monika Segl is acknowledged for assistance in radiocarbon analyses. We are grateful to Michael Schulz and Jürgen Pätzold for valuable discussions and suggestions on an early version of the manuscript. Data presented in this study will be stored in the WDC PANGAEA under www.pangaea/home/kuhlmann. This study was supported by the DFG Forschungszentrum Ozeanränder.

7. GENERAL CONCLUSIONS

The results of the presented thesis, "Reconstruction of paleoceanography and terrigeneous sedimentation in the Canary Islands Region: Application of core-logging tools", can be divided in three main parts.

a. The intensive work on the core-logging tools MSCL and, particularly, the XRF Core Scanner, has improved the application of these systems, especially in terms of calibration of the semiquantitative element intensity (counts per second) into concentrations.

b. The application of the core-logging tools for paleoceanographic investigations emphasizes their advantages in providing rapid and non-destructive measurements. These methodological opportunities, combined with a large number of sediment cores located in a relatively small region off NW Africa were used for detailed investigation of a climate-relevant upwelling system on glacial-interglacial time scales. The important supply of lithogenic material to the marine sediments provided insights in the different pathways of the terrigeneous material.

c. The utilization of previous regional studies resulted in the determination of very high accumulation areas. We selected the sediment record providing the highest sedimentation rates of the region, GeoB 6007, for a detailed high-resolution investigation. Now we are able to extract similarities at a resolution comparable to that provided by ice-core data. From this study we present suggestions for the imprint of modern NAO mechanisms on the subtropical region off NW Africa.

7.1 Calibration of XRF-Scanner data

The XRF Core Scanner at the University of Bremen provides a relatively fast and non-destructive element intensity analysis of the elements from K (atomic nr. 19) to Sr (atomic nr. 38). In this study we test the accuracy of the system and demonstrate major applications for the interpretation of sediment cores. Our results show that the XRF Core Scanner cannot completely substitute standard analytical measurements of element concentrations such as ICP or XRF on discrete samples. This is especially true both for highest accuracy requirements and for low element concentrations near or below the detection limit of the XRF Core Scanner. It has been shown that among other sediment properties, porosity of the sediments only has a minor influence on XRF Core Scanner measurements. The limitations are related to the fact that the XRF measurements are taken on the surface of a sediment core, therefore on a material that

is not homogenized or otherwise prepared for optimal measurement conditions. The comparison of data from standard geochemical methods with XRF Core Scanner measurements show, however, that the general elemental signal is reflected very well, with good accuracy and at a very high resolution. All these are enormous advantages compared to relatively expensive and time-consuming standard analytical methods.

It was shown that XRF Core Scanner-derived element intensities can be converted to absolute concentrations with the help of geochemical reference measurements. This calibration was applied successfully to the sediment cores located in the Canary Islands region with ages up to 300 kyr. It will be a useful tool for further investigations of the sediments at the NW African continental margin. It has to be tested in the future whether, and how, this calibration can be transferred to other sediment types of different ages from different regions.

7.2 Paleoceanographic reconstruction

With the combination of a high-resolution spatial density of investigation sites and rapid high-resolution analysis of the sediment cores, we were able to develope an extraordinarily successful approach for detailed investigation and understanding of the highly dynamic upwelling region off NW Africa between 27 and 33° N. The application of core-logging tools enabled us to present age control for a large number of sediment cores (chapter 4 manuscript 1). These data provided the basis for an additional project funded by the Deutsche Forschungsgemeinschaft: "Reconstruction of variability of the biogenic and lithogenic sedimentation in the Canary Islands region during the last glacial period using time slice analysis", which is being carried out in close cooperation with other disciplines (micropaleontology and geochemistry). Detailed answer have been provided to the question that is raised frequently in the literature regarding local and regional influences on the sediment accumulation off NW Africa (chapter 4 manuscript 1). The bulk sediment accumulation rates provided us the opportunity to detect the local influence of sea-level variations caused by the morphology and lateral extent of the shelf areas. The characteristic cape morphology at Cape Yubi extended 50 – 100 km to the north during sea-level lowstand in the last glacial maximum. Therefore the high-accumulation area has its largest extent in this time period. The highest absolute amount of accumulation at Cape Yubi is observed during the deglaciation pointing to strongest trade wind-related upwelling conditions during the last 40,000 years. There is an indication that the varying windfield causes shifts in surface-water conditions at Cape Ghir, which are mirrored in the underlying sediments. The

actualistic approach compares modern conditions indicating a southwestward extent of the Cape Ghir filament during phases of extraordinarily high wind stress, with the glacial pattern resulting from the bulk sediment accumulation rates in this area. The interpreted higher wind stress during deglacial and glacial periods provide the same local pattern off Cape Ghir as is observed during high wind speed events under modern conditions. This study clearly identifies the influences of local and regional factors and explains the different reasons for these findings, emphasizing the advantages of regional as opposed to single core studies (chapter 4 manuscript 1).

The analysis of Fe accumulation as an indicator of terrigeneous sediment supply provides new insights into the extent of the NW African monsoonal climate system and the implications for transport mechanisms of terrigeneous material (chapter 5 manuscript 2). The accumulation of lithogenic material reflects considerable regional variations within the relatively small investigation area during the last 130,000 years. We identified three main areas reflecting: a) terrigenous material exclusively delivered via dust input (further offshore), b) influence of riverine input during wet phases of interglacial periods (near to the coast around Cape Yubi), and c) permanent influence of riverine input (near the coast north of 30 °N). The area of Cape Yubi (~ 27 °N) received increased terrigeneous sediment supply during the early-Holocene and OIS 5. We interpret this as being caused by the northward propagation of the NW African monsoon providing summer precipitation, which is drained through wadi systems. These results are in contrast to the suggestions of modeling approaches, but corroborate palynomorphical and hydrological studies in NW Africa. It is suggested that monsoonal and especially vegetational feedback mechanisms account for the differences between paleodata and modelling studies (chapter 5, manuscript 2).

7.3. High-resolution Holocene investigations

The detailed knowledge of the sedimentary conditions in the investigation area enabled us to carry out investigations on sediment archives with extremely high time resolution. A combined analysis of climate archives from the arctic North Atlantic region and the subtropical eastern North Atlantic Ocean was conducted in order to investigate mechanisms of the North Atlantic oscillation (chapter 6, manuscript 3). A drastic change in the environmental conditions was detected at about 8,500 years ago, which is in contrast to studies carried out further to the south describing the mid-Holocene climatic change at 5,000 years ago. Spectral and wavelet analysis of the subtropical Holocene terrigeneous record reflected by the K intensity confirmed the

results of the visual inspection. The periodicity detected in the early-Holocene (~300 year) is comparable to studies of southern origin. The characteristic period for the later Holocene (~900 year) is known from temperature reconstructions from the GISP 2 ice core. These results allowed to conclude that the investigated site off NW Africa (~30 °N) underwent a change from the influence of climatic conditions of southern origin (NW African monsoon) to an influence of mechanisms that also laft their imprint on Greenland temperatures at about 8,500 years ago. It was discovered that the mechanism that is known from the modern NAO can explain the relationship of terrigeneous sedimentation off NW Africa with Greenland temperatures. The changing strengths and positions of the Icelandic low and the subtropical high are related to Greenland temperatures. The pressure gradient is linked via trade wind intensity and the windfield of the westerlies to the humidity budget of northern NW Africa and therefore to river discharge. This influence is reflected in the terrigeneous sedimentation in the investigation area.

8. PERSPECTIVES

Although we have presented a first step in regional calibration of the semi-quantitative element intensity obtained with the XRF Core Scanner, future evaluations will determine to what extent the linear calibration can be transferred to different kinds of sediment types of varying ages in different regions. As an initial investigation we recently applied the presented formula successfully to sediments from the North Atlantic west of Ireland and to the South Atlantic West of South Africa. The next step should be to define the threshold values of general sedimentary characteristics that limit the application of this approach.

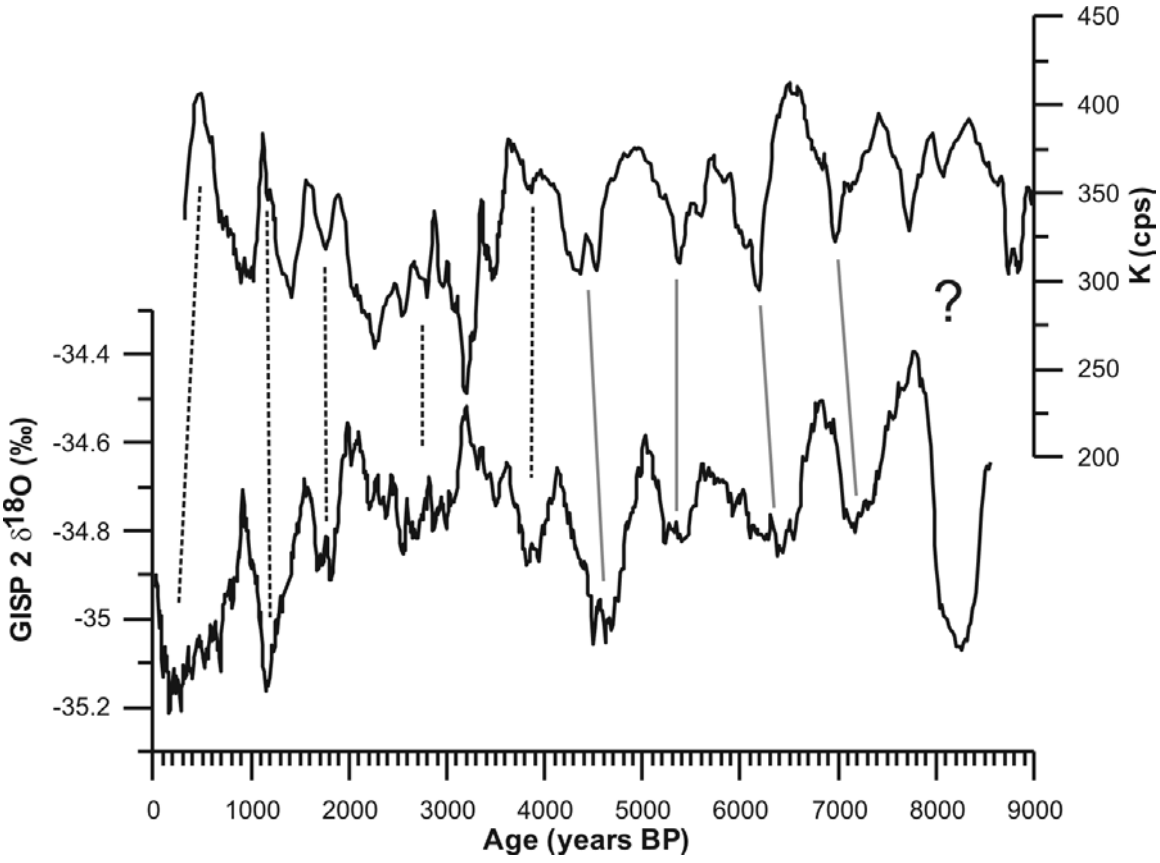

Figure 9.1 NW African terrigeneous input reflected in the K intensity record (cps = counts per second) obtained with the XRF Scanner of site GeoB 6007 is presented in the upper panel, applying a running average of 21 points. The $\delta^{18}O$ record of the GISP 2 ice core, reflecting Greenland temperatures is presented below, applying a running average of 35 points. The results of spectral analysis reveal the same periodicity (909 and 890 yr. respectively). The records correlate well in the earlier Holocene (indicted by blue vertical lines). Please note the shift to an anticorrelation (indicated by red vertical lines) at about 4,200 yr. B.P..

The area south of the Canary Islands region should be the focus of further studies. Based on remote sensing data, we expect that the average marine productivity here is even higher, because upwelling occurs nearly the whole year and the filament abundance is much higher. Additionally, this region is situated in the center of the main dust plume penetrating from Saharan and Sahelian region into the North Atlantic Ocean. Therefore we expect the sedimentation rates at sites near the coast to be even higher than in the Canary Islands Region and to represent the climatic and paleoceanographic history of this area in even greater detail. This may provide the opportunity to achieve a resolution comparable to ice cores and permit us to find a closer relationship to the long-term, continuous sediment-trap series of the Cape Blanc sediment trap. In particular, the relationship of this region to modern climate mechanisms like NAO and ENSO will be of increasing interest for understanding the roles that the subtropics and tropics play in climate development. As a first step in this direction, an analysis of the phase relationship between the terrigeneous signal of the most high-resolution core at Cape Ghir (GeoB 6007) and the GISP 2 ice-core record (Fig. 9.1) should be carried out. A possible explanation of the varying phase relationship, characterized by intervals of both, correlation and anticorrelation, may be found in the future with the help of modeling studies aiming to generate different states of the interaction of the North Atlantic and NW African monsoonal climate system.

9. REFERENCES

Abratis, M., Schmincke, H.-U. and Hansteen, T.H., 2002. Composition and evolution of submarine volcanic rocks from the central and western Canary Islands. International Journal of Earth Sciences, 91(4): 562-582.

Aléon, J., Chaussidon, M., Marty, B., Schütz, L. and Jaenicke, R., 2002. Oxygen isotopes in single micrometer-sized quartz grains: tracing the source of Saharan dust over long-distance atmospheric transport. Geochimica et Cosmochimica Acta, 66(19): 3351-3365.

Alley, R.B., Mayewski, P.A., Sowers, T., Stuiver, M., Taylor, K.C. and Clark, P.U., 1997. Holocene climatic instability: A prominent, widespread event 8200 yr ago. Geology, 25(6): 483-486.

Ancochea, E., Huertas, M.J., Cantagrel, J.M., Coello, J., Fúster, J.M., Arnaud, N. and Ibarrola, E., 1999. Evolution of the Cañadas edifice and its implications for the origin of the Cañadas Caldera (Tenerife, Canary Islands). Journal of Volcanology and Geothermal Research, 88(3): 177-199.

Andreae, M.O., 1996. Raising dust in the greenhouse. Nature, 380: 389-390.

Andres, W., 1977. Studien zur jungquartären Reliefentwicklung des südwestlichen Anti-Atlas und seines saharischen Vorlandes. In: M. Domrös, H. Eggers, E. Gormsen and W. Klaer (Editors), Mainzer Geographische Studien.

Antoine, D., André, J.-M. and Morel, A., 1996. Oceanic primary production, 2. Estimation at global scale from satellite (coastal zone color scanner) chlorophyll. Global Biogeochemical Cycles, 10(1): 57-69.

Arimoto, R., Duce, R.A., Ray, B.J., Ellis Jr., W.G., Cullen, J.D. and Merrill, J.T., 1995. Trace elements in the atmosphere over the North Atlantic. Journal of geophysical Research, 100(D!): 1199-1213.

Arimoto, R., 2001. Eolian dust and climate: relationships to sources, tropospheric chemistry, transport and deposition. Earth-Science Reviews, 54(1-3): 29-42.

Arístegui, J., Sangrá, P., Hernámdez-Leon, S., Cantón, M., Hernández-Guerra, A. and Kerling, J.L., 1994. Island-induced eddies in the Canary Islands. Deep-Sea Research, Part I, 41(10): 1509-1525.

Arístegui, J., Tett, P., Hernández-Guerra, A., Basterretxea, G., Montero, M.F., K.Wild, Sangrá, P., Hernández-León, S., Cantón, M., García-Braun, J.A., Pacheco, M. and Barton, E.D., 1997. The influence of island-generated eddies on chlorophyll distribution: a study of mesoscale variation around Gran Canaria. Deep Sea Research Part I, 44(1): 71-96.

Arz, H.W., Pätzold, J. and Wefer, G., 1998. Correlated millenial-scale changes in surface hydrography and terrigeneous sediment yield inferred from last-glacial marine deposits off Brazil. Quaternary Research, 50(2): 157-166.

Arz, H.W., Gerhardt, S., Pätzold, J. and Röhl, U., 2001. Millennial-scale changes of surface- and deep-water flow in the western tropical Atlantic linked to Northern Hemisphere high-latitude climate during the Holocene. Geology, 29(3): 239-242.

Arz, H.W., Pätzold, J., Müller, P.J. and Moammar, M.O., 2003. Influence of Northern Hemisphere climate and global sea level rise on the restricted Red Sea marine environment during termination I. Paleoceanography, 18(2): 1053.

Avila, A., Queralt-Mitjans, I. and Malarcón, M., 1997. Mineralogical composition of African dust delivered by red rains over northeastern Spain. Journal of Geophysical Research, 102(D18): 21977-21996.

Balsam, W.L., Otto-Bliesner, B.L. and Deaton, B.C., 1995. Modern and last glacial maximum eolian sedimentation patterns in the Atlantic Ocean interpreted from sediment iron oxide content. Paleoceanography, 10(3): 493-507.

Bard, E., Fairbanks, R., Arnold, M., Maurice, P., Duprat, J., Moyes, J. and Duplessy, J.-C., 1989. Sea-level estimates during the last deglaciation based on $d^{18}O$ and accelerator mass spectrometry ^{14}C ages measured in *Globigerina bulloides*. Quaternary Research, 31: 381-391.

Bard, E., Hamelin, B., Arnold, M., Montaggioni, L., Cabioch, G., Faure, G. and Rougerie, F., 1996. Deglacial sea-level record from Tahiti corals and the timing of global meltwater discharge. Nature, 382: 241-244.

Barlow, L.K., Rogers, J.C., Serreze, M.C. and Barry, R.G., 1997. Aspects of climate variability in the North Atlantic sector: Discussion and relation to the Greenland Ice Sheet Project 2 high-resolution isotopic signal. Journal of Geophysical Research, 102(C12): 26,333-26,344.

Barnola, J.M., Raynaud, D., Korotkevich, Y.S. and Lorius, C., 1987. Vostok ice core provides 160,000-year record of atmospheric CO2. Nature, 329: 408-414.

Barton, E.D., 1998. Eastern Boundary of the North Atlantic: Northwest Africa and Iberia. In: A.R. Robinson and K. Brink (Editors), The Global Coastal Ocean. The Sea. John Wiley & Sons, New York, Chichester, Weinheim, Brisbane, Singapore, Toronto, pp. 29-67.

Barton, E.D., Arístegui, J., Tett, P., Cantón, M., García-Braun, J., Hernández-León, S., Nykjaer, L., Almeida, C., Almunia, J., Ballesteros, S., Basterretxea, G., Escánez, J., García-Weill, L., Hernández-Guerra, A., López-Laatzen, F., Molina, R., Montero, M.F., Navarro-Pérez, E., Rodríguez, J.M., Van Lenning, K., Vélez, H. and Wild, K., 1998. The transition zone of the Canary Current upwelling region. Progress in Oceanography, 41: 455-504.

Basterretxea, G., Barton, E.D., Tett, P., Sangrá, P., Navarro-Perez, E. and Arístegui, J., 2002. Eddy and deep chlorophyll maximum response to wind-shear in the lee of Gran Canaria. Deep Sea Research Part I, 49(6): 1087-1101.

Behrenfeld, M.J. and Falkowski, P.G., 1997. Photosynthetic rates derived from satellite-based chlorophyll concentration. Limnology and Oceanography, 42(1): 1-20.

Bender, M., Sowers, T., Dickson, M.-L., Orchardo, J., Grootes, P., Mayewski, P.A. and Meese, D.A., 1994. Climate correlations between Greenland and Antarctica during the past 100,000 years. Nature, 372: 663-666.

Bergametti, G., Gomes, L., Coude-Gaussen, G., Rognon, P. and le Coustumer, M.-N., 1989. African dust observed over Canary Islands: Source-regions identification and transport pattern for some summer situations. Journal of Geophysical Research, 94(D12): 14855-14864.

Berger, W.H. and Keir, R.S., 1984. Glacial-Holocene changes in atmospheric CO2 and the deep-sea record. In: J.E. Hansen and T. Takahashi (Editors), Climate Processes and Climate Sensitivity. Geophysical Monographs. American Geophysical Union, Washington, DC, pp. 337-351.

Bertrand, P., Shimmield, G., Martinez, P., Grousset, F., Jorissen, F., Paterne, M., Pujol, C., Bouloubassi, I., Buat-Menard, P., Peypouquet, J.P., Beaufort, L., Sicre, M.-A., Lallier-Verges, E., Foster, J.M., Tenois, Y. and Program, O.p.o.t.S., 1996. The Glacial ocean productivity hypothesis: the importance of regional temporal and spatial studies. Marine Geology, 130: 1-9.

Bertrand, P., Pdersen, T.F., Martinez, P., Calvert, S. and Shimmield, G., 2000. Sea level impact on nutrient cycling in coastal upwelling areas during deglaciation: Evidence from nitrogen isotopes. Global Biogeochemical Cycles, 14(1): 341-355.

Bianchi, G.G. and McCave, I.N., 1999. Holocene periodicity in North Atlantic climate and deep-ocean flow south of Iceland. Nature, 397: 515-517.

Blackman, R.B. and Tukey, J.W., 1958. The measurement of power spectra from the point of view of communication engineering. Dover, New York, 190 pp.

Bloemendal, J., King, J.W., Hall, F.R. and Doh, S.-J., 1992. Rock magnetism of late Neogene and Pleistocene deep-sea sediments: Relationship to sediment source, diagenetic processes, and sediment lithology. Journal of Geophysical Research, 97(B4): 4361-4375.

Bond, G., Showers, W., Cheseby, M., Lotti, R., Almasi, P., de Menocal, P., Priore, P., Cullen, H., Hajdas, I. and Bonoani, G., 1997. A preservative millennial-scale cycle in North Atlantic Holocene and glacial climates. Science, 278: 1257-1266.

Bond, G., Kromer, B., Beer, J., Muscheler, R., Evans, M.N., Showers, W., Hoffmann, S., Lotti-Bond, R., Hajdas, I. and Bonani, G., 2001. Persistent Solar Influence on North Atlantic Climate During the Holocene. Science, 294(5549): 2130-2136.

Bozzano, G., Kuhlmann, H. and Alonso, B., 2002. Storminess control over African dust input to the Moroccan Atlantic margin (NW Africa) at the time of maxima boreal summer insolation: a record of the last 220 kyr. Palaeogeography, Palaeoclimatology, Palaeoecology, 183(1-2): 155-168.

Broecker, W.S. and Peng, T.-H., 1993. What caused the glacial to interglacial CO_2 to change? In: M. Heimann (Editor), The Global Carbon Cycle. Springer, Berlin, pp. 95-115.

Broecker, W.S. and Henderson, G.M., 1998. The sequence of events surrounding Termination II and their implications for the cause of glacial-interglacial CO2 changes. Paleoceanography, 13(4): 352-364.

Cantagrel, J.M., Arnaud, N.O., Ancochea, E., Fúster, J.M. and Huertas, M.J., 1999. Repeated debris avalanches on Tenerife and genesis of Las Cañadas caldera wall (Canary Islands). Geology, 28(8): 739-742.

Caquineau, S., Gaudichet, A., Gomes, L., Magonthier, M.-C. and Chatenet, B., 1998. Saharan dust clay ratio as a relevant tracer to assess the origin of soil derived aerosols. Geophysical Research Letters, 25(7): 983-986.

Caquineau, S., Gaudichet, A., Gomes, L. and Legrand, M., 2002. Mineralogy of Saharan dust transported over northwestern tropical Atlantic Ocean in relation to source regions. Journal of Geophysical Research, 107(15): AAC4/1-AAC4/12.

Chester, R. and Johnson, L.R., 1971. Atmospheric dusts collected off the West African Coast. Nature, 229: 105-107.

Chiapello, I., Bergametti, G., Gomes, L., Chatenet, B., Dulac, F., Pimenta, J. and Santos Suares, E., 1995. An additional low layer transport of Sahelian and Saharan dust over the North-Eastern Tropical Atlantic. Geophysical Research Letters, 22(23): 3191-3194.

Chiapello, I., Bergametti, G., Chatnet, B., Bousquet, P., Dulac, F. and Santos Soares, E., 1997. Origins of African dust transported over the northeastern tropical Atlantic. Journal of Geophysical Research, 102(D12): 13701-13709.

Chiapello, I., Goloub, P., Tanré, D., Marchand, A., Herman, J. and Torres, O., 2000. Aerosol detection by TOMS and POLDER over oceanic regions. Journal of Geophysical Research, 105(D6): 7133-7142.

Claussen, M., Kubatzki, C., Brovkin, V., Ganopolski, A., Hoelzmann, P. and Pachur, H.-J., 1999. Simulation of an abrupt change in Saharan vegetation in the mid-Holocene. Geophysical Research Letters, 26(14): 2037-2040.

Claussen, M., Brovkin, V., Kubatzki, C. and Petoukhov, V., 2003. Climate Change in Northern Africa: The Past is not the Future. Climatic Change, 57(1): 99-118.

Claustre, H., Morel, A., Hooker, S.B., Babin, M., Antoine, D., Oubelkheir, K., Bricaud, A., Leblanc, K., Quéguiner, B. and Maritorena, S., 2002. Is desert dust making oligotrophic waters greener? Geophysical Research Letters, 29(10): 107.

Colarco, P.R., Toon, O.B., Reid, J.S., Livingston, J.M., Russell, P.B., Redemann, J., Schmid, B., Maring, H.B., Savoie, D., Welton, E.J., Campbell, J.R., Holben, B.N.

and Levy, R., 2003. Saharan dust transport to the Caribbean during PRIDE: 2. Transport, vertical profiles, and deposition in simulations of in situ and remote sensing observations. Journal of Geophysical Research, 103(D19): 8590.

Coude-Gaussen, G., Rognon, P., Bergametti, G., Gomes, L., Strauss, B., Gros, J.M. and le Coustumer, M.-N., 1987. Saharan dust on Fuerteventura Island (Canaries): Chemical and mineralogical characteristics, air mass trajectories and probable sources. Journal of Geophysical Research, 92(D8): 9753-9771.

Damnati, B., Petit-Maire, N., Fontugne, M., Meco, J. and Williamson, D., 1996. Quaternary palaeoclimates in the eastern Canary Isands. Quaternary International, 31: 37-46.

Damnati, B., 2000. Holocene lake records in the Northern Hemisphere of Africa. Journal Of African Earth Sciences, 31(2): 253-262.

Davenport, R., Neuer, S., Hernández-Guerra, A., Rueda, M.J.L., Octavio, Fischer, G. and Wefer, G., 1999. Seasonal and interannual pigment concentration in the Canary Islands region from CZCS data and comparison with observations from the ESTOC. International Journal of Remote Sensing, 20(7): 1419-1433.

Davenport, R., Neuer, S., Helmke, P., Perez-Marrero, J. and Llinas, O., 2002. Primary productivity in the northern Canary Islands region as inferred from SeaWiFS imagery. Deep Sea Research Part II, 49(17): 3481-3496.

Davis, B.A.S., Brewer, S., Stevenson, A.C., Guiot, J. and Contributors, D., 2003. The temperature of Europe during the Holocene reconstructed from pollen data. Quaternary Science Reviews, 22(15-17): 1701-1716.

de Lange, G.J., Jarvis, I. and Kujpers, A., 1987. Geochemical characteristics and provenance of late Quaternary sediments from the Madeira Abyssal Plain. In: P.P.E. Weaver and J. Thomson (Editors), Geology and geochemistry of abyssal plains. Geological Society Special Publications. Blackwell Scientific Publications, Oxford, pp. 147-165.

Delany, A.C., Delany, A.C., Parkin, D.W., Griffin, J.J., Goldberg, E.D. and Reimann, B.E.F., 1967. Airborne dust collected at Barbados. Geochimica Cosmochimica Acta, 31: 885-909.

deMenocal, P., Ortiz, J., Guilderson, T., Adkins, J., Sarnthein, M., Baker, L. and Yarusinsky, M., 2000a. Abrupt onset and termination of the African Humid Period: rapid climate responses to gradual insolation forcing. Quaternary Science Reviews, 19(1-5): 347-361.

deMenocal, P., Ortiz, J., Guilderson, T. and Sarnthein, M., 2000b. Coherent high- and low-latitude climate variability during the Holocene warm period. Science, 288: 2198-2202.

deMenocal, P.B. and Rind, D., 1993. Sensitivity of Asian and African climate to variations in seasonal insolation, glacial ice cover, sea surface temperature, and Asian Orography. Journal of Geophysical Research, 98(D4): 7265-7287.

Díaz, J.P., Expósito, F.J., Torres, C.J., Herrera, F., Prospero, J.M. and Romero, M.C., 2001. Radiative properties of aerosols in Saharan dust outbreaks using ground-based and satellite data: Applications to radiative forcing. Journal of Geophysical Research, 106(D16): 18304-18416.

Dubief, J., 1979. Review of the North African climate with particular emphasis on the production of eolian dust in the Sahel Zone and in the Sahara. In: C. Morales (Editor), Saharan Dust. SCOPE. John Wiley & Sons, Chichester, pp. 27-48.

Duce, R.A., Liss, P.S., Merrill, J.T., Atlas, E.L., Buat-Menard, P., Hicks, B.B., Miller, J.M., Prospero, J.M., Arimoto, R., Church, T.M., Ellis, W., Galloway, J.N., Hansen, L., Jickells, T.D., Knap, A.H., Reinhardt, K.H., Schneider, B., Soudine, A., Tokos, J.J., Tsunogai, S., Wollast, R. and Zhou, M., 1991. The atmospheric

input of trace species to the world ocean. Global Biogeochemical Cycles, 5(3): 193-259.

Dupont, L.M. and Hooghiemstra, H., 1989. The Saharan-Sahelian boundary during the Brunhes chron. Acta Botanica Neerlandica, 38(4): 405-415.

Dupont, L.M., 1993. Vegetation zones in NW Africa during the Brunhes chron reconstructed from marine palynological data. Quaternary Science Reviews, 12: 189-202.

Dupont, L.M., 1999. Pollen and spores in marine sediments from the East Atlantic. A view from the ocean into the African continent. In: G. Fischer and G. Wefer (Editors), Use of Proxies in Paleoceanography: Examples from the South Atlantic. Springer, Berlin Heidelberg.

Edgar, C.J., Wolff, J.A., Nichols, H.J., Cas, R.A.F. and Martí, J., 2002. A complex Quaternary ignimbrite-forming phonolitic eruption: the Poris Member of the Diego Hernández Formation (Tenerife, Canary Islands). Journal of Volcanology and Geothermal Research, 118(1-2): 99-130.

Ercilla, G., Alonso, B., Perez-Belzuz, F., Estrada, F., Baraza, J., Farran, M., Canals, M. and Masson, D., 1998. Origin, sedimentary processes and depositional evolution of the Agadir turbidite system, central eastern Atlantic. Journal of the Geological Society London, 155(6): 929-939.

Fairbanks, R.G., 1989. A 17,000 year glacio-eustatic sea level record: influence of glacial melting rate on the Younger Dryas event and deep-ocean circulation. Nature, 342: 637-642.

Falkovich, A.H., Ganor, E., Levin, Z., Formenti, P. and Rudich, Y., 2001. Chemical and mineralogical analysis of individual mineral dust particles. Journal of Geophysical Research, 106(D16): 18029-18036.

Fischer, G. and Wefer, G., 1999. Use of proxies in oceanography: examples from the South Atlantic. Springer, Berlin, 735 pp.

Formenti, P., Elbert, W., Maenhaut, W., Haywood, J. and Andreae, M.O., 2003. Chemical composition of mineral dust aerosol during the Saharan Dust Experiment (SHADE) airborne campaign in the Cape Verde region, September 2000. Journal of Geophysical Research, 108(D18): 8576.

Frankenberg, P. (Editor), 1978. Florengeographische Untersuchungen im Raume der Sahara. Bonner Geographische Abhandlungen, 58. Ferd. Dümmlers, Bonn.

Freudenthal, T., Neuer, S., Meggers, H., Davenport, R. and Wefer, G., 2001. Influence of lateral particle advection and organic matter degradation on sediment accumulation and stable nitrogen isotope ratios along a productivity gradient in the Canary Islands region. Marine Geology, 177(1-2): 93-109.

Freudenthal, T., Meggers, H., Henderiks, J., Kuhlmann, H., Moreno, A. and Wefer, G., 2002. Upwelling intensity and filament activity off Morocco during the last 250,000 years. Deep Sea Research Part II, 49(17): 3655-3674.

Friddell, J.E., Thunell, R.C., Guilderson, T.P. and Kashgarian, M., 2003. Increased northeast Pacific climatic variability during the warm middle Holocene. Geophysical Research Letters, 30(11): 1560.

Game, P.M., 1964. Observations on a dustfall in the eastern Atlantic, February, 1962. Journal of Sedimentary Petrology, 34(2): 355-359.

Ganopolski, A., Kubatzki, C., Claussen, M., Brovkin, V. and Petoukhov, V., 1998. The influence of vegetation-atmosphere-ocean interaction on climate during the mid-Holocene. Science, 280: 1916-1919.

Gasse, F., Téhet, R., Durand, A., Gilbert, E. and Fontes, J.-C., 1990. The arid-humid transition in the Sahara and the Sahel during the last deglaciation. Nature, 346: 141-146.

Gasse, F., 2000. Hydrological changes in the African tropics since the Last Glacial Maximum. Quaternary Science Reviews, 19(1-5): 189-211.

Geb, M., 2000. Factors favouring precipitation in North Africa: seen from the viewpoint of present-day climatology. Global and Planetary Change, 26(1-3): 85-96.

Geldmacher, J. and Hoernle, K., 2000. The 72 Ma geochemical evolution of the Madeira hotspot (eastern North Atlantic): recycling of Paleozoic (500 Ma) oceanic lithosphere. Earth and Planetary Science Letters, 183(1-2): 73-92.

Geldmacher, J., Hoernle, K., Bogaard, P.v.d., Zankl, G. and Garbe-Schönberg, D., 2001. Earlier history of the 70-Ma-old Canary hotspot based on the temporal and geochemical evolution of the Selvagen Archipelago and neighboring seamounts in the eastern North Atlantic. Journal of Volcanology and Geothermal Research, 111(1-4): 55-87.

Glaccum, R.A. and Prospero, J.M., 1980. Saharan aerosols over the tropical North Atlantic - Mineralogy. Marine Geology, 37: 295-321.

Goudie, A.S. and Middleton, N.J., 2001. Saharan dust storms: nature and consequences. Earth-Science Reviews, 56(1-4): 179-204.

Grootes, P.M. and Stuiver, M., 1997. Oxygen 18/16 variability in Greenland snow and ice with 10^{-3}- to 10^{5}-year time resolution. Journal of Geophysical Research, 102(C12): 26455-26470.

Guieu, C., Loye-Pilot, M.-D., Ridame, C. and Thomas, C., 2002. Chemical characterization of the Saharan dust end-member: some biogeochemical implications for the western Mediterranean Sea. Journal of Geophysical Research, 107(15): ACH5/1-ACH5/11.

Gunn, D.E. and Best, A.I., 1998. A new automated nondestructive system for high resolution multi-sensor core logging of open sediment cores. Geo-Marine Letters, 18(1): 70-77.

Haag, M., 2000. Reliability of relative palaeointensities of a sediment core with climatically-triggered strong magnetisation changes. Earth and Planetary Science Letters, 180(1-2): 49-59.

Hagen, E., 2001. Northwest African upwelling scenario. Oceanologica Acta, 24(1): 113-128.

Hastenrath, S., 1996. Climate Dynamics of the Tropics. Atmospheric Sciences Library, 8. Kluwer Academic, Dordrecht.

Haug, G.H., Hughen, K.A., Sigman, D.M., Peterson, L.C. and Röhl, U., 2001. Southward migration of the Intertropical Convergence Zone through the Holocene. Science, 293(5533): 1304-1308.

Helmke, P., Davenport, R., Kuhlmann, H., (subm.). Wind stress-related filament structures off Cape Ghir, NW Africa. Deep-Sea Research.

Henderiks, J., Freudenthal, T., Meggers, H., Nave, S., Abrantes, F., Bollmann, J. and Thierstein, H.R., 2002. Glacial-interglacial variability of particle accumulation in the Canary Basin: a time-slice approach. Deep Sea Research Part II, 49(17): 3675-3705.

Hernández-Guerra, A., Aristegui, J., Canton, M. and Nykjaer, L., 1993. Phytoplankton pigment patterns in the Canary Islands area as determined using Coastal Zone Colour scanner data. International Journal of Remote Sensing, 14(7): 1431-1437.

Hernández-Guerra, A., Fraile-Nuez, E., Borgesa, R., López-Laatzen, F., Vélez-Belchí, P., Parrilla, G. and Müller, T.J., 2003. Transport variability in the Lanzarote passage (eastern boundary current of the North Atlantic subtropical Gyre). Deep Sea Research Part I, 50(2): 189-200.

Herrmann, L., Stahr, K. and Sponholz, B., 1997. Identifizierung trockenzeitlicher und regenzeitlicher Staubquellen im östlichen Westafrika. Würzburger Geographische Arbeiten, 92: 189-211.

Hoelzmann, P., Jolly, D., Harrison, S.P., Laarif, F., Bonnefille, R. and Pachur, H.-J., 1998. Mid-Holocene land-surface conditions in northern Africa and the Arabian Peninsula: A data set for the analysis of biogeophysical feedbacks in the climate system. Global Biogeochemical Cycles, 12(1): 35-51.

Hoepffner, N., Sturm, B., Finenko, Z. and Larkin, D., 1999. Depth-integrated primary production in the eastern tropical and subtropical North Atlantic basin from ocean colour imagery. International Journal of Remote Sensing, 20(7): 1435-1456.

Holz, C., Stuut, J.-B.W., Henrich, R. (subm.). Terrigeneous sedimentation along the continental margin off NW Africa: implications from grain-size analyses of surface sediments. Sedimentology

Hooghiemstra, H., Bechler, A. and Beug, H.-J., 1987. Isopollen maps for 18,000 years B.P. of the Atlantic Offshore of northwest Africa: evidence for paleowind circulation. Paleoceanography, 2(6): 561-582.

Hooghiemstra, H., 1989. Variations of the NW African trade wind regime during the last 140,000 years: changes in pollen flux evidenced by marine sediment records. In: M. Leinen and M. Sarnthein (Editors), Paleoclimatology and Paleometeorology: Modern and Past Patterns of Atmospheric Transport. Kluwer Academic Publishers, Dordrecht, pp. 733-770.

Hsu, C.-P.F. and Wallace, J.M., 1976. The global distribution in annual and semiannual cycles in precipitation. Monthly Weather Review, 104(9): 1093-1101.

Huertas, M.J., Arnaud, N.O., Ancochea, E., Cantagrel, J.M. and Fúster, J.M., 2002. 40Ar/39Ar stratigraphy of pyroclastic units from the Cañadas Volcanic Edifice (Tenerife, Canary Islands) and their bearing on the structural evolution. Journal of Volcanology and Geothermal Research, 115(3-4): 351-365.

Imbrie, J., Hays, J.D., Martinson, D.G., McIntyre, A., Mix, A.C., Morley, J.J., Pisias, N.G., Prell, W.L. and Shackleton, N.J., 1984. The orbital theory of Pleistocene climate: Support from a revised chronology of the marine d^{18}O record. In: W.H. Berger, J. Imbrie, J.D. Hays, J. Kukla and J. Saltzmann (Editors), Milankovitch and Climate, Part 1. Reidel, Hingham, Mass., pp. 269-305.

Jahn, B., Donner, B., Müller, P.J., Röhl, U., Schneider, R.R. and Wefer, G., 2003. Pleistocene variations in dust input and marine productivity in the northern Benguela Current: Evidence of evolution of global glacial–interglacial cycles. Palaeogeography, Palaeoclimatology, Palaeoecology, 193(3-4): 515-533.

Jansen, J.H.F., Gaast, S.J.V.d., Koster, B. and Vaars, A.J., 1998. CORTEX, a shipboard XRF-scanner for element analyses in split sediment cores. Marine Geology, 151(1-4): 143-153.

Jarvis, I., Moreton, J. and Gérard, M., 1998. Chemostratigraphy of Madeira Abyssal Plain Miocene-Pleistocene turbidites, Site 950. Proceedings of the ODP, Scientific Results, 157: 535-558.

Johnson, J. and Stevens, I., 2000. A fine resolution model of the eastern North Atlantic between the Azores, the Canary Islands and the Gibraltar Strait. Deep Sea Research Part I, 47(5): 875-899.

Jolly, D., Harrison, S.P., Damnati, B. and Bonnefille, R., 1998. Simulated climate and biomes of Africa during the late quaternary: comparison with pollen and lake status data. Quaternary Science Reviews, 17(6-7): 629-657.

Joussaume, S., Taylor, K.E., Braconnot, P., Mitchell, J.F.B., Kutzbach, J.E., Harrison, S.P., Prentice, I.C., Broccoli, A.J., Abe-Ouchi, A., Bartlein, P.J., Bonfils, C., Dong, B., Guiot, J., Herterich, K., Hewitt, C.D., Jolly, D., Kim, J.W., Kislov, A.,

Kitoh, A., Loutre, M.F., Masson, V., McAvaney, B., McFarlane, N., de Noblet, N., Peltier, W.R., Peterschmitt, J.Y., Pollard, D., Rind, D., Royer, J.F., Schlesinger, M.E., Syktus, J., Thompson, S., Valdes, P., Vettoretti, G., Webb, R.S. and Wyputta, U., 1999. Monsoon changes for 6000 years ago: results of 18 simulations from the Paleoclimate Modeling Intercomparison Project (PMIP). Geophysical Research Letters, 26(7): 859-862.

Kaufmann, Y.J., Tanré, D. and Boucher, O., 2002. A satellite view of aerosols in the climate system. Nature, 419: 215-223.

Keigwin, L.D., 1996. The Little Ice Age and the Medieval Warm Period in the Sargasso Sea. Science, 274: 1504-1508.

Keigwin, L.D. and Pickard, R.S., 1999. Slope water current over the Laurentian fan on interannual to millenial time scales. Science, 286: 520-523.

Klügel, A., Hoernle, K.A., Schmincke, H.-U. and White, J.D.L., 2000. The chemically zoned 1949 eruption on La Palma (Canary Islands): Petrologic evolution and magma supply dynamics of a rift zone eruption. Journal of Geophysical Research, 105(B3): 5997-6016.

Knoll, M., Hernández-Guerra, A., Lenz, B., Laatzen, F.L., Machín, F., Müller, T.J. and Siedler, G., 2002. The Eastern Boundary Current system between the Canary Islands and the African Coast. Deep Sea Research Part II, 49(17): 3427-3440.

Knutti, R., Stocker, T.F., Joos, F. and Plattner, G.-K., 2002. Constraints on radiative forcing and future climate change from observations and climate model ensembles. Nature, 416: 719-723.

Koopmann, B., 1981. Sedimentation von Saharastaub im subtropischen Nordatlantik während der letzten 25.000Jahre. "Meteor" Forschungsergebnisse, C(35): 23-59.

Krastel, S., Schmincke, H.-U., Jacobs, C.L., R., R., Le Bars, T.P. and Alibés, B., 2001. Submarine landslides around the Canary Islands. Journal of Geophysical Research, 106(B3): 3977-3997.

Kremling, K. and Streu, P., 1993. Saharan dust influenced trace element fluxes in deep North Atlantic subtropical waters. Deep Sea Research Part I, 40(6): 1155-1168.

Kushnir, Y., 1999. Climatology: Europe's winter prospects. Nature, 398(6725): 289-291.

Kutzbach, J.E. and Liu, Z., 1997. Response of the African monsoon to orbital forcing and ocean feedbacks in the middle Holocene. Science, 728: 440-443.

Lamb, H.F., Gasse, F., Benkaddour, A., El Hamouti, N., vann der Kaas, S., Perkins, W.T., Pearce, N.J. and Roberts, C.N., 1995. Relation between century-scale Holocene arid intervals in tropical and temperate zones. Nature, 373: 134-136.

Lamy, F., Hebbeln, D., Röhl, U. and Wefer, G., 2001. Holocene rainfall variability in southern Chile: a marine record of latitudinal shifts of the Southern Westerlies. Earth and Planetary Science Letters, 185(3-4): 369-382.

Lézine, A.-M., Casanova, J. and Hillaire-Marcel, C., 1990. Across an early Holocene humid phase in western Sahara: Pollen and isotope stratigraphy. Geology, 18: 264-267.

Llinás, O., Rueda, M.J., Marrero, J.P., Pérez-Martell, E., Santana, R., Villagarcía, M.G., Cianca, A., Godoy, J. and Maroto, L., 2002. Variability of the Antarctic intermediate waters in the Northern Canary Box. Deep Sea Research Part II, 49(17): 3441-3453.

Loutre, M.R., Berger, A., Bretagnon, P. and Blanc, P.-L., 1992. Astronomical frequencies for climate research at the decadal to century time scale. Climate Dynamics, 7: 181-194.

MacLeod, K.G., Huber, B.T., Pletsch, T., Röhl, U. and Kucera, M., 2001. Maastrichtian foraminiferal and paleoceanographic changes on Milankovitch time scales. Paleoceanography, 16(2): 133-154.

Mahowald, N.M., Bryant, R.G., del Corral, J. and Steinberger, L., 2003. Ephemeral lakes and desert dust sources. Geophysical Research Letters, 30(2): 1074.

Mahowald, N.M. and Kiehl, L.M., 2003. Mineral aerosol and cloud interactions. Geophysical Research Letters, 30(9): 1475.

Marret, F. and Turon, J.-L., 1994. Paleohydrology and paleoclimatology off Northwest Africa during the last glacial-interglacial transition and the Holocene: Palynological evidences. Marine Geology, 118: 107-117.

Martí, J., Mitjavila, J. and Arana, V., 1994. Stratigraphy, structure and geochronology of the Las Canadas caldera (Tenerife, Canary Islands). Geological Magazine, 131(6): 715-727.

Martinez, P., Bertrand, P., Shimmield, G.B., Cochrane, K., Jorissen, F.J., Foster, J. and Dignan, M., 1999. Upwelling intensity and ocean productivity changes off Cape Blanc (northwest Africa) during the last 70,000 years: geochemical and micropalaeontological evidence. Marine Geology, 158(1-4): 57-74.

Martinez, P., Bertrand, P., Calvert, S.E., Pedersen, T.F., Shimmield, G.B., Lallier-Vergès, E. and Fontugne, M.R., 2000. Spatial variations in nutrient utilization, production and diagenesis in the sediments of a coastal upwelling regime (NW Africa): Implications for the paleoceanographic record. Journal of Marine Research, 58: 809-835.

Martinson, D.G., Pisias, N.G., Hays, J.D., Imbrie, J., Moore, T.C. and Shackleton, N.J., 1987. Age dating and the orbital theory of the ice ages: development of a high-resolution 0 to 300.000 year chronostratigraphy. Quaternary Research, 27: 1-29.

Masson, D.G., Niel, B.v. and Weaver, P.P.E., 1997. Flow processes and sediment deformation in the Canary Debris Flow on the NW African Continental Rise. Sedimentary Geology, 110(3-4): 163-179.

Mayewski, P.A., Meeker, L.D., Twickler, M.S., Whitlow, S., Yang, Q., Lyons, W.B. and Prentice, M., 1997. Major features and forcing of high-latitude northern hemisphere atmospheric circulation using a 110,000-year-long glaciochemical series. Journal of Geophysical Research, 102(C12): 26345-26366.

McIntyre, A., Ruddiman, W.F., Karlin, K. and Mix, A.C., 1989. Surface water response of the equatorial Atlantic Ocean to orbital forcing. Paleoceanography, 4: 19-55.

Measures, C.I. and Brown, E.T., 1996. Estimating dust input to the Atlantic Ocean using surface water aluminium concentrations. In: S. Guerzoni and R. Chester (Editors), The impact of desert dust across the Mediterranean. Environmental Science and Technology Library. Kluwer Academic Publishers, Dodrecht, pp. 301-311.

Meggers, H., Freudenthal, T., Nave, S., Targarona, J., Abrantes, F. and Helmke, P., 2002. Assessment of geochemical and micropaleontological sedimentary parameters as proxies of surface water properties in the Canary Islands region. Deep Sea Research Part II, 49(17): 3631-3654.

Middleton, N.J., Betzer, P.R. and Bull, P.A., 2001. Long-range transport of 'giant' aeolian quartz grains: linkage with discrete sedimentary sources and implications for protective particle transfer. Marine Geology, 177(3-4): 411-417.

Milankovic, M., 1930. Mathematische Klimalehre und astronomische Theorie der Klimaschwankungen. In: W. Köppen and R. Geiger (Editors), Handbuch der Klimatologie. Gebrüder Bornträger, Berlin.

Milliman, J.D. and Meade, R.H., 1983. World-wide delivery of river sediment to the oceans. Journal of Geology, 91(1): 1-21.

Mittelstaedt, E., 1991. The ocean boundary along the northwest African coast: Circulation and oceanographic properties at the sea surface. Progress in Oceanography, 26: 307-355.

Mix, A.C., 1989. Pleistocene paleoproductivity: Evidence from organic carbon and foraminiferal species. In: W.H. Berger, V.S. Smetacek and G. Wefer (Editors), Productivity of the Ocean: Present and Past. Wiley-Interscience, Bath, pp. 313-340.

Moreno, A., Targarona, J., Henderiks, J., Canals, M., Freudenthal, T. and Meggers, H., 2001. Orbital forcing of dust supply to the North Canary Basin over the last 250 kyr. Quaternary Science Reviews, 20: 1327-1339.

Moreno, A., Nave, S., Kuhlmann, H., Canals, M., Targarona, J., Freudenthal, T. and Abrantes, F., 2002. Productivity response in the North Canary Basin to climate changes during the last 250000 yr: a multi-proxy approach. Earth and Planetary Science Letters, 196(3-4): 147-159.

Müller, T.J. and Siedler, G., 1992. Multi-year current time series in the eastern North Atlantic Ocean. Journal of Marine Research, 50: 63-98.

Myhre, G. and Stordal, F., 2001. Global sensitivity experiments of the radiative forcing due to mineral aerosols. Journal of Geophysical Research, 106(D16): 18193-18204.

Neuer, S., Ratmeyer, V., Davenport, R., Fischer, G. and Wefer, G., 1997. Deep water particle flux in the Canary Island region: seasonal trends in relation to long-term satellite derived pigment data and lateral sources. Deep Sea Research Part I, 44(8): 1451-1466.

Neuer, S., Alfke, R., Bergenthal, M., Bittkau, A., Böhme, L., Bothmer, H., Cianca, A., Diekamp, V., Freudenthal, T., Gerdes, A., Godoy, J., Grimm, G., Hayn, C., Hebbeln, D., Huebner, H., Kahl, G., Klein, T., Köster, J., Laglera, L., Langer, J., Benz, B., Meggers, H., Meinecke, G., Metzler, W., Moroto, L., Nave, S., Ochsenhirt, W., Ratmeyer, V., Rosiak, U., Rueda, M.-J., Ruhland, G., Schiebel, R., Schüssler, U., Struck, U., Themann, S., Villagarcia, M., von Oppen, C. and Waldmann, C., 2000. Report and preliminary results of METEOR cruise M 45/5, Bremen - Las Palmas, October 1 - November 3, 1999. Berichte aus dem Fachbereich Geowissenschaften der Universität Bremen, 163: 93.

Norris, R.D. and Röhl, U., 1999. Carbon cycling and chronology of climate warming during the Palaeocene/Eocene transition. Nature, 401: 775-778.

Nykjaer, L. and Van Camp, L., 1994. Seasonal and interannual variability of coastal upwelling along northwest Africa and Portugal from 1981 to 1991. Journal of Geophysical Research, 99(C7): 14197-14207.

Olivera, F., 1996. Water Balance of the Souss Basin - Morocco. University of Texas at Austin, Austin, TX, http://www.ce.utexas.edu/prof/maidment/GISHydro/olivera/morocco/report.htm.

Ortiz, J.D. and Rack, F.R., 1999. Non-invasive sediment monitoring methods. In: F. Abrantes and A.C. Mix (Editors), Reconstructing Ocean History: A Window into the Future. Kluwer Academic / Plenum Publishers, New York, pp. 343-379.

Overpeck, J.T., Peterson, L.C., Kipp, N., Imbrie, J. and Rind, D., 1989. Climate change in the circum-North Atlantic region during the last deglaciation. Nature, 338: 553-557.

Paillard, D., Labeyrie, L. and Yiou, P., 1996. Macintosh program performs time-series analysis. EOS Transactions American Geophysical Union, 77: 379.

Pälike, H., Shackleton, N.J. and Röhl, U., 2001. Astronomical forcing in Late Eocene marine sediments. Earth and Planetary Science Letters, 193(3-4): 589-602.

Perlwitz, J., Tegen, I. and Miller, R.L., 2001. Interactive soil dust aerosol model in the GISS GCM, 1, Sensitivity of the soil dust cycle to radiative properties of soil dust aerosols. Journal of Geophysical Research, 106(D16): 18167-18192.

Peterson, L.C., Haug, G.H., Hughen, K.A. and Röhl, U., 2000. Rapid Changes in the Hydrologic Cycle of the Tropical Atlantic During the Last Glacial. Science, 290: 1947-1951.

Petit-Maire, N., 1989. Interglacial environments in presently hyperarid Sahara: paleoclimatic implications. In: M. Leinen and M. Sarnthein (Editors), Paleoclimatology and Paleometeorology: Modern and Past Patterns of Global Atmospheric Transport. Kluwer Academic Publishers, Dordrecht, pp. 637-661.

Petit-Maire, N., Commelin, D., Fabre, J. and Fontugne, M., 1990. First evidence for Holocene rainfall in the Tanezrouft hyperdesert and its margins. Palaeogeography, Palaeoclimatology, Palaeoecology, 79: 333-338.

Potts, P.J., 1987. A Handbook of Silicate Rock Analysis. Blackie, Glasgow, 622 pp.

Prahl, F.G., Cowie, G.L., Lange, G.J.D. and Sparrow, M.A., 2003. Selective organic matter preservation in "burn-down" turbidites on the Madeira Abyssal Plain. Paleoceanography, 18(2): 1052.

Prospero, J.M. and Nees, R.T., 1986. Impact of the North African drought and El Niño on mineral dust in the Barbados trade winds. Nature, 320: 735-738.

Prospero, J.M., 1990. Mineral-aerosol transport to the North Atlantic and North Pacific: The impact of African and Asian sources. In: A.H. Knap (Editor), The long-range atmospheric transport of natural and contaminant substances. Mathematical and Physical Sciences. Kluwer Academic Publishers, Dodrecht, pp. 59-86.

Prospero, J.M., 1996. The atmospheric transport of particles to the ocean. In: V. Ittekkot, P. Schäfer, S. Honjo and P.J. Depetris (Editors), Particle flux in the ocean. John Wiley & Sons, Chichester, pp. 19-52.

Prospero, J.M., Ginoux, P., Torres, O., Nicholson, S.E. and Gill, T.E., 2002. Environmental characterization of global sources if atmospheric soil dust identified with the nimbus 7 total ozone mapping spectrometer (TOMS) absorbing aerosol product. Review of Geophysics, 40(1): 2-1/2-31.

Pye, K., 1987. Aeolian dust and dust deposits. Academic Press, London.

Ramaswamy, V., Nair, R.R., Manganini, S., Haake, B. and Ittekkot, V., 1991. Lithogenic fluxes to the deep Arabian Sea measured by sediment traps. Deep-Sea Research II, 38(2): 169-184.

Ratmeyer, V., Balzer, W., Bergametti, G., Chiapello, I., Fischer, G. and Wyputta, U., 1999a. Seasonal impact of mineral dust on deep-ocean particle flux in the eastern subtropical Atlantic Ocean. Marine Geology, 159(1-4): 241-252.

Ratmeyer, V., Fischer, G. and Wefer, G., 1999b. Lithogenic particle fluxes and grain size distributions in the deep ocean off northwest Africa: Implications for seasonal changes of aeolian dust input and downward transport. Deep Sea Research, 46(8): 1289-1337.

Raymo, M.E., 1997. The timing of major climate terminations. Paleoceanography, 12(4): 577-585.

Renssen, H., Brovkin, V., Fichefet, T. and Goosse, H., 2003. Holocene climate instability during the termination of the African Humid Period. Geophysical Research Letters, 30(4): 1184.

Rihm, R., Jacobs, C.L., Krastel, S., Schmincke, H.-U. and Alibés, B., 1998. Las Hijas Seamounts-the next Canary Island? Terra Nova, 10: 121-125.

Rimbu, N., Lohmann, G., Kim, J.-H., Arz, H.W. and Schneider, R., 2003. Arctic/North Atlantic Oscillation signature in Holocene sea surface temperature trends as obtained from alkenone data. Geophysical Research Letters, 30(6): 1280.

Rodehorst, U., Schmincke, H.-U. and Sumita, M., 1998. Geochemistry and petrology of Pleistocene ash layers erupted at las Cañadas edifice, (Tenerife). In: P.P.E.

Weaver, H.-U. Schmincke, J.V. Firth and W. Duffield (Editors), Proceedings of the ODP, Scientific Results, pp. 315-328.

Röhl, U. and Abrams, L.J., 2000. High-resolution, downhole, and nondestructive core measurements from sites 999 and 1001 in the Caribbean Sea: Application to the late paleocene thermal maximum. In: R.M. Leckie, H. Sigurdsson, G.D. Acton and G. Draper (Editors), Proceedings of the ODP, Scientific Results, pp. 191-203.

Röhl, U., Bralower, T.J., Norris, R.D. and Wefer, G., 2000. New chronology for the late Paleocene thermal maximum and its environmental implications. Geology, 28(10): 927-930.

Röhl, U., Ogg, J.G., Geib, T.L. and Wefer, G., 2001. Astronomical calibration of the Danian time scale. In: R.D. Norris, D. Kroon and A. Klaus (Editors), Western North Atlantic Paleogene and Cretaceous Paleoceanography. Geological Society Special Publication. Geological Society, London, pp. 163-183.

Rossignol-Strick, M. and Duzer, D., 1979. Late Quaternary pollen and dinoflagellate cysts in marine cores off West Africa. "Meteor" Forschungsergebnisse, C(30): 1-14.

Ruddiman, W.F. and Janecek, T.R., 1989. Pliocene-Pleistocene biogenic and terrigenous fluxes at equatorial Atlantic sites 662, 663 and 664. In: W.R. Ruddiman and M. Sarnthein (Editors), Proceedings of the ODP, Scientific Results, pp. 211-240.

Sarnthein, M., Tetzlaff, G., Koopmann, B., Wolter, K. and Pflaumann, U., 1981. Glacial and interglacial wind regimes over the eastern subtropical Atlantic and North-West Africa. Nature, 193: 193-196.

Sarnthein, M., Thiede, J., Pflaumann, U., Erlenkeuser, H., Fütterer, D., Koopmann, B., Lange, H. and Seibold, E., 1982. Atmospheric and oceanic circulation patterns off Northwest Africa during the past 25 million years. In: U. von Rad, K. Hinz, M. Sarnthein and E. Seibold (Editors), Geology of the northwest African continental margin. Springer-Verlag, Berlin, Heidelberg, pp. 545-604.

Sarnthein, M., Winn, K., Duplessy, J.-C. and Fontugne, M.R., 1988. Global variations of surface ocean productivity in low and mid latitudes: Influence on CO2 reservoirs of the deep ocean and atmosphere during the last 21.000 years. Paleoceanography, 3(3): 361-399.

Sassen, K., DeMott, P.J., Prospero, J.M. and Poellot, M.R., 2003. Saharan dust storms and indirect aerosol effects on clouds: CRYSTAL-FACE results. Geophysical Research Letters, 30(12): 1633.

Saydam, A.C. and Senyuva, H.Z., 2002. Deserts: Can they be the potential suppliers of bioavailable iron? Geophysical Research Letters, 29(11): 19/1-19/3.

Schemainda, R., Nehring, D. and Schulz, S., 1975. Ozeanologische Untersuchungen zum Produktionspotential der nordwestafrikanischen Wasserauftriebsregion 1970 - 1973. Geodätische und Geophysikalische Veröffentlichungen, 4(16).

Schlesinger, W.H., 1997. Biogeochemistry, An Analysis of Global Change. Academic Press, San Diego, 588 pp.

Schlitzer, R., 2002. Ocean Data View. http://ww.awi-bremenhaven.de/GEO/ODV,2002.

Schmincke, H.-U., 2000. Seamounts und Vulkaninseln, Vulkanismus. Wissenschaftliche Buchgesellschaft, Darmstadt, pp. 63-86.

Schollaert, S.E. and Merrill, J.T., 2001. Cooler sea surface west of the Sahara Desert correlated to dust events. Geophysical Research Letters, 25(18): 3529-3532.

Schulz, E., Akhtar-Schuster, M., Agwu, C., Beck, C., L.Dupont, S.Jahns, Niedermeyer, M., Ousseini, I. and U.Salzmann, 2000. The Holocene landscape and vegetation history of northern and western Africa. Univerität Würzburg, Geographie.

Schulz, M. and Paul, A., 2002. Holocene Climate Variability on Centennial-to-Millennial Time Scales: Climate Records from the North-Atlantic Realm. In: G. Wefer, W.H. Berger, K.-E. Behre and E. Jansen (Editors), Climate Development and History of the North Atlantic Realm. Springer-Verlag, Berlin, Heidelberg, pp. 41-54.

Schütz, L., Jaenicke, R. and Pietrek, H., 1981. Saharan dust transport over the North Atlantic Ocean. Geological Society of America Spec. Pap., 186: 87-100.

Schütz, L. and Sebert, M., 1987. Mineral aerosols and source indentification. Journal of Aerosol Sciences, 18(1): 1-10.

Schütz, L.W., Prospero, J.M., Buat-Ménard, P., Carvalho, R.A.C., Cruzado, A., Harriss, R., Heidam, N.Z. and Jaenicke, R., 1990. The long-range transport of mineral aerosols: group report. In: A.H. Knap (Editor), The long-range atmospheric transport of natural and contaminant substances. Mathematical and Physical Sciences. Kluwer Academic Publishers, Dodrecht, pp. 197-229.

Shipboard, Scientific Party, 1995. Background objectives and principal results of drilling the clastic apron of Gran Canaria (VICAP). Proceedings of the ODP, Initial Reports, 157: 11-25.

Siegenthaler, U. and Sarmiento, J.L., 1993. Atmospheric carbon dioxide and the ocean. Nature, 365: 119-125.

Stramma, L., 1984. Geostrophic transport in the warm water sphere of the eastern subtropical North Atlantic. Journal of Marine Research, 42: 537-558.

Stramma, L. and Siedler, G., 1988. Seasonal changes in the North Atlantic Subtropical Gyre. Journal of Geophysical Research, 93(C7): 8111-8118.

Street-Perrot, F.A. and Perrot, R.A., 1990. Abrupt climate fluctuations in the tropics: the influence of Atlantic Ocean circulation. Nature, 343: 607-612.

Stuiver, M. and Braziunas, T., F., 1993. Modeling atmospheric ^{14}C influences and ^{14}C ages of marine samples to 10,000 BC. Radiocarbon, 35(1): 137-189.

Stuiver, M., Reimer, P.J., Bard, E., Beck, W., Burr, G.S., Hughen, K.A., Kromer, B., McCormac, G., van der Plicht, J. and Spurk, M., 1998. INTCAL98 radiocarbon age calibration, 24,000-0 cal BP. Radiocarbon, 40(3): 1041-1083.

Summerhayes, C.P., Milliman, J.D., Briggs, S.R., Bee, A.G. and Hogan, C., 1976. Northwest African shelf sediments: Influence of climate and sedimentary processes. Journal of Geology, 84: 277-300.

Swan, A.R.H. and Sandilands, M., 1995. Introduction to geological data analysis. Blackwell Science, Oxford, 446 pp.

Tetzlaff, G. and Wolter, K., 1980. Meteorological patterns and the transport of mineral dust from the North African continent. In: M. Sarnthein, E. Seibold and P. Rognon (Editors), Palaeoecology of Africa. A.A. Balkema, Rotterdam, pp. 31-42.

Tetzlaff, G., Peters, M., Janssen, W. and Adams, L.J., 1989. Aeolian dust transport in West Africa. In: M. Leinen and M. Sarnthein (Editors), Paleoclimatology and Paleometeorology: Modern and Past Patterns of Atmospheric Transport. NATO ASI Series. Kluwer Academic Publishers, Dordrecht, pp. 185-203.

Thompson, L.G., Mosley-Thompson, E., Davies, M.E., Henderson, K.A., Brecher, H.H., Zagorodnov, V.S., Mashiotta, T.A., Lin, P.-N., Mikhalenko, V.N., Hardy, D.R. and Beer, J., 2002. Kilimanjaro ice core records: Evidence of Holocene climate change in tropical Africa. Science, 298: 859-593.

Tiedemann, R., Sarnthein, M. and Stein, R., 1989. Climatic changes in the western Sahara: Aeolo-marine sediment record of the last 8 million years (sites 657-661). In: W. Ruddiman and M. Sarntheim (Editors), Proceedings of the ODP, Scientific Results, pp. 241-261.

Torrence, C. and Compo, G.P., 1998. A practical guide to wavelet analysis. Bulletin of the American Meteorological Society, 79(1): 61-78.

Torres-Padrón, M.E., Gelado-Caballero, M.D., Collado-Sánchez, C., Siruela-Matos, V.F., Cardona-Castellano, P.J. and Hernández-Brito, J.J., 2002. Variability of dust inputs to the CANIGO zone. Deep Sea Research Part II, 49(17): 3455-3464.

Tuenter, E., Weber, S.L., Hilgen, F.J. and Lourens, L.J., 2003. The response of the African summer monsoon to remote and local forcing due to precession and obliquity. Global and Planetary Change, 36(4): 219-235.

Uchupi, E., Emery, K.O., Bowin, C.O. and Phillips, J.D., 1976. Continental Margin off Western Africa: Senegal to Portugal. American Association of Petroleum Geologists Bulletin, 60(5): 809-876.

Van Camp, L., Nykjaer, L., Mittelstaedt, E. and Schlittenhardt, P., 1991. Upwelling and boundary circulation off Northwest Africa as described by infrared and visible satellite observations. Progress in Oceanography, 26: 357-402.

van den Bogaard, P., 1998. $^{40}Ar/^{39}Ar$ ages of Pliocene-Pleistocene fallout tephra layers and volcaniclastic deposits in the sedimentary aprons of Gran Canaria and Tenerife (Sites 953, 954, and 956). In: P.P.E. Weaver, H.-U. Schmincke, J.V. Firth and W. Duffield (Editors), Proceedings of the ODP, Scientific Results, pp. 329-341.

Vidal, L., Bickert, T., Wefer, G. and Röhl, U., 2002. Late Miocene stable isotope stratigraphy of SE Atlantic ODP Site 1085: Relation to Messinian events. Marine Geology, 180(1-4): 71-85.

von Dobeneck, T. and Schmieder, F., 1999. Using rock magnetic proxy records for orbital tuning and extended time series analysis into the Super- and Sub-Milankovitch bands. In: G. Fischer and G. Wefer (Editors), Use of Proxies in Paleoceanography: Examples from the South Atlantic. Springer, Berlin, Heidelberg, pp. 601-633.

Vörösmarty, C.J., Fekete, B.M., Meybeck, M. and Lammers, R.B., 2000. Global system of rivers: Its role in organizing continental land mass and defining land-to-ocean linkages. Global Biogeochemical Cycles, 14(2): 599-621.

Watts, A.B. and Masson, D.G., 2001. New sonar evidence for recent catastrophic collapses of the north flank of Tenerife, Canary Islands. Bulletin of Volcanology, 63(1): 8-19.

Weaver, P.P.E. and Schultheiss, P.J., 1990. Current methods for obtaining, logging and splitting marine sediment cores. Marine Geophysical Researches, 12: 85-100.

Weaver, P.P.E., Rothwell, R.G., Ebbing, J., Gunn, D. and Hunter, P.M., 1992. Correlation, frequency of emplacement and source directions of megaturbidites on the Madeira Abyssal Pain. Marine Geology, 109(1-2): 1-20.

Weaver, P.P.E., Wynn, R.B., Kenyon, N.H. and Evans, J., 2000. Continental margin sedimentation, with special reference to the north-east Atlantic margin. Sedimentology, 47(Suppl. 1): 239-256.

Weber, M.E., Niessen, F., Kuhn, G. and Wiedicke, M., 1997. Calibration and application of marine sedimentary physical properties using a multi-sensor core logger. Marine Geology, 136(3-4): 151-172.

Wefer, G. and Fischer, G., 1993. Seasonal patterns of vertical fluxes in equatorial and coastal upwelling areas of the eastern Atlantic. Deep -Sea Research I, 40(8): 1613-1645.

Wefer, G., Abrantes, F., Bassek, D., Bollmann, J., Bozzano, G., Diekamp, V., Dittert, L., Eberwein, A., Klump, J., Kuhlmann, H., Lindblom, S., Meggers, H., Meinecke, G., Metzler, W., Moustafa, Y., Peters, M., Ratmeyer, V., Rieß, W., Rosiak, U., Segl, M., Skoglund, S., Targarona, J., Vaqueiro, S., Waldmann, C.,

Wenzhöfer, F. and Zabel, M., 1997. Report and preliminary results of METEOR cruise M 37/1 Lisbon - Las Palmas; 04.12.96-23.12.96. Berichte aus dem Fachbereich Geowissenschaften der Universität Bremen, 90: 79.

Wefer, G., Berger, W.H., Richter, C.L. and Shipboard Scientific Party, S.S., 1998. 13. Site 1085. Proceedings of the ODP, Initial Reports, 175: 385-428.

Wefer, G., Segl, M., Bassek, D., Buhlmann, K., Deeken, A., Dehning, K., Diekamp, V., Drünert, F., Eberwein, A., Franke, P., Freudenthal, T., Geisen, M., Godoy, J., Gonzáles-Davila, M., Günther, L., Hayn, C., Hendriks, J., Irmisch, A., Jeronimo, D., Kotte, N., Koy, U., Kretschmar, F., Langer, J., Makaoui, A., Maroto, L., Meggers, H., Meinecke, G., Metzler, W., Moreno, A., Nave, S., Neuer, S., Nowald, N.R., V., Rieß, W., Rosiak, U., Schroeter, M., Sprengel, C., Targarona, J., Thiele, J., Tierstein, H., von Oppen, C. and Waldmann, C., 1999. Report and preliminary results of METEOR cruise M 42/4 Las Palmas - Las Palmas - Vienna do Castelo; 26.09.1998 - 26.10.1998. Berichte aus dem Fachbereich Geowissenschaften der Universität Bremen, 132: 104.

Wegener, A., 1915. Die Entstehung der Kontinente und Ozeane. Vieweg-Verlag, Braunschweig, 94 pp.

Weischert, W. and Endlicher, W., 1999. Regionale Klimatologie Teil 2: Die Alte Welt. Teubner Studienbücher der Geographie. B.G. Teubner, Stuttgart, Leipzig, 625 pp.

Westerhold, T. (2003) The middle-Miocene carbonate crash: relationship to Neogene changes in ocean circulation and climate changes. PhD. Thesis, University of Bremen, Germany.

White, F., 1983. The vegetation of Africa. Natural Resources Research, 20(UNESCO, Paris): 356.

Windom, H.L., 1976. Lithogenous material in marine sediments. In: J.P. Riley and R. Chester (Editors), Chemical Oceanography. Academic Press, London, pp. 103-135.

Wynn, R.B., Masson, D.G., Stow, D.A.V. and Weaver, P.P.E., 2000. The Northwest African slope apron: a modern analogue for deep-water systems with complex seafloor topography. Marine and Petroleum Geology, 17: 253-265.

Yu, G. and Harrison, S.P., 1996. An evaluation of the simulated water balance of Eurasia and northern Africa at 6000 y BP using lake status data. Climate Dynamics, 12(11): 723-735.

Zahn, R., Schönfeld, J., Kudrass, H.-R., Park, M.-H., Erlenkeuser, H. and Grootes, P., 1997. Thermohaline instability in the North Atlantic during meltwater events: Stable isotope and ice-rafted detritus records from core SO75-26KL, Portuguese margin. Paleoceanography, 12(5): 696-710.

Zhao, M., Eglinton, G., Haslett, S.K., Jordan, R.W., Sarnthein, M. and Zhang, Z., 2000. Marine and terrestrial biomarker records for the last 35,000 years at ODP site 658C off NW Africa. Organic Geochemistry, 31(9): 919-930.

Zhao, M., Dupont, L., Eglinton, G. and Teece, M., 2003. n-Alkane and pollen reconstruction of terrestrial climate and vegetation for NW Africa over the last 160 kyr. Organic Geochemistry, 34(1): 131-143.

Danksagung

Für die Vergabe und die Betreuung der vorliegenden Arbeit bedanke ich mich herzlich bei Prof. Dr. Gerold Wefer, der einschließlich des gesamten Fachbereiches Geowissenschaften der Universität Bremen eine ideale wissenschaftliche Arbeitsumgebung zur Verfügung stellten. Prof. Dr. Gerhard Bohrmann danke ich für die Übernahme des Zweitgutachtens.

Mein besonderer Dank gilt Dr. Helge Meggers und Dr. Tim Freudenthal, die die wichtigsten wissenschaftlichen Ansprechpartner für mich waren und mich im Verlauf der Arbeit intensiv betreut und unterstützt haben. Sowohl die kollegiale und freundschaftliche Zusammenarbeit, als auch die anregende und zuweilen lebhafte Atmosphäre werden mir in bester Erinnerung bleiben.

Für die Unterstützung und Hilfsbereitschaft bei der Arbeit mit den Kernlogging-Systemen danke ich Dr. Ursula Röhl und Heike Pfletschinger. Für die besonders angenehme Atmosphäre während der vielen Monate im ODP Kernlager gilt der Dank Alexius Wülbers und Walter Hale, dem auch für die Korrektur der englischsprachigen Texte herzlich gedankt sei. Einen großen Beitrag zum Gelingen dieser Arbeit durch die vielen gemeinsamen nicht nur wissenschaftlichen Aktivitäten haben Boris Dorschel, Sebastian Meier, Peer Helmke und Nicolas Nowald geleistet, dafür sei auch ihnen herzlich gedankt.

Bei den Kollegen an der Universität Barcelona (Spanien) bedanke ich mich für eine sehr lehrreiche und interessante Zeit. Für die freundliche und hilfsbereite Aufnahme in die Arbeitsgruppe und die sehr gute Zusammenarbeit danke ich Prof. Dr. Miguel Canals, Dr. Ana Moreno, Graziella Bozzano und Dr. Joan Fabres, sowie Elisenda Segui und Montserrat Guart Fernández für die Betreuung bei der Röntgenfluoreszenz- und Korngrößenanalyse.

Weiterhin hat diese Arbeit von der vielfachen Unterstützung und Diskussionsbereitschaft der vielen (z.T. ehemaligen) Kollegen im Fachbereich sehr profitiert. Stellvertretend für sie alle sei hier gedankt: Astrid Eberwein, Daniela Hofmann, Thomas Westerhold, Rik Tjallingii, Oscar Romero, Ulrike Holzwarth, Dorit Siggelkow, Christine Holz, Matthias Zabel, Helge Arz, Jürgen Pätzold, Torsten Bickert, Carmen Murken, Gisela Boelen, Wolfgang Bevern.

Darüber hinaus möchte ich mich besonders bei meinen Eltern und meiner Schwester bedanken, die mir ein großer Rückhalt waren.

Die Deutsche Forschungsgemeinschaft hat die vorliegende Arbeit im Rahmen von zwei Projekten (We 992/31-1; We 992/41-1) finanziell unterstützt. Der Deutsche Akademische Austauschdienst (DAAD) gewährte ein Kurzzeitstipendium für den Aufenthalt an der Universität in Barcelona. Die Kommission zur Förderung des Wissenschaftlichen Nachwuchses der Universität Bremen (FNK) förderte die Arbeit durch Reisekostenzuschüsse.